DISSERTATIONES
TECHNOLOGIAE
CIRCUMIECTORUM
UNIVERSITATIS
TARTUENSIS
30

ERGO RIKMANN

Autotrophic nitrogen removal and relevant equilibrial processes

DISSERTATIONES TECHNOLOGIAE CIRCUMIECTORUM
UNIVERSITATIS TARTUENSIS
30

DISSERTATIONES TECHNOLOGIAE CIRCUMIECTORUM
UNIVERSITATIS TARTUENSIS
30

ERGO RIKMANN

Autotrophic nitrogen removal and relevant equilibrial processes

UNIVERSITY OF TARTU
Press

Institute of Chemistry, Faculty of Science and Technology, University of Tartu, Tartu, Estonia.

Dissertation was accepted for the commencement of the degree of *Doctor philosophiae* in environmental technology at the University of Tartu on 21st of August 2019, by the Scientific Council on Environmental Technology, Faculty of Science and Technology, University of Tartu.

Supervisors: Prof. Toomas Tenno, PhD
Institute of Chemistry
University of Tartu
Estonia

Research Fellow Anne Menert, PhD
Institute of Molecular and Cell Biology
University of Tartu
Estonia

Opponent: Prof. William Hogland, PhD
Department of Biology and Environmental Science
Linnaeus University
Sweden

Commencement: Room 1020, Chemicum, 14A Ravila Street, Tartu,
on October 4rd in 2019, at 14.15.

Publication of this thesis is granted by Institute of Chemistry, University of Tartu and by the Doctoral School 'Functional materials and Technologies' receiving funding from the European Social Fund under project '1.2.0401.09-0079 in Estonia'.

ISSN 1736-3349
ISBN 978-9949-03-168-9 (print)
ISBN 978-9949-03-169-6 (pdf)

University of Tartu Press
www.tyk.e

TABLE OF CONTENTS

LIST OF PUBLICATIONS INCLUDED IN THE THESIS

The current thesis is based on the following publications, which are listed below and referred to by their Roman numerals in the text of thesis:

I **Rikmann E**, Zekker I, Tomingas M, Tenno T, Menert A, Loorits L, Tenno T. (**2012**) Sulfate-reducing anaerobic ammonium oxidation as a potential treatment method for high nitrogen-content wastewater. *Biodegradation* 23(4): 509–524; 10.1007/s10532-011-9529-2.

II **Rikmann E**, Zekker I, Tomingas M, Vabamäe P, Kroon K, Saluste A, Tenno T, Menert A, Loorits L, dC Rubin SSC, Tenno T. (**2014**) Comparison of sulfate-reducing and conventional Anammox upflow anaerobic sludge blanket reactors. *J Biosci Bioeng* 118(4): 426–433; 10.1016/j.jbiosc.2014.03.012.

III **Rikmann E**, Zekker I, Tenno T, Saluste A, Tenno T. (**2018**) *Inoculum*-free start-up of biofilm- and sludge-based deammonification systems in pilot scale. *Int J Environ Sci Technol* 15(1): 133–148; 10.1007/s13762-017-1374-3.

IV Tenno T, **Rikmann E,** Zekker I, Tenno T, Daija L, Mashirin A. (**2016**). Modelling equilibrium distribution of carbonaceous ions and molecules in a heterogeneous system of $CaCO_3$–water–gas. *P Est Acad Sci Chem* 65(1): 68–77; 10.3176/proc.2016.1.07.

V Tenno T, Uiga K, Mashirin A, Zekker I and **Rikmann E**. (**2017**) Modeling Closed Equilibrium Systems of H_2O–Dissolved CO_2–Solid $CaCO_3$ *J Phys Chem A* 121: 3094–3100; 10.1021/acs.jpca.7b00237.

VI Tenno T, **Rikmann E**, Uiga K, Zekker I, Mashirin A, and Tenno T. **(2018)**. A novel proton transfer model of closed equilibrium systems of H_2O–CO_2–$CaCO_3$–NH_X. *P Est Acad Sci Chem* 67(3): 260–270; 10.3176/proc.2018.3.04.

Papers are reprinted with the permission of copyright owner and publisher.

Author's contribution:

Ref. I Author operated the reactors and wrote the manuscript.

Ref. II Author performed ca 50% of experimental work and wrote the manuscript.

Ref. III Author operated the reactors and wrote the manuscript.

Ref. IV Author performed the experimental work and participated in the writing of the manuscript.

Ref. V Author participated in the experimental work and writing of the manuscript.

Ref. VI Author participated in the experimental work and writing of the manuscript.

LIST OF ABBREVIATIONS AND ACRONYMS

16S rDNA	section of prokaryotic DNA that codes for a strand of ribosomal RNA, and which is used for measuring bacterial taxonomy, phylogeny and the rate of divergence;
AnamMBBR	anerobic moving bed biofilm reactor performing Anammox process used in pilot study of this thesis;
ANAMMOX	ANaerobic AMMonium OXidation process;
Anita™Mox	technology based on one-stage deammonification moving-bed biofilm reactor for partial nitrification to nitrite and autotrophic N-removal from N-rich effluents;
AOB	ammonia-oxidizing bacteria;
BABE®	Bio-Augmentation Batch Enhanced technology;
BLAST	Basic Local Alignment Search Tool software;
BOD	biological oxygen demand;
BOD_7	biological oxygen demand, incubation period 7 days;
C/N	carbon to nitrogen ratio;
CANDO	technology of Coupled Aerobic–anoxic Nitrous Decomposition Operation;
CANON	Completely Autotrophic Nitrogen-removal Over Nitrite DeamSBR technology;
COD	chemical oxygen demand;
DeamMBBR	intermittently aerated moving bed biofilm reactor performing deammonification process used in pilot study of this thesis;
DEAMOX	DEnitrifying AMmonium OXidation process;
DeamSBR	intermittently aerated sludge-based sequencing batch reactor performing deammonification process used in pilot study of this thesis;
DEMON®	sequencing batch reactor based deammonification technology;
DGGE	denaturing gradient gel electrophoresis;
DIB	deammonification in biofilm;
DNA	deoxyribonucleic acid;
DO	dissolved oxygen;
FA	free ammonia (unionized ammonia in aqueous solution, also designated as $(NH_3)_W$);
FNA	free nitrous acid (undissociated HNO_2 in aqueous solution);
GC-clamp	a stretch of GC-rich sequences used in DGGE. Also refers to a small number of G or C frequently used at the 3'-end of a PCR primer such that the 3'-end of a primer will form stable complex with the target DNA;
HM	humic matter;
HPLC	high performance liquid chromatography;
HRT	hydraulic retention time;
IC	inorganic carbon;

MBBR	moving bed biofilm reactor;
MEGA	Molecular Evolutionary Genetics Analysis software, https://www.megasoftware.net/;
NDAMO	nitrite-dependent anaerobic methane oxidation;
NitriSBR	aerobic sequencing batch nitritation reactor preceding AnamMBBR and used in pilot study of this thesis;
NOB	nitrite-oxidizing bacteria;
OLAND	technology of Oxygen-Limited Autotrophic Nitrification-Denitrification;
ORP	oxidation-reduction potential;
PANDA	technology of Partial Augmented Nitritation Denitritation with Alkalinity Recovery;
PCR	polymerase chain reaction;
qPCR	quantitative polymerase chain reaction;
rDNA	ribosomal deoxyribonucleic acid;
ROS	reactive oxygen species;
SBR	sequencing batch reactor;
SHARON®	technology of Single reactor system for High activity Ammonium Removal Over Nitrite;
SRAO	sulfate reducing ammonium oxidation;
SRT	sludge retention time;
TN	total nitrogen;
TNLR	total nitrogen loading rate;
TNRE	total nitrogen removal efficiency;
TNRR	total nitrogen removal rate;
TSS	total suspended solids;
UASB	upflow anaerobic sludge bed;
UASBR	upflow anaerobic sludge bed reactor;
WWTP	wastewater treatment plant

The capital letters in the explanatory text of designations of certain wastewater treatment technologies, genomic data analysis software, and certain biological processes indicate how an abbreviation is derived.

Most papers in the field of environmental technology use the acronym FA for free ammonia and FNA for free nitrous acid, respectively. The same acronyms often also denote the concentrations of free ammonia and free HNO_2.

1. INTRODUCTION

From the viewpoint of energy-efficient nitrogen removal, deammonification process has significant advantages over conventional denitrification – it does not require any external carbon source, enables to save up to 63% of aeration costs, produces up to 90% less excess sludge and requires smaller process tanks owing to the lower active volume. As a result, wastewater treatment costs are significantly lower. An additional advantage is diminished emission of greenhouse gases such as CO_2 and NO_X [1–3]. The anammox-related technology has the potential to achieve a neutral or even positive energy balance in complete wastewater treatment cycle [4–6] by combining anaerobic treatment of excess sludge with use of upflow anaerobic sludge bed reactors (UASBRs) in the following nitrogen removal stage [7]. The water from the dewatering of anaerobically treated excess sludge (reject water) contributes around 15÷40% of the total nitrogen (TN) load in a wastewater treatment plant (WWTP) [8]. Reject water from an efficiently operated anaerobic digester has the organic carbon to inorganic nitrogen (C/N) ratio of ≤1, which is too low for treating it in conventional nitrification–denitrification systems. These are strong arguments for treating this stream separately using anammox-based technology.

The metabolic versatility of anammox organisms, involving use of various substrates and electron acceptors has been demonstrated [9]. Among other alternative electron acceptors, SO_4^{2-} reduction by anammox bacteria has been experimentally observed [10–13].

In few earlier studies, start-up of sulphate-reducing ammonium oxidation (SRAO) process has been achieved using synthetic substrates [10–15]. If feasible for real wastewaters, it may provide opportunities to further reduce the need for aeration to produce nitrite for anammox bacteria. In this thesis, feasibility of SRAO was investigated using real reject water (**paper I**). The performance of process was compared to 'conventional' anammox process (**paper II**).

Laboratory-scale nitritation, deammonification and anammox processes were successfully started-up at Univerity of Tartu in various configurations (biofilm reactors, upflow anaerobic sludge bed and sequencing batch reactors) without specific inocula and using reject water from anaerobic digestion of municipal sludge [3, 16–23]. In this thesis, based on the experiences from laboratory studies cited, scaling up of bench-scale developments to a pilot scale under real technological conditions in a WWTP was performed (**paper III**). Three different configurations of processes under investigation were launched: a two-stage system consisting of separated nitritation reactor and anammox biofilm reactor, a biofilm-based deammonification reactor and a sludge-based deammonification sequencing batch reactor (SBR). Suitable boundary conditions for the start-up of autotrophic nitrogen removal were identified and autotrophic nitrogen removal was achieved in all three systems commenced. The pH of the liquid phase of the process turned out to be a key factor affecting the success of the start-up process. The control over dissolved oxygen (DO) and concentration of suspended solids also played an important role.

Reject water is a complex multi-component system. The concentrations of its components are determined by multiple pH-dependent equilibrial processes which are interconnected over protons. The main equilibrial processes are carbonaceous equilibrium $(CO_2)_W$–HCO_3^-–CO_3^{2-} and ammoniacal equilibrium $(NH_3)_W$–NH_4^+; other important equilibria include phosphate, sulphide and nitrous acid equilibrium[1]. A mathematical model for the description of chemical equilibrium processes in an open system $(CO_2)_G$–H_2O–$(CO_2)_W$–H_2CO_3–HCO_3^-–CO_3^{2-}–$(CaCO_3)_S$ and calculation of pH and concentrations of all species in the liquid phase (CO_3^{2-}, HCO_3^-, H_2CO_3, Ca^{2+}, H^+, and OH^-) at different concentrations of $(CO_2)_G \rightleftharpoons (CO_2)_W$ was presented in **paper IV**[2]. Analogously, a mathematical model for a closed equilibrium system H_2O–$(CO_2)_W$–H_2CO_3–HCO_3^-–CO_3^{2-}–$(CaCO_3)_S$ at different certain values of $[CO_2]_{W0}$ was developed in **paper V**[3]. The interconnection between carbonaceous and ammoniacal equilibrium was taken under observation in **paper VI** by modelling the closed system H_2O–$(CO_2)_W$–$(CaCO_3)_S$–NH_4Cl. All three models are also experimentally validated.

[1] Subscript 'W' denotes aqueous phase; thus $(CO_2)_W$ and $(NH_3)_W$ are free (unionised) CO_2 and NH_3, respectively, dissolved in aqueous phase.

[2] Subscript 'G' denotes gaseous phase; thus $(CO_2)_G$ is CO_2 present in the gaseous phase. $(CO_2)_G$ also denotes atmospheric CO_2. Subscript 'S' denotes solid phase, thus $(CaCO_3)_S$ is undissolved solid $CaCO_3$.

[3] Square brackets denote concentration of given species (molecules, ions, ion pair or total species). Moreover, subscripted '0' denotes initial concentration of the given species. Thus, $[CO_2]_{W0}$ denotes initial concentration of dissolved CO_2 in the aqueous phase.

2. LITERATURE REVIEW

2.1. Anammox process

Disappearance of some of the supposedly accumulated NH_4^+ in the anoxic marine environments was observed as early as 1965. Based on this fact, the hypothesis was proposed that a group of unknown microorganisms produced N_2 when oxidating NH_4^+ by using NO_3^- as an electron acceptor. In 1977, the possibility of oxidation of NH_4^+ by using both NO_2^- and NO_3^- as electron acceptors was confirmed *via* thermodynamic calculations and the existence of anaerobic ammonia-oxidising (anammox) bacteria in nature was predicted [24–26]. The anammox process was first discovered in a denitrifying fluidized bed reactor treating reject water (supernatant) from a methanogenic reactor, and was confirmed by nitrogen and redox balances in continuous-flow experiments [27]. The autotrophic anammox bacteria belonging to phylum *Planctomycetales* are able to convert NH_4^+ to N_2 with nitrite as electron acceptor under anaerobic conditions. Eq 1 represents the anammox catabolism. Combining the anammox catabolism and anabolism using the experimentally obtained yield of bicarbonate on ammonium (0.066 mol HCO_3^- / mol NH_4^+) results in the Eq 2 describing the overall anammox reaction [4–5]:

$$NH_4^+ + NO_2^- \rightarrow N_2 + 2\ H_2O \quad (1)$$

$$NH_4^+ + 1.32\ NO_2^- + 0.066\ HCO_3^- + 0.13\ H^+ \rightarrow 1.02\ N_2\uparrow + 0.26\ NO_3^- + \\ + 0.066\ CH_2O_{0.5}N_{0.15} + 2.03\ H_2O \quad (2)$$

Equations (1) and (2) have been applied as intrinsic stoichiometry of anammox process since 1999 in almost all of the studies worldwide. However, in a recent study the operation of high purity free suspended cell anammox bacteria, a different stoichiometric equation has been purposed [28]:

$$NH_4^+ + 1.146\ NO_2^- + 0.071\ HCO_3^- + 0.057\ H^+ \rightarrow 0.986\ N_2 + \\ + 0.161\ NO_3^- + 0.071\ CH_{1.74}O_{0.31}N_{0.20} + 2.002\ H_2O \quad (3)$$

Deammonification represents a short-cut in the bacterial conversion of NH_4^+ to N_2 and comprises two steps: about a half the amount of NH_4^+ is oxidised to NO_2^- and then residual NH_4^+ and NO_2^- are transformed to elementary nitrogen in an anoxic pathway. The first step involves aerobic oxidation of NH_X-N by ammonia-oxidizing bacteria (AOB), a process called nitritation. Eq 4 represents the catabolism of nitritation [29–30].

$$NH_4^+ + 1.5\ O_2 \rightarrow NO_2^- + H_2O + 2\ H^+ \quad (4)$$

The overall reaction of cell synthesis and oxidation of ammoniacal species in nitritation process is represented with the Eq 5 as follows:

$$NH_4^+ + 1.38\ O_2 + 1.98\ HCO_3^- \rightarrow 0.018\ C_5H_7O_2N + 0.98\ NO_2^- + \\ + 2.93\ H_2O + 1.89\ CO_2 \quad (5)$$

In the second step, the anammox reaction takes place, leading to formation of N_2 and a small amount of NO_3^-. Nitrate can also be formed in the oxidation of nitrite by nitrite-oxidising bacteria (NOB) [30]. The latter is considered undesirable in deammonification, since it reduces the efficiency of anammox process. To some extent, denitrification takes place in anammox and deammonification systems, depending on the availability of substrate. Due to low C/N ratio in reject water and high content of ammoniacal species (500÷1000 mg NH_X-$N \cdot L^{-1}$ in Tallinn WWTP (**paper III**) and up to 1300 mg NH_X-$N \cdot L^{-1}$ in Tartu WWTP [22]), an anammox-based technology would be suitable to treat the reject water from anaerobic sludge treatment separately in order to reduce the total nitrogen load in the WWTP-s.

Various reactor configurations have been used to start-up the anammox process in laboratory, pilot and industrial scale, including fluidized bed reactors [2, 31], sequencing batch biosludge-based [32–33] and biofilm reactors [34], up-flow anaerobic sludge blanket [35] and membrane bioreactors [36], among other reactor types [37–38]. Examples of industrial autotrophic nitrogen removal technologies requiring inoculation at start-up phase include SHARON® [39], CANON [40], OLAND [41], DEAMOX [42], BABE® and PANDA [43–45], DIB [46] and DEMON [47], Anita™Mox [48] and CANDO [49] technologies.

2.2. SRAO process

Initially, the anammox bacteria were considered to be highly specialized chemolithoautotrophs. However, the genomic sequencing of *Kuenia stuttgartiensis* revealed that anammox bacteria could actually be regarded metabolic generalists rather than specialists. In spite of distinct adaptations required for anammox metabolism, it appeared to be compatible with a versatile lifestyle, which interconnected the biological cycles of nitrogen, carbon and metals, such as iron and manganese [26]. Metabolic versatility was found also characteristic to other anammox organisms such like *Anammoxoglobus propionicus*, *Brocadia anammoxidans, Brocadia fulgida* and *Scalindua spp* [50].

The electron donors that are alternative to NH_4^+ include C_1–C_3 carboxylic acids, methanol, mono- and dimethyl amines, hydrogen and Fe^{2+}. The alternative electron acceptors, on the basis of genomic data, include Fe^{3+}, FeOOH and MnO_2. In addition, at least in case of *Kuenenia stuttgartiensis*, oxygen was proposed as a putative electron acceptor [26]. 'Disguised denitrification' has also been reported as an alternative pathway. In this process, NO_3^- is primarily converted into NO_2^- and part of it is reduced into NH_4^+. Hereafter, NH_4^+ and NO_2^- are combined to yield nitrogen by the 'conventional' anammox cycle [50].

Recently, applying a metaproteomic approach to study the microbial consortia in anoxic groundwater of a pristine limestone-fracture aquifer in Germany, Starke R et al found that the order candidate *Brocadiales*, in addition to anammox reaction, was featuring all major carbon fixation strategies, ammonification and denitrification as well as assimilatory sulfate reduction and dissimilatory sulfite reduction to sulphide [51].

The SRAO process was first assumed by Fdz.-Polanco F et al to explain 'abnormal' losses of NH_X-N and SO_4^{2-} observed in an anaerobic fluidized-bed reactor treating yeast wastewater. The authors demonstrated the feasibility of methanogenesis and SRAO in a single reactor and proposed a summary equation describing the two-staged process [52]:

$$SO_4^{2-} + 2\ NH_4^+ \rightarrow S + N_2 + 4\ H_2O \qquad \Delta G_0 = -46\ kJ \cdot mol^{-1} \qquad (6)$$

Proposed stages were:

$$NH_4^+ + SO_4^{2-} \rightarrow S + NO_2^- + 2\ H_2O \qquad \Delta G_0 = +314\ kJ \cdot mol^{-1} \qquad (7)$$

$$NH_4^+ + NO_2^- \rightarrow N_2 + 2\ H_2O \qquad \Delta G_0 = -360\ kJ \cdot mol^{-1} \qquad (8)$$

The other pathways of SRAO reported in the literature are given in Tab 1.

Table 1. Possible pathways for SRAO processes

N°	Reaction	References
	SRAO reaction with sulfide formation:[4]	[11, 53–54]
(9)	$4\ NH_4^+ + 3\ SO_4^{2-} \rightarrow 4\ NO_2^- + 3\ HS^- + 4\ H_2O + 5\ H^+$ Combined with anammox reaction:[5]	
(10)	$8\ NH_4^+ + 3\ SO_4^{2-} \rightarrow 4\ N_2 + 3\ HS^- + 12\ H_2O + 5\ H^+$	
	SRAO with NO_3^- formation taking place in parallel with conversion of NH_X-N into N_2:	[55]
(11)	$4\ SO_4^{2-} + 3\ NH_4^+ + 2\ HCO_3^- \rightarrow 4\ S + 3\ NO_3^- + 2\ H_2O + 2\ CO_2$	
	SRAO with formation of NO_3^- and HS^- (in marine environments, coupled with heterotrophic denitrification)	[56]
(12)	$NH_4^+ + SO_4^{2-} \rightarrow NO_3^- + HS^- + H_2O + H^+$	
(13)	$5\ "CH_2O" + 4\ NO_3^- + 4\ H^+ \rightarrow 5\ CO_2 + 2\ N_2 + 7\ H_2O$	
(14)	$4\ NH_4^+ + 4\ SO_4^{2-} + 5\ "CH_2O" \rightarrow 5\ CO_2 + 2\ N_2 + 11\ H_2O + 4\ HS^-$	

Various authors [13, 55, 57–60] have mentioned an over-consumption of NH_X-N in relation to available electron acceptors by anammox consortia under anoxic conditions. One of possible explanations of this phenomenon is the generation

[4] $\Delta G_0 = +338\ kJ \cdot mol^{-1}$

[5] $\Delta G_0 = -22\ kJ \cdot mol^{-1}$

of ROS (e.g. H_2O_2, hydroxyl-, peroxide or superoxide radicals) released by bacteria in stress or from decaying cells. The reactive oxygen species (ROS) can be produced biologically as a result of bacterial respiration under anoxic conditions involving organic carbon or any other electron acceptor. Dismutation of O_2^- anion by superoxide dismutases produces H_2O_2. As a detoxification mechanism, the catalase enzymes readily break H_2O_2 in an aerobic pathway to water and O_2, with the latter taken up by AOB and NOB [55, 57–60].

If the amount of O_2 (produced from ROS) is small and only NO_2^- is produced in nitritation, the reaction products are SO_4^{2-} and N_2 [61]:

$$3\ HS^- + 8\ NO_2^- + 5\ H^+ \rightarrow 3\ SO_4^{2-} + 4\ N_2 + \\ + 4\ H_2O,\ \Delta G^{0'} = -2944\ kJ \cdot mol^{-1} \quad (15)$$

If there is abundant O_2 to perform nitrification, S and N_2 are generated [62]:

$$S^{2-} + 0.4\ NO_3^- + 2.4\ H^+ \rightarrow S + 0.2\ N_2 + 1.2\ H_2O \quad (16)$$

A few recent studies have documented the link between anammox and sulfide-dependent denitrification [63–65]. Although several studies have documented the coupling of anammox with organotrophic denitrification [66–69] as well as with lithotrophic denitrification [31, 63–65], the collected evidence in the present study suggests complex interactions between nitrogenous and sulfurous compounds during the coupling between anammox and sulfide-dependent denitrification as mentioned also in [61] and shonw in Fig 1.

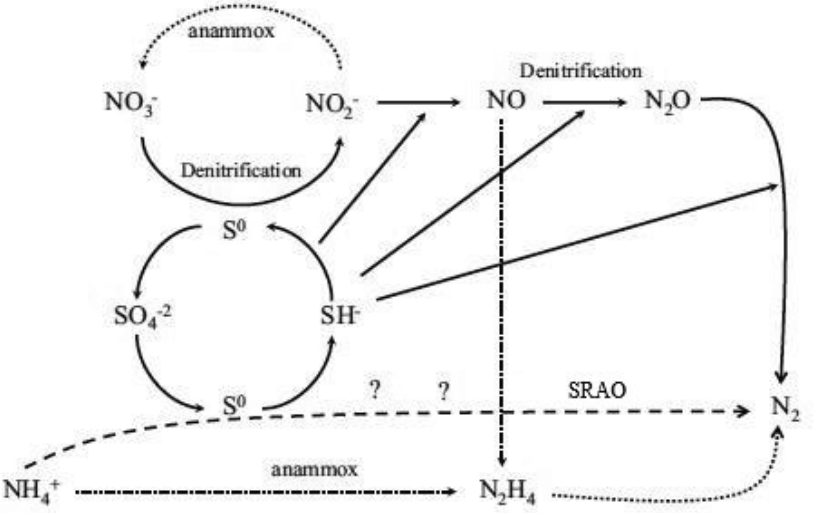

Figure 1. Interconnections between nitrogenous and sulfurous compounds in case of simultaneous occurrence of anaerobic ammonium oxidation (anammox), SRAO and sulfide-dependent denitrification. Question marks represent unknown putative intermediates of SRAO [61].

2.2.1. Microorganisms involved in SRAO and autotrophic denitrification

Liu S et al isolated a new *Planctomycete* bacterium, which performs oxidation of NH_4^+ into NO_2^- by using SO_4^{2-} as an electron acceptor in compliance with the Eq 7, and named it *Anammoxoglobus sulphate* [10]. Prachakittikul P et al reported an identification of several anammox strains found in SRAO cultures, possibly involved in SRAO processes. These included clones SRAO-10, (KM210532) most closely related to uncultured *Planctomycetales* clone T13J-B80 and clone SRAO-22 (KM210536), most closely related to uncultured *Planctomycetales* clone MP-R114 [13].

A non-*planctomycete*, *Bacillus benzoevorans* strain ASR, was reported to perform the overall two-staged SRAO reaction (Eq 6) in addition to other metabolic pathways involving utilization of various organic compounds [15]. Hence, the SRAO process may be a more common metabolic pathway in the nature and not restricted to only few genera of bacteria. Some denitrifying species of γ-proteobacteria – *Pseudomonas* sp. HPC262, *Pseudomonas stutzeri* strain SLG510A3-81 and *Pseudomonas stutzeri* strain SLG510A3 have been isolated from anaerobic environment containing sulfides, nitrogen compounds and recalcitrant organics [70].

2.3. Start-up of anammox process

One of the key limitations in the application of anammox process is its long start-up period due to a low cellular yield and slow growth rate of the anammox bacteria, which have a doubling time of approximately 7÷20 days [32, 50, 71]. Thus, enrichment and propagation of anammox biomass is a critical factor for a successful start-up process.

In sludge-based configurations, various seed sludge types have been used to initiate the propagation of the anammox biomass, including aerobic [33, 37], nitrifying [36, 71], denitrifying [72] and methanogenic sludge [73, 74], as well as sludge from a SBR system [35, 75]. In case of using a biofilm reactor, it is demonstrated that biofilms from from nitrification-denitrification or nitritation-denitritation systems could be converted into deammonifying one [16, 46]. For the shortening of start-up process, ready-to-use biofilms or suspended / granular biomass could be purchased from companies such as Purac AB, DEMON GmbH and Paques BV.

2.3.1. Start-up of deammonification – is inoculum required?

An alternative to using inoculum is in-situ cultivation of deammonifying biomass [8, 76], which relies on the ability of suspended wastewater microorganisms to attach onto surface of virgin carrier material that provides the suitable

structure for biomass adherance. No additional seeding biomass is used and the influent wastewater is the only source of anammox bacteria and AOB [8, 76]. Although time-consuming (4÷6 months or more) [17], cultivation of 'home-grown' biomass would enable a WWTP or biogas plant to be independent from biomass suppliers and ensure that the biomass is adapted to the composition of the wastewater and conditions of the particular facility. Kanders L et al concluded that systems' seeding with proper bacteria did not contribute to a shorter start-up time in comparison to *inoculum*-free commencement [76]. The latter start-up strategy has been mentioned in relatively few studies [8, 76]. A modification of this strategy is partial seeding with a small fraction of pre-colonized carriers in order to reduce the time required for the development of a mature deammonification biofilm on the brand new carriers. An example of this strategy includes the Anita™Mox [48]. On the other hand, Schneider Y et al found that seeding with fully functional deammonification biofilm was not an efficient start-up strategy for moving bed biofilm reactor (MBBR) deammonification systems [77].

As reported by Christensson M et al, the start-up times were shortened to 2÷4 months in two Swedish WWTP-s (Sjölunda and Sundet) using Anita™Mox process seeded with pre-colonized carriers comprising 3÷15% of total carrier mass. Concomitantly, a real-time aeration control strategy was applied. During start-up period, the total nitrogen loading rate (TNLR) was kept slightly above the capacity of the seeding media and steadily increased. A removal rate of 1.2 kg-NH_X-N·m^{-3}·d^{-1} with 90% NH_X-N removal efficiency was obtained (a) without any pre-treatment of the reject water, (b) without any addition of methanol or other carbon source, acid or base solution, (c) with no mechanical mixing (i.e. continuous aeration was sufficient for mixing carriers) and (d) without any heating [48]. Chen H et al achieved a shortening of start-up time from 96 to 40 days using a mixture of anammox and denitrifying sludge, compared to denitrifying sludge, which was used in bioreactors fed with a synthetic wastewater [78].

2.3.2. Operation parameters as key factors of start-up

Sensitivity of anammox bacteria towards elevated concentrations of DO, NO_2^-, free nitrous acid (FNA), and free ammonia (FA) during the start-up phase has been widely reported [76–80]. Concentration of FA is estimated in many studies of biological treatment of wastewater by using Eq 17 [79–81, 84–86]:

$$FA = \frac{[NH_4^+ - N] \times 10^{pH}}{\frac{K_{b,NH_3}}{K_W} + 10^{pH}} \quad (17)$$

where:

$$\frac{K_{b,NH_3}}{K_W} = e^{\frac{6344}{273+t}} \quad (18)$$

In the equations (17) and (18), K_{b,NH_3} is the basicity constant of NH_3, K_W is the ion-product constant of water, t is the temperature in ºC and $[NH_4^+\text{-N}]$ is the concentration of ammonium nitrogen, usually expressed as mg-N·L^{-1}.

The term $[NH_4^+\text{-N}]$ in Eq 17 actually represents summary concentration of two species, nitrogen found in ammonium ions and nitrogen found in molecules of dissolved free ammonia, which are at equilibrium; thus elsewhere in this thesis, more accurate denotion $[NH_X\text{-N}]$ is preferred.

FA concentrations inhibitory to anammox process are reported to be in a wide range: 1.7÷150 mg-N·L^{-1} [79–80, 87–89], depending on the maturity and composition of the biomass.

Concentration of FNA is estimated from Eq 19 in most studies of biological nitrogen removal [84, 90–93]:

$$FNA = \frac{[NO_2^- - N]}{K_{a,HNO_2} \times 10^{pH}} \quad (19)$$

where:

$$K_{a,HNO_2} = e^{-\frac{2300}{273+t}} \quad (20)$$

In the equations (17) and (18), K_{a,HNO_2} is the acidity constant of HNO_2, t is the temperature in ºC and $[NO_2^-\text{–N}]$ is the concentration of summary nitrous nitrogen (nitrogen found in nitrite ions and in undissociated HNO_2 molecules), usually expressed as mg-N·L^{-1}.

Using the equations (17) and (19) in case of complex wastewaters neglects the participation of FA and FNA in various chemical equilibrium processes. Except for the model presented by Hafner and Bisogni for the calculation of FA in anaerobic digesters [94], no alternative methods to estimate FA or FNA have been presented in literature surveyed by the author of this thesis.

In order to control FA and FNA and maintain suitable boundary conditions during start-up period for AOB-anammox consortia, most studies available in the literature report the use of diluted real high-ammonia wastewater or synthetic wastewater with NH_X-N concentrations below 200 mg-N·L^{-1}. The dilution factor is decreased the as the bacterial consortium develops [19, 45, 76, 95]. The main benefit of undiluted reject water would be the opportunity to take advantage of the mesophilic temperature of reject water. However, possible FA inhibition and potential for the excessive generation of nitrite owing to higher NH_X-N content in the influent during start-up period still remains a challenge [81]. For these reasons, only few studies [96–97] report the use of undiluted reject water from the inception of bioreactor operation.

2.3.3. Aeration control

A key factor for the successful start-up of single-stage deammonification process is the DO control. An excessive aeration may result in the accumulation of NO_2^- reaching an inhibitory level to anammox bacteria. Moreover, a persisting DO concentration exceeding 1.5 mg $O_2 \cdot L^{-1}$ promotes the growth of NOB and leads to an accumulation of NO_3^-, which, in turn, causes a drop in pH and results in an out-competing of anammox bacteria by the NOB. For the above-mentioned reasons, the aeration control in a range of 0÷1.5 mg $O_2 \cdot L^{-1}$ has been used in earlier laboratory-scale studies with intermittent aeration application [16, 19, 21, 23].

A real-time DO control strategy, based on maximized nitrite production while preventing its further oxidation to nitrate, is a key add-on feature to the Anita™Mox technology. A control loop continuously calculates the amount of $NO_3^-N_{produced}$ / NH_X-$N_{removed}$ based on signals from online sensors in the inlet and outlet of the reactor. The value of the $NO_3^-N_{produced}$ / NH_X-$N_{removed}$ ratio higher than 0.11 indicates oxygen excess and the DO set-point should be decreased. If the $NO_3^-N_{produced}$ / NH_X-$N_{removed}$ ratio is lower than 0.11, DO set-point should be increased to achieve further increase NH_X-N removal [48].

In the DEMON process, the aeration control is based on pH-stasis. The controller is established out of three main parameters – time, pH and DO – listed according to their order of hierarchy. The aeration system is activated only within a very tight pH-bandwidth of 0.01. The set-point of DO control is specified at a low range, close to 0.3 mg$\cdot L^{-1}$ in order to prevent rapid nitrite accumulation and to maintain a continuous repression of the second oxidation step of nitrite to nitrate [98].

2.4. Carbonaceous equilibrium and its effect on autotrophic nitrogen removal

The biological treatment of reject water is affected by the pH-dependent equilibrial processes that govern the concentrations of ammoniacal, carbonaceous and phosphatous species, nitrous acid forms and other ions and molecules, which are relevant for the microorganisms as substrates, nutrients, inhibitors or toxins. Within this thesis, the carbonaceous and ammoniacal equilibria have been taken under observation. The carbonaceous equilibrium has been analysed in detail on the basis of heterogenous systems involving solid $CaCO_3$, aqueous and gas phase. The carbonaceous equilibria are analysed, providing a wider, global context, not limited just to reject water treatment.

2.4.1. Importance of carbonaceous equilibria in the nature

The carbonaceous equilibrium constitutes the most important acid-base equilibrium in the global redox carbon cycle spanning Earth's various geospheres: hydrosphere, atmosphere, upper part of lithosphere and biosphere. The carbon cycle can be formally presented as a closed loop consisting of the two branches – oxidative and reductive. It has two main processes, one of which is photosynthesis, where the carbonaceous species are turned into the reduced state e.g. organic matter. Another process, mineralization of organics, provides the reverse transition [99]. In the biosphere the CO_2 participates in biological processes either as the end product of respiration or as a substrate for biosynthesis in autotrophic and photosynthetic organisms [100]. The carbonaceous equilibrium also bears an essential role in buffer system of the body fluids of Metazoan organisms [101].

The chemical species that make up the carbonate system in most natural waters comprise of gaseous and dissolved CO_2, carbonic acid (H_2CO_3), bicarbonate (HCO_3^-), carbonate (CO_3^{2-}) and carbonate-containing solids, e.g. $CaCO_3$. Carbonates and bicarbonates may form complexes and ion pairs with metal cations such as Ca^{2+} and Mg^{2+} [102]. $CaCO_3$ is the principal component of the limestone rocks and the skeletons of most marine invertebrates. There are two common $CaCO_3$ minerals, calcite and aragonite. Under equilibrium conditions at ambient temperature and pressure, calcite is more stable while aragonite is often the phase deposited biologically and the conversion to calcite occurs slowly [103]. There is no single universal factor that controls calcite and aragonite precipitation in natural water bodies [104]. Less stable forms include vaterite, amorphous calcium carbonate, etc [103–104]. The dissolution of carbonate-bearing minerals such as limestone is a major source of carbonaceous species in natural waters; other sources include direct entry of CO_2 from the atmosphere to water and metabolic activity of the organisms in the water and soil [102, 105]. Although calcium ions do not show any adverse effect on human health, they promote the carbonate scale formation, which impairs water supply by blockage of valves, pumps and pipelines, impart an alkali taste to the water, and can also cause other aesthetic problems [105]. Scaling also affects wastewater facilities. By its influence on the carbonaceous equilibrium, $CaCO_3$ affects both chemical and biological wastewater treatment processes [102].

The World Ocean's carbonate systems constitute the main sink for $(CO_2)_G$ from the atmosphere. Atmospheric CO_2 concentrations have oscillated between 200 and 280 ppm over the 400 000 years before the industrial period [106], but increased by approximately a third since the start of the Industrial Revolution in the late eighteenth century, to 409.5 ppm in April 2019 [107], and are currently rising by about 1.7 ppm per year. Around 20% of anthropogenic CO_2 emitted to the atmosphere is taken up by the terrestrial biosphere and 30% dissolves into the oceans [106], leading to an increase of ocean acidity by 0.1 pH units since pre-industrial times [108].

For equilibrium between dissolved and atmospheric CO_2 at a certain partial pressure $P(CO_2)_G$, the concentration of $(CO_2)_W$ is in equilibrium with $(CO_2)_G$. Carbonate systems can either be closed systems in which the dissolved carbonic species do not exchange matter with the gas phase (CO_2 in soil or atmosphere), or open systems, in which the liquid is open to gas phase, i.e. exchanges matter with the gas phase. The closed systems can be homogenous without the presence of solid $CaCO_3$, or heterogeneous where the solid $CaCO_3$ is present. The open systems can be either binary (without $CaCO_3$) or ternary ($CaCO_3$ is present). In an open equilibrium system, a constant $P(CO_2)_G$ fixes the concentration of dissolved CO_2 independently of the concentration of dissolved $CaCO_3$. In a closed system, the concentration of dissolved CO_2 will change as the summarized concentration of all dissolved carbonaceous species $\sum[CO_x]_W$ is altered [103].

2.4.2. Literature overview of modelling of the system H_2O–$(CO_2)_W$– $(CaCO_3)_S$

Dissolution and precipitation of calcium carbonate in the system H_2O–$(CO_2)_W$–$(CaCO_3)_S$ has been extensively researched because of the relevance of these equilibrial processes in many fields, which include, but are not limited of, geochemistry, oceanography, marine biology, CO_2 sequestration, isotope-based paleoclimatical studies, soil sciences, environmental sciences, water supply and industrial engineering [109–110]. The equilibrium state of a carbonate system is defined by equilibrium constants, charge balance (the electrical neutrality criterion) [103, 111] and molar balance (mass conservation criterion) [110]. Various equilibrial and kinetic models have been proposed for describing of equilibium system H_2O–$(CO_2)_W$–$(CaCO_3)_S$ [103,109–111]. A detailed systematic interpretation of all processes taking place in a system H_2O–$(CO_2)_W$ –$(CaCO_3)_S$ during its evolution to equilibrium state is, however, still lacking. For calculations of $[CO_2]_W$, $[H_2CO_3]$, $[HCO_3^-]$, $[CO_3^{2-}]$, $[Ca^{2+}]$, $[H^+]$, $[OH^-]$, in some models also the ion pairs such as $[CaCO_3^0]$, $[CaOH^+]$ and $[CaHCO_3^+]$ [103, 109, 112–113], are used[6]. An ion pair is a pair of oppositely charged ions temporarily held together by the electrostatic attraction force without formation of a covalent bond. Experimentally, an ion pair in the solution behaves as one unit in determining conductivity, kinetic behaviour, osmotic properties, etc. of that solution. A certain population of these pairs is supposed to exist at any given time, since the formation and dissociation of ion-pairs are continuous equilibrial processes [114].

[6] Square brackets denote concentration of the given species, i.e. $[CO_2]_W$ indicates the concentration of free CO_2 in the water phase, $[H_2CO_3]$ the concentration of carbonic acid etc. $CaCO_3^0$ is a neutral ion pair assumed to form in association of a Ca^{2+} ion with CO_3^{2-} ion. $CaOH^+$ and $CaHCO_3^+$ are positive ion pairs assumed to form when a Ca^{2+} ion associates with a OH^- or HCO_3^- ion, respectively.

Some authors assume that aqueous carbonaceous species react with water via processes of hydrolysis and Ca^{2+} ions interact with water and anions from solution to yield ion pairs. This assumption should be critically analysed. The following processes have been proposed for characterization of the equilibrium system H_2O–$(CO_2)_W$–$(CaCO_3)_S$ [112–113]:

$$(CaCO_3)_S \rightleftharpoons Ca^{2+} + CO_3^{2-} \tag{21}$$

$$(CaCO_3)_S \rightleftharpoons CaCO_3^{0} \tag{22}$$

$$CaCO_3^{0} \rightleftharpoons Ca^{2+} + CO_3^{2-} \tag{23}$$

$$CO_3^{2-} + H_2O \rightleftharpoons HCO_3^{-} + OH^{-} \tag{24}$$

$$HCO_3^{-} + H_2O \rightleftharpoons H_2CO_3 + OH^{-} \tag{25}$$

$$H_2CO_3 \rightleftharpoons H_2O + (CO_2)_W \tag{26}$$

$$Ca^{2+} + H_2O \rightleftharpoons Ca(OH)^{+} + H^{+} \tag{27}$$

$$Ca^{2+} + HCO_3^{-} \rightleftharpoons CaHCO_3^{+} \tag{28}$$

$$Ca^{2+} + OH^{-} \rightleftharpoons Ca(OH)^{+} \tag{29}$$

Reactions (21)–(23) describe dissolution of $(CaCO_3)_S$ (solid $CaCO_3$), (24)–(26) are subsequent hydrolysis reactions and (27)–(29) describe formation of ion pairs.

Arakaki T and Mucci A adapted a surface complexation model to describe the assumed chemical structure and reactivity of calcite-water interface. They proposed that surface speciation on the solid-liquid phase boundary during equilibrial dissolution of calcite crystals is governed by the following cycle of surface reactions [109]:

$$>CO_3^{-} + 2H^{+} + Ca^{2+} \rightleftharpoons >Ca^{+} + H_2CO_3 \tag{30}$$

$$>Ca^{+} + H_2CO_3 \rightleftharpoons >CO_3H^{0} + CaHCO_3^{+} \tag{31}$$

$$>CO_3H^{0} + CaHCO_3^{+} \rightleftharpoons >Ca^{+} + H_2CO_3 + CaCO_3^{0} \tag{32}$$

These reactions involve adsorption of dissolved ions onto liquid-solid boundary layer of $CaCO_3$ crystals. The symbol '>' denotes species associated with the surface of $CaCO_3$ crystals (adsorbed ions). Thus $>CO_3^{-}$ and $>Ca^{+}$ indicate surface-bound paired ions with resultant electric charges –1 and +1, respectively, while $>CO_3H^{0}$ is an electrically neutral paired ion. In addition, reversible ion pairing between Ca^{2+} and CO_3^{2-} was included in the proposed model [109].

Complex surface reactions on calcite-solute boundaries have also been proposed in studies on zeta potential of calcite particles [112, 115].

A proton-centric model presented in this thesis that shows a good coincidence between experimental research and theoretical calculations does not support above-mentioned interpretations applying ion pairs.

2.4.3. Effect of carbonaceous equilibrium on autotrophic nitrogen removal

Due to limestone bedrocks, in many places in Estonia, potable water has an elevated content of dissolved Ca^{2+} (up to 1.8 mmol·L^{-1} in Tallinn, as of 2016) and carbonaceous species (up to 3.1 mmol·L^{-1} HCO_3^- in Tallinn) [116]. The content of Ca^{2+} around 2 mmol·L^{-1}, total hardness 3.2 mmol·L^{-1} and bicarbonaceous alkalinity 8.6 mmol·L^{-1} were mean values in municipal wastewater (Tallinn WWTP, January 2014, unpublished data). During the sludge digestion process nearly equal amounts of ammonium and carbonaceous species (in mmol·L^{-1}) are released into the supernatant [117]. Due to additional presence of phosphate species and significant concentrations of Ca^{2+} and Mg^{2+}, many equilibrial processes occur in the reject water.

Use of Eq 17 for estimation of FA is based on the assumption that NH_4^+ is the only species in equilibrium with $(NH_3)_W$. However, this approach is not sufficient for modelling processes in supernatant from an anaerobic digester, where a variety of factors, including interactions between ammoniacal and carbonaceous equilibria and sedimentation of struvite or $CaCO_3$ have to be taken into account [94]. The authors presented a model of speciation for ammonia in the liquid phase of anaerobic digesters, based on Pitzer's ion-interaction approach. The Pitzer model extends the Debye-Hückel equation, using a virial expansion for the excess Gibbs energy to account for the ionic strength dependence of the short range forces in binary and ternary ion interactions [118]. There are no non-thermodynamic, equilibrial models taking into consideration all conjugated acid-base processes in the system containing both carbonaceous and ammoniacal species in literature surveyed by the author of this thesis.

2.5. Aims of study

Based on the literature survey, the following specific objectives were set:

1) To find out the conditions for start-up of SRAO, evaluate the feasibility of SRAO and compare the efficiency and stability of the SRAO process against conventional anammox in laboratory scale (**papers I** and **II**);
2) To find out the influence of different reactor configurations on start-up of conventional autotrophic nitrogen removal at laboratory and pilot-scale. In case of pilot study, the operational conditions were dictated by a real technological process in the WWTP and no anammox-specific inoculum was used (**paper III**);

3) To identify the main setting conditions influencing the effective start-up of anammox process (as stated under Aim 2) and develop a stategy for process control (**paper III**);
4) To develop non-thermodynamic mathematical models for the equilibrial processes affecting the biological nitrogen removal, such as carbonaceous and ammoniacal equilibria. These models must take into consideration all conjugated acid-base processes in the system (**papers IV**, **V**, and **VI**).

3. MATERIALS AND METHODS

3.1. Laboratory-scale experiments with sulfate as alternative electron acceptor

3.1.1. Configurations of reactors

Three laboratory-scale reactors were operated in parallel (Fig 2): a SRAO MBBR with an effective volume of 3.3 L, a SRAO UASBR (0.75 L) and a conventional anammox UASBR (1.5 L).

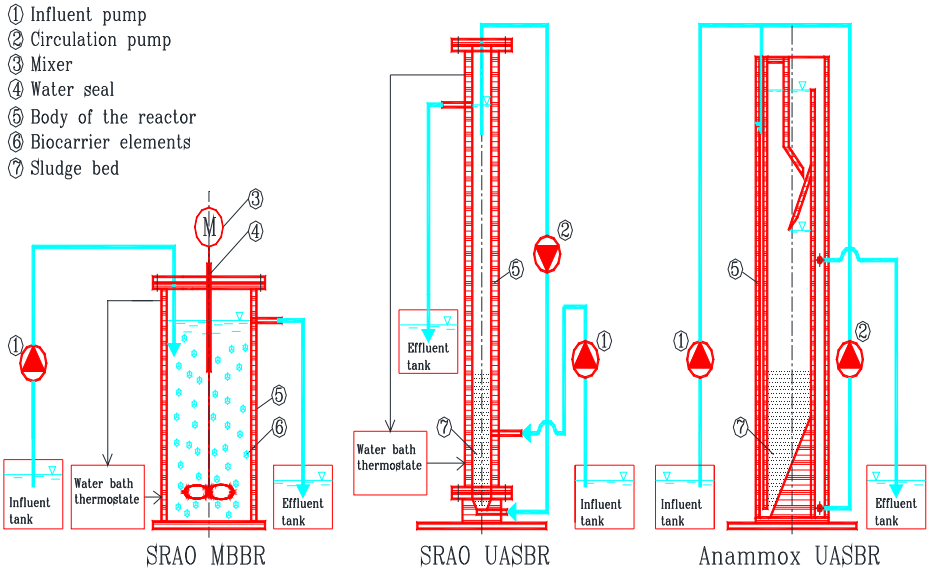

Figure 2. Schemes of the laboratory reactors

A detailed description of initiation and operation of each reactor as well batch assays is given in **papers I** and **II**.

3.1.2. Influent

The influent was based on reject water from dewatering of anaerobically digested municipal wastewater sludge. The reject water contained sufficient amounts of micro- and macronutrients needed for propagation of the anammox process [16] and served as a source of both ammoniacal nitrogen NH_X-N and anammox bacteria. Dilution of reject water was prepared by mixing reject water with tap water. As a SO_4^{2-} source, K_2SO_4 was added to the influent of SRAO reactors, while $NaNO_2$ was added to the influent of Anammox UASBR as a

source of NO_2^-. The influent had the following ratios of essential parameters: chemical oxygen demand to total nitrogen ratio COD:TN = 0.78:1 (range 0.39÷1.10) and chemical oxygen demand to biological oxygen demand ratio $COD:BOD_7$ = 1.95:1 (range 1.82÷2.03).

3.1.3. Analytical methods

Samples of the influents and effluents from both the MBBR and the UASBR were collected at least once a week for prompt chemical analyses and physico-chemical measurements.

The analyses of concentrations of NH_X-N, nitrous nitrogen NO_2^--N, nitrate nitrogen NO_3^--N, HCO_3^-, sulphate sulphur SO_4^{2-}-S, HS^- / S^{2-}, and COD were performed using the standard methods according to [119]. Hydrazine was determined spectrophotometrically using a Hach Lange DR2800 type spectrophotometer. Prior to the application of the Hach Lange HydraVer 2 reagent (containing *p*-dimethylaminobenzaldehyde), 0.5% solution of sulfamic acid was added to the sample as described by George M et al [120], in order to eliminate interference from NO_x^- (NO_2^- + NO_3^-). A spectro-photometric method was applied for measurement of hydroxylamine as well, at the wavelenght of 705 nm as reported by Frear DS and Burrell RC [121]. Humic and fulvic substances were analyzed by high-performance liquid chromatography (HPLC) according to the method described by Ibrahim MBM et al [122].

The DO concentration was measured by portable oxygen meter (Marvet Junior MJ2000, Estonia) and pH by a portable pH meter (Evikon, Estonia, or SensIon, Hach Lange). The oxidation-reduction potential (ORP) was measured by a Eutech redox electrode connected with a Jenway pH meter in the mV mode. The chemical analyses were performed either by the autor of the thesis or by laboratory assistant Anne Paaver.

Data and statistical analyses were performed by the MS Excel 2010 Analysis ToolPak. Homogeneity of group variances and the difference between group means were checked using the F-test and the two-way t-test, respectively. The level of significance was set at $\alpha < 0.05$. The data analysis was performed by the author of the thesis in cooperation with Ivar Zekker and other co-autors of **papers I** and **II**.

3.1.4. DNA extraction, nested PCR and DGGE

The deoxyribonucleic acid (DNA) of biomass was extracted with the MoBio PowerSoil DNA extraction kit (MoBio Laboratories Inc.) according to the manufacturer's instructions. Fingerprinting of *Planctomycetes* and *Nitrospira* communities was conducted via polymerase chain reaction (PCR) and denaturing gradient gel electrophoresis (DGGE). The first PCR round for amplification of *Planctomycetes* was performed with a wide-range primer set, Eub27f / Eub1492r

as reported by Lane DJ [123], and the second PCR round was performed with a *Planctomycetes*-specific primer Pla46f with a GC-clamp (GC CGC CGC GCG GCG GGC GGG GCG GGG GC) as reported by Neef A at al [124]. The second round was coupled with an anammox-specific primer Amx368r as reported by Sànchez-Melsió A et al [125].

Nested PCR was carried out according to thermocycling parameters as described by Sànchez-Melsió A et al [125]. PCR was also performed to identify *Nitrospira* strains with the primer set NSR1113f / NSR1264r, which are specific for *Nitrospira* 16S rDNA, using a PCR program described by Dionisi HM et al [126]. DGGE for detecting diversity of most abundant microorganisms was conducted using the eubacterial primer set GC-BacV3f / 907r as described in previous studies [127–129].

3.1.5. Sequencing and phylogenetic analysis

PCR for sequencing was performed with the BigDye® Terminator v3.1 Cycle Sequencing Kit (Life Technologies Corporation, USA). The sequences acquired were compared to the available database sequences via a Basic Local Alignment Search Tool software (BLAST) search and the related sequences were obtained from the GenBank. In order to determine the phylogenetic position of the anammox 16S rRNA gene sequence acquired, it was compared with available database sequences via a BLAST search, obtaining the related sequences from the GenBank. Further analysis was carried out with Molecular Evolutionary Genetics Analysis (MEGA) software version 5.0 applying the neighbor-joining method. The analytical procedures and data analysis were performed in Tallinn University of Technology, Chair of Biotechnology, by Anne Menert and Liis Loorits.

3.2. Operation of pilot plant

3.2.1. Pilot plant

The automated pilot plant consisted of three independent parallel operational units that were initiated simultaneously. The automatic control system used a Unitronics Vision V1040 controller. The main process tanks (AnamMBBR, DeamMBBR and DeamSBR) had a total volume of 3 m^3 each. The AnamMBBR was equipped with an auxiliary nitritation reactor (NitriSBR) with a total volume of 0.3 m^3 – the first stage in the NitriSBR-AnamMBBR system. The NitriSBR was a sludge-based sequencing batch reactor, serving as a pre-nitritation tank in a pair consisting of the NitriSBR and the AnamMBBR. The latter was a biofilm-based anoxic anammox reactor – the second stage of the two-stage system. The DeamSBR was a sludge-based deammonification SBR. The DeamMBBR was a single-stage biofilm-based intermittently aerated

deammonifying moving bed biofilm reactor. A detailed description of the pilot plant is given in **paper III**.

At initiation, 50% of active volume in both biofilm reactors AnamMBBR and DeamMBBR was loaded with blank biofilm carriers (BioElementsLight type RK, specific surface 750 $m^2 \cdot m^{-3}$, density 930 $kg \cdot m^{-3}$ – see **paper III**). No *inoculum* was used and reject water from dewatering of anaerobically digested municipal wastewater sludge was the sole source of anammox bacteria. During oxic periods, the maximum DO setpoints were 5 mg-$O_2 \cdot L^{-1}$ in the NitriSBR and 0.8 mg-$O_2 \cdot L^{-1}$ in both DeamSBR and DeamMBBR. Operation of the pilot plant was performed by the author of this thesis in cooperation with other co-autors of **paper III**.

The scheme of pilot plant is shown in Fig 3 and a photo of pilot plant in Fig 4.

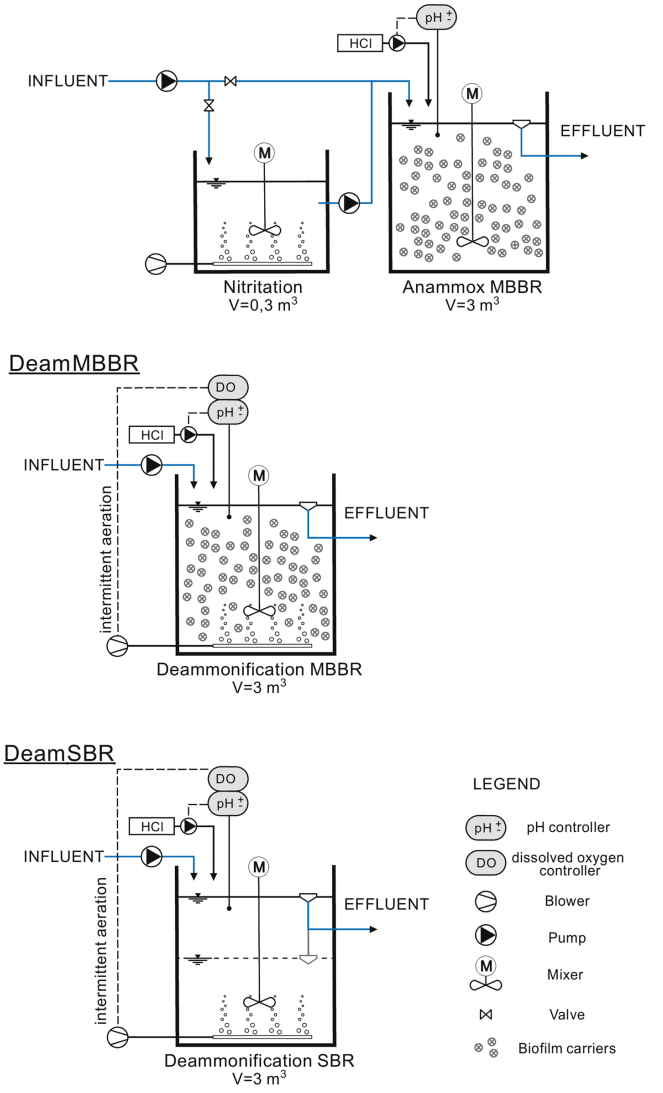

Figure 3. Scheme of pilot plant

Figure 4. Photo of pilot plant

3.2.2. Influent

The influent of the pilot plants consisted of undiluted reject water from WWTP's anaerobic digester deposited by centrifugation (Tab 2).

Table 2. Characteristics of the influent of the pilot plant

Characteristic, unit	Mean ± SD
TN, mg-N·L^{-1}	718 ± 117
NH_X-N, mg-N·L^{-1}	717 ± 117
NO_2^--N, mg-N·L^{-1}	0.20 ± 0.35
NO_3^--N, mg-N·L^{-1}	0.38 ± 0.57
COD, mg-O_2·L^{-1}	312 ± 125
BOD_7, mg-O_2·L^{-1}	100 ± 60
P, mg-P·L^{-1}	10 ± 3
Alkalinity, mmol·L^{-1}	60 ± 8
NH_X-N / alkalinity molar ratio	0.87 ± 0.05
Hardness, mmol·L^{-1}	3.65 ± 0.85
Total suspended solid, mg·L^{-1}	500 ± 214

3.2.3. Analytical methods

[NH_X-N], [NO_2^--N], [NO_3^--N], and (COD) were determined using standard methods [119]. The inorganic carbon (IC) was analyzed using an Analytic Jena MULTI NC (Germany) instrument. Alkalinity was determined titrimetrically, using potentiometric titration with 0.1 M HCl. The pH was measured potentiometrically.

Most chemical analyses were performed by laboratory assistent Anne Paaver in Laboratory of Environmental Chemistry, University of Tartu. Data analysis was performed by the author of this thesis, in cooperation with other co-authors of **paper III**.

3.2.4. Calculations of FA and FNA

FA and FNA were estimated using equations (17) and (19), respectively [81].

3.2.5. Estimation of anammox abundance by qPCR

Samples of biomass were harvested trice on days 318, 528 and 681. qPCR was conducted in Tallinn University of Technology, Chair of Biotechnology, using two primer sets Amx694F (GGGGAGAGTGGAACTTCTG) and Amx960R (GCTCCACCGCTTGTGCGAGC), which amplify approximately 285 base pair fragments from most anammox bacteria's 16S rDNA gene [130]. The detailed description of procedure of estimation of anammox abundance is given in **paper III**.

3.3. Experimental validation of theoretical models

The description of experimental validation of developed matemathical models for open heterogenous system H_2O–$(CO_2)_G$–$(CO_2)_w$–H_2CO_3–HCO_3^-–CO_3^{2-}–$(CaCO_3)_S$, closed heterogenous system H_2O–$(CO_2)_w$–H_2CO_3–HCO_3^-–CO_3^{2-}–$(CaCO_3)_S$ and closed heterogenous system H_2O–$(CO_2)_W$–$(CaCO_3)_S$–$(NH_X)_W$ is given in **papers IV, V** and **VI**, respectively.

The experimental validation of the model presented in **paper IV** was performed by the autors of the thesis. The validation of models presented in **papers V** and **VI** was performed by author of this thesis and by doctoral student Kalev Uiga.

4. RESULTS AND DISCUSSION

4.1. SRAO experiments

4.1.1. Summary of reactors' operation

The SRAO MBBR was seeded with carriers from a laboratory MBBR performing a conventional anammox process. NO_2^- as the electron acceptor was replaced with SO_4^{2-}, which resulted in a decrease in the total nitrogen (TN) removal efficiency. During the 350-day operational period, the total nitrogen removal rate (TNRR) fluctuated in a range of 0÷0.12 kg-N·m^{-3}·d^{-1} (avg. 0.03 kg-N·m^{-3}·d^{-1}) and total nitrogen removal efficiency (TNRE) in a range of 0÷72% (avg. 24%, Fig 5). The conversion rate of SO_4^{2-} also showed large fluctuations (avg. 0.01 kg-S·m^{-3}·d^{-1}, Fig 6). The average ORP in the effluent was +130 mV and the average estimated FA was 6 mg·L^{-1}. The MBBR process resulted in a decrease in pH by about 0.4 units to an average value of 8 in the effluent. In spite of differences in the operating temperatures (36 ºC in the SRAO MBBR and 20 ºC in the SRAO UASBR) and in the reactors' configuration, the performance of these reactors was similar in terms of both, TN removal and sulphate reduction.

In the UASBR, the TNRE fluctuated in a range of 1÷75% (avg. 23%) and TNRR in a range of 0÷0.09 kg-N·m^{-3}·d^{-1} (avg. 0.03 kg-N·m^{-3}·d^{-1}) (Fig 5). The average conversion rate of SO_4^{2-} was nearly equal to one of the MBBR (Fig 6), as were the estimated FA values and pH. The average ORP in the effluent of UASBR was +149 mV.

In the Anammox UASBR which was seeded with sludge from the same source as the SRAO UASBR, the nitrogen removal rapidly increased in first 40 days. Then, after a period of instability, the Anammox UASBR achieved a nitrogen removal over 90% in days around 130÷160, followed a new period of instability, related to an increase in NO_3^- in the liquid phase of the reactor. After day 250, the reactor achieved a stable nitrogen removal around 70%. The average TNRR over the entire operation period was 0.25 kg-N·m^{-3}·d^{-1} and the average TNRE was 69% (Fig 5).

FA inhibition in the SRAO reactors was unlikely, as the inocula were adapted to FA concentrations present in the reactors or even higher values. The same can be assumed for sulfide, as its concentrations in the effluents of both reactors were below 100 µg·L^{-1}. At pH around 8, the less harmful form HS^- predominated over more toxic free H_2S. Negative ORP values were reported to be propitious for the SRAO reaction [11], thus, positive values of ORP, observed in this study, might be a factor contributing to the modest efficiency of the SRAO process. For comparison, other researches of the SRAO process, using synthetic wastewaters have achieved 40÷45% NH_4^+ removal efficiencies [12, 14, 15] while Fdz.-Polanco F et al [52] have reported 30÷55% total Kjeldahl nitrogen removal studying treatment of vinasse-based wastewater.

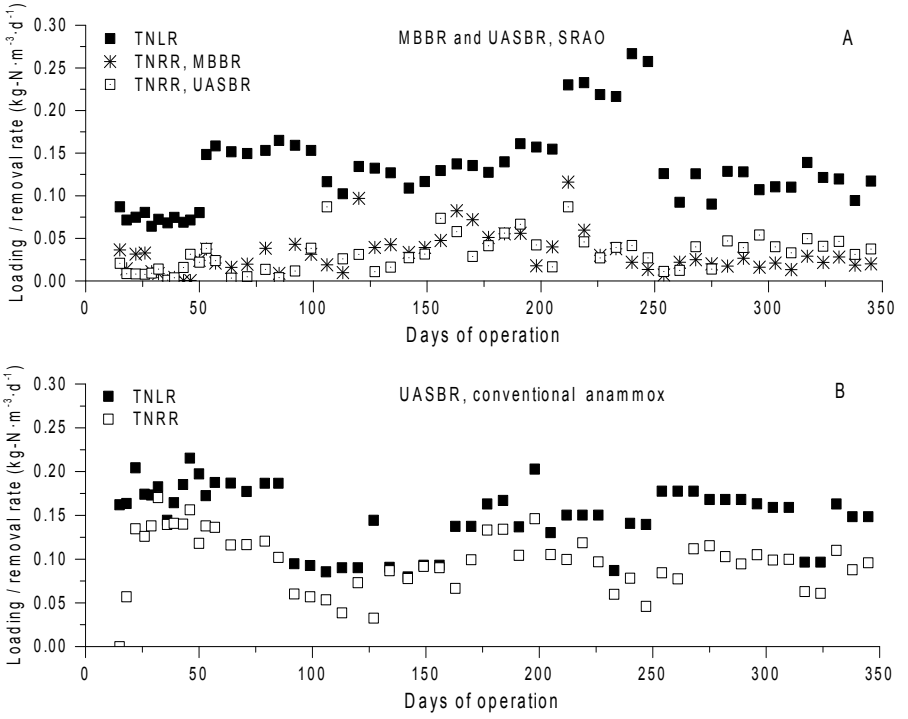

Figure 5. TNLR and TNRR in the laboratory reactors: A – SRAO reactors; B – conventional anammox reactor

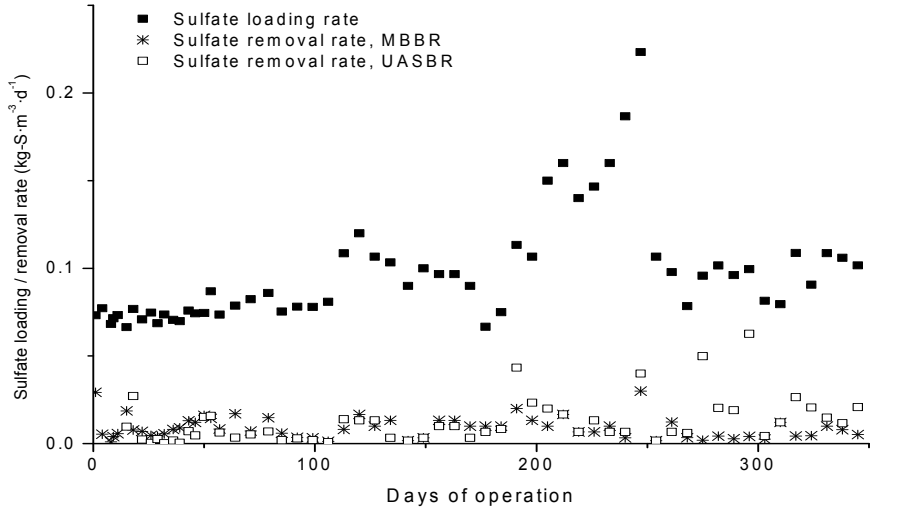

Figure 6. Sulfate loading and removal rates in SRAO reactors

After day 239, anammox intermediates (hydrazine and hydroxylamine, forms of $N_2H_5SO_4$ and $NH_2OH{\times}HCl$, respectively) were injected into all reactors. More stable process was observed in all reactors, but the effect was the most pronounced in the SRAO UASBR. Interestingly, also sulfate conversion increased in the SRAO UASBR, indicating that intermediates might stimulate the SRAO process in this reactor.

The operation of laboratory SRAO reactors as well as the Anammox reactor is described in more detail in **papers I** and **II**.

4.1.2. Stoichiometry of SRAO and conventional Anammox

The molar ratio of NH_4^+ oxydised in SRAO process was consistently more than twice higher than the amount of SO_4^{2-} reduced. This ratio was different from most other studies of SRAO [10, 12, 15, 52], which reported stoichiometric ratios close to 2:1. Only few studies [57–59] report higher NH_4^+ removal ratios, similar to the results in this thesis.

The possible effect of Fe^{3+} and Mn^{4+} in anoxic biological oxidation of NH_4^+ can be neglected on the ground of their low concentration in the reject water (<1 $mg{\cdot}L^{-1}$). The DO content in the influent was ≤0.2 $mg{\cdot}L^{-1}$ and O_2 leakage was minimized by use of a water-seal for the stirrer rod and keeping the discharge gates of the effluent tubes beneath water level in the vessels receiving effluent.

The possible explanations for over-consumption of NH_X-N could be:

1) The activity of AOB and NOB that generate NO_X^-, which, in turn, is denitrified in both autotrophic and heterotrophic pathways. The AOB and NOB live on either limited O_2 leakage, or microbially produced ROS, or both. Autotrophic denitrification uses sulphur and reduced sulfurous compounds. Another hypothetical way for generation of oxygen in anoxic medium is intra-aerobic pathway of nitrite-dependent anaerobic methane oxidising (NDAMO) bacteria, which have been also found in sludge of wastewater treatment plants [131]. There is, however, no solid evidence of presence of NDAMO in this study. Sulfur-utilizing autotrophic denitrification results in a partial recovery of SO_4^{2-}. Aerobic NH_X-N oxidation combined with autotrophic denitrification thus increases the $\Delta NH_4^+/\Delta SO_4^{2-}$ ratio in both ways, by the oxidation of an additional amount of NH_X–N and re-oxidation of reduced sulfurous spices. These reactions proceed according to equations (33)–(36), published by Li W et al [132]:

$$S + {}^6/_5\, NO_3^- + {}^2/_5\, H_2O \rightarrow SO_4^{2-} + {}^3/_5\, N_2 + {}^4/_5\, H^+ \qquad (33)$$
$$\Delta G_0 = -548\ kJ{\cdot}mol^{-1}$$

$$HS^- + {}^8/_5\, NO_3^- + {}^7/_5\, H^+ \rightarrow SO_4^{2-} + {}^4/_5\, N_2 + {}^4/_5\, H_2O \qquad (34)$$
$$\Delta G_0 = -739\ kJ{\cdot}mol^{-1}$$

$$S + 2\, NO_2^- \rightarrow SO_4^{2-} + N_2 \qquad (35)$$
$$\Delta G_0 = -676\ kJ{\cdot}mol^{-1}$$

$$HS^- + {}^8/_3\ NO_2^- + {}^7/_3\ H^+ \rightarrow SO_4^{2-} + {}^4/_3\ N_2 + {}^4/_3\ H_2O \qquad (36)$$
$$\Delta G_0 = -981\ kJ \cdot mol^{-1}$$

The presence of denitrifying sulfur-oxidizing *Sulfurimonas denitrificans* DSM1251 [133] in the *inoculum* as well as in the UASBR sludge, and very low (<100 μg·L kJ·mol^{-1}) sulphide concentrations provide a clear evidence in favour of this denitrification mechanism. In another work, a stable co-culture of anammox bacteria and *Sedimenticola sp.,* consuming sulfide, nitrate, NH_X-N, and inorganic carbon (IC) was reported, with *Sedimenticola sp.* acting in the same role as *Sulfurimonas denitrificans* DSM 1251 in this study [64].

2) Adsorption, desorption and ion exchange by the extracellular polymers of biomass. These processes have been shown to occur in case of activated sludge, aerobic granular sludge and anammox granules, but can potentially take place in case of other types of biomass [134, 135];
3) The humic matter (HM) present even at small concentration, either in oxidized or reduced forms, acts as redox mediator boosting both biological and abiotic oxidation of S^{2-} into elementary sulphur and reduction of NO_2^- and NO_3^- into N_2 thus amplifying the effect of O_2 leakage [62]. About ⅔ of organics present in reject water expressed as total organic carbon (TOC) was constituted of HM. The effect of HM on both SRAO and conventional anammox was shown in batch tests. HM and it's low-molecular quinoid analogues can serve as terminal electron acceptors during the anaerobic oxidation of wide range of organic compounds, including organic acids, phenols and toluene [136–139] and inorganic species such as HS^- [140], $S_2O_3^{2-}$ and Fe^{2+} [141]). The oxidation products are S_0 or polysulfides, SO_4^{2-}, and Fe^{3+}, respectively. On the other hand, reduced HM serve as electron donors for the anaerobic reduction. NO_2^-, NO_3^-, N_2O are reduced into N_2 and ClO_4^- into Cl^- [136, 142, 143]. Whether HM mediates the anammox process or can HM itself be an alternative electron acceptor for anammox bacteria, is needed to be studied further.

Higher substrate concentrations and low ORP were shown to be favourable for the SRAO process. Yuan Y et al [55] reported a new pathway for the SRAO process where N_2 was formed as a product. The authors concluded that the NH_X-N to SO_4^{2-}-S ratio had little effect on the overall conversion efficiency of NH_X-N, while lower NH_X-N to SO_4^{2-}-S ratio lead to higher SO_4^{2-}-S conversion rate. At higher NH_X-N to SO_4^{2-}-S ratio a higher fraction of NH_X-N was converted into N_2 and less NO_3^- formed, while lower NH_X-N to SO_4^{2-}-S ratio promoted NO_3^- accumulation (the latter result was not mentioned in earlier studies). A simultaneous oxidation of NH_X-N to N_2 and NO_3^- also explains a drop in pH observed by Yuan Y et al [55]:

$$4\ SO_4^{2-} + 3\ NH_4^+ + 2\ HCO_3^- \rightarrow 4\ S + 3\ NO_3^- + 2H_2O + 2CO_2 \qquad (37)$$

4.1.3. Microorganisms involved in SRAO

The phylogenetic neighbour-joining trees of some key organisms detected in the inoculum of SRAO reactors, reflecting the relationships between identified sequences, are shown in Fig 7 and Fig 8. Numbers at the nodes are percentages of bootstrap values. Branch lengths correspond to sequence differences as indicated by the scale bar.

In the seeding biocarriers for the MBBR, *Candidatus Nitrospira defluvii* **(**Gen Bank: EU559167) and the following uncultured microorganisms were detected (presented in **paper I**, see Fig 7): *Planctomycetales bacterium clone P4* (GenBank: DQ304521.2), *Nitrospira sp. clone 53* (Gene Bank: HQ424565), *Nitrospira sp. clone S1-62* (GenBank ID: HQ674926.1)*, Bacteroidetes bacterium clone VC5 (genus Ferruginibacter,* Gen Bank: AY211071*)*, *Chloroflexi bacterium clone QEDQ2AB09* (GenBank CU923588.1), and *bacterium clone: 13C-M6* (family *Saprospiraceae,* GenBank AB205722). In addition, uncultured *anaerobic ammonium-oxidizing bacterium clone W1* (Genbank: HQ906639.1) was found (not shown in Figure 7).

In the seeding sludge of UASBR, the following uncultured microorganisms were found (**papers I** and **II**, Fig 8): *Verrucomicrobiales* bacterium clone *ATB-KS-1929* (GenBank: EF686989) and clone *De2102* (GenBank: HQ183974) unclassified *Planctomycetaceae* bacterium JJB347 [21] (GenBank: GQ143799) and compost bacterium isolate *10b* (GenBank: AY489036), unclassified *Porphyromonadaceae* bacterium clone *Dok23* (GenBank: FJ710742), and unclassified *Cryomorphaceae* bacterium clone *LCFA-B01* (GenBank: AB244308). Also found in the sludge of wastewater treatment facility of Salutaguse yeast factory, but not shown in Fig 8 was *Carnobacterium maltaromaticum* (strain IUET-ME1, GenBank: MF503245.1). Differently from other similar biological wastewater treatment schemes applied for treatment of wastewater from yeast industry, residual sludge from the anoxic stage was returned to the beginning of the process scheme (mixing tank). Thus retaining of anammox microorganisms in the system was facilitated with recirculation of sludge. The returned anoxic sludge retained also methanogenic activity as reported by Zub S et al [144].

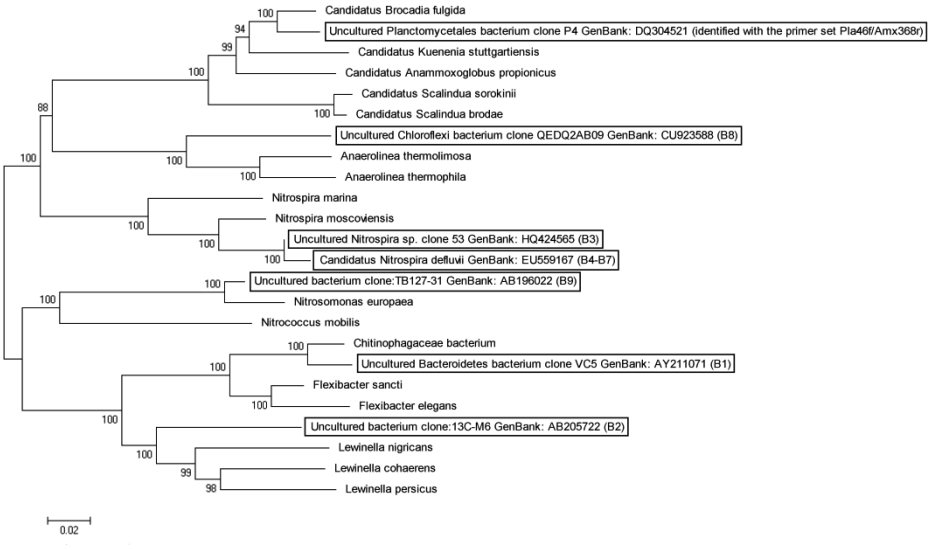

Figure 7. 16S rDNA phylogenetic tree of some key microorganisms detected in the inocula of the MBBR

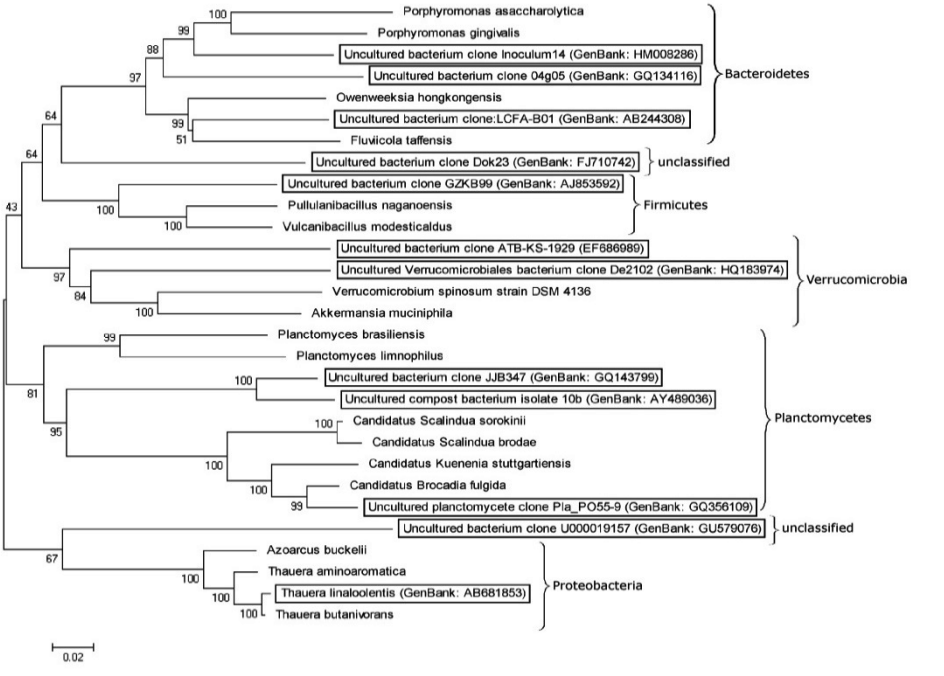

Figure 8. 16S rDNA phylogenetic tree of some key microorganisms detected in the inocula of the UASBR

4.2. Start-up of pilot plant

4.2.1. Overview of operation of the pilot plant

The main characteristics of operational units in pilot study (DeamMBBR, DeamSBR and AnamSBR) are shown in Tab 3. The operation of the pilot plant can be divided into 3 periods, designated as period I (initial start-up without pH adjustment), period II (start-up after pH adjustment) and period III (operation after start-up period).

During period I, the development of autotrophic microbial consortia removing dissolved nitrogenous forms was delayed. The conditions turned out to be unfavourable for propagation of functional bacteria, most probably due to FA inhibition. This demonstrates the urgency for the development of an accurate technique to evaluate the FA concentration in reject water containing up to 1 $g \cdot L^{-1}$ NH_X-N. Since an accurate model for calculation of FA in the complex wastewater with high-ammonia content has still not been developed, the Anthoniesen's formula (Eq 17) has been used in this thesis. After implementation of automatic pH adjustment, autotrophic nitrogen-removing consortia were developed in all systems within 4÷6 months (period II). During period III, the maximum TNRR of 1.04 kg-$N \cdot m^{-3} \cdot d^{-1}$ was achieved in the DeamMBBR, trice exceeding the TNRR value achieved in the DeamSBR. In the AnamMBBR, the maximum TNRR was limited by the volume of the nitritation reactor NitriSBR. A detailed overview of the operation of the pilot plant is given in **paper III**.

The concentrations of ammoniacal and carbonaceous species ($(NH_3)_W \rightleftharpoons NH_4^+$ and $(CO_2)_W \rightleftharpoons HCO_3^- \rightleftharpoons CO_3^{2-}$) are determined by equilibrium processes. In an anaerobic digester, where biogas in which about 1/3 of content is CO_2, is in contact with liquid phase, the optimum pH for methane production is close to neutral [145]. The pH in an anaerobic digester is affected by multiple factors, including the equilibrium process $(CO_2)_G \rightleftharpoons (CO_2)_W$. During dewatering of digested sludge by centrifugation, $(CO_2)_W$ becomes into contact with ambient air and degassing of CO_2 from liquid phase occurs, which results in the pH of reject water 7.9÷8.3 (**paper III**), higher than 7.0÷7.5, which is the optimal pH range for deammonification [47]. The pH value of around 8 shifts the equilibrium of the process $NH_4^+ \rightleftharpoons NH_3 + H^+$ towards the formation of FA. Increased FA concentration (exceeding 8÷10 mg NH_3-$N \cdot L^{-1}$) acted as an inhibitor for anammox bacteria, thus, pH adjustment was required (**paper III**).

Table 3. Main characteristics of operational units in pilot study

Operation period	DeamMBBR		DeamSBR		AnamMBBR	
Period I (start-up before pH adjustment)	**Days 1-236**		**Days 1-221**		**Days 1-236**	
	Average	**Max.**	**Average**	**Max.**	**Average**	**Max.**
TNLR, kg-N·m^{-3}·d^{-1}	0.37±0.05	0.48	0.37±0.05	0.48	0.35±0.06	0.44
TNRR, kg-N·m^{-3}·d^{-1}	0.05±0.04	0.15	0.05±0.04	0.17	0.04±0.03	0.12
TNRE, %	13±11	38	15±12	45	10±8	40
Alkalinity, mmol·L^{-1}	36.0±11.5	75.3	36.0±12.3	73.9	44.8±6.4	57.7
pH	7.80±0.28	8.21	7.78±0.41	8.13	7.80±0.29	8.25
Estimated FA, mg-N·L^{-1}	30±15	56	24±9	39	37±19	69
NO_3^--N_{formed} / $TN_{removed}$	0.023		0.020		close to 0	
Period II (start-up, after pH adjustment)	**Days 237-377**		**Days 222-410**		**Days 237-426**	
	Average	**Max.**	**Average**	**Max.**	**Average**	**Max.**
TNLR, kg-N·m^{-3}·d^{-1}	0.15±0.05	0.28	0.19±0.05	0.08	0.10±0.03	0.15
TNRR, kg-N·m^{-3}·d^{-1}	0.04±0.02	0.06	0.03±0.02	0.10	0.03±0.01	0.05
TNRE, %	24±11	43	20±12	42	28±10	47
Alkalinity, mmol·L^{-1}	21.6±11.9	42.3	17.1±9.8	41.6	20.7±7.6	35.0
pH	7.06±0.23	7.41	7.22±0.41	8.30	7.25±0.35	7.99
Estimated FA, mg-N·L^{-1}	6±6	24	6±3	16	6±4	16
NO_3^--N_{formed} / $TN_{removed}$	0.044		0,013		0.006	
Period III (operation after start-up period)	**Days 378-720**		**Days 411-700**		**Days 427-720**	
	Average	**Max.**	**Average**	**Max.**	**Average**	**Max.**
TNLR, kg-N·m^{-3}·d^{-1}	0.43±0.37	1.11	0.18±0.11	0.48	0.06±0.02	0.11
TNRR, kg-N·m^{-3}·d^{-1}	0.38±0.34	1.04	0.13±0.07	0.30	0.04±0.01	0.06
TNRE, %	82±15	98	73±14	95	72±24	99
Alkalinity, mmol·L^{-1}	6.1±3.5	21.6	5.0±4.8	27	13.6±10.9	36.8
pH	6.97±0.36	7.45	7.17±0.31	7.94	7.91±0.36	8.62
Estimated FA, mg-N·L^{-1}	1±1	8	1±1	7	1±1	7
NO_3^--N_{formed} / $TN_{removed}$	0.124		0.104		0.025	

4.2.2. Operation of DeamMBBR

During period I, the average TNRE and TNRR were low. The average pH value of 7.80±0.28 and the NO_3^--N_{formed} / $TN_{removed}$ ratio of 0.002 showed that NH_3 stripping played the main role in TN removal. Denitrification, using dissolved COD, contributed 10÷30% of total nitrogen removal as the average removal efficiency of dissolved COD was 17%. The propagation of deammonifying biomass was inhibited and it was assumed that FA inhibition was the primary reason as the estimated FA concentration exceeded 10 mg-N·L^{-1} (Tab 3).

During period II, the alkalinity was decreased almost twice from 36.0 mmol·L^{-1} to 21.4 mmol·L^{-1}. The pH was decreased to a nearly neutral value, resulting in a curtailed stripping of ammonia. A slight increase in TNRE was achieved, compared to period II. Denitrification using soluble COD contributed less than 10% of total nitrogen removal (average COD removal was 27%), indicating emerging anammox process. Yet, denitrification significantly affected the NO_3^--N_{formed} / $TN_{removed}$ ratio, as well as efficient suppression of NOB. Nitrite level was transiently increased during this period (Fig 10) probably due to discrepancy in the growth rates of AOBs and anammox bacteria. The excessive nitritation was suppressed by changing set-points of DO concentration and by variation of the length of anoxic period. The estimated FA was decreased 5-fold compared to the previous period. Since day 377, the TNRE exceeded 50% and a slight accumulation of NO_3^--N was observed, denoting conclusion of the start-up process. By the end of the period III, a 13-fold increase in TNRR was achieved, from 0.08 to 1.04 kg-N·m^{-3}·d^{-1}. This was nearly twice as high as the TNRR achieved in a MBBR by Mehrdad M et al (0.4÷0.6 kg-N·m^{-3}·d^{-1}) [8]. Denitrification, using soluble COD, was estimated to contribute less than 10% of total nitrogen removal, with average COD removal of 31%.

In the first half of the period III, however, there was a short period of increased NOB activity and the effluent NO_3^--N reached up to 200 mg·L^{-1}. In order to facilitate the growth of anammox bacteria, longer hydraulic retention time (HRT) values were applied in the beginning of the period III, which, however, resulted in an accumulation of suspended biomass. This, in turn, combined with decreased alkalinity (4÷11 mmol·L^{-1}) and FA (<1 mgNH_3-N·L^{-1}), unintentionally led to prodigious growth of NOB. Earlier bench-scale studies [22, 146] showed that suspended biomass in a deammonifying MBBR increases nitritating and nitrifying activity, but not anammox activity. The NOB activity was suppressed by DO control and shortening of HRT. Lower DO set point values resulted in DO peak concentrations below 1.5 mg-O_2·L^{-1}. The higher NO_3^--N_{formed} / $TN_{removed}$ ratio reflected both intensified anammox activity and activity of NOB. The FA concentration was around 1 mg-N·L^{-1}, below inhibition threshold for any of main autotrophic bacterial groups oxidizing nitrogen compounds (anammox bacteria, AOB and NOB).

Time courses of TNLR, TNRR and TNRE in DeamMBBR are given in Fig 9. Time courses for the effluent parameters of DeamMBBR are given in Fig 10. The figures show an increase in TNRE after day 377, short period of nitrate accumulation before day 500 and rapid increase in nitrogen removal afterwards.

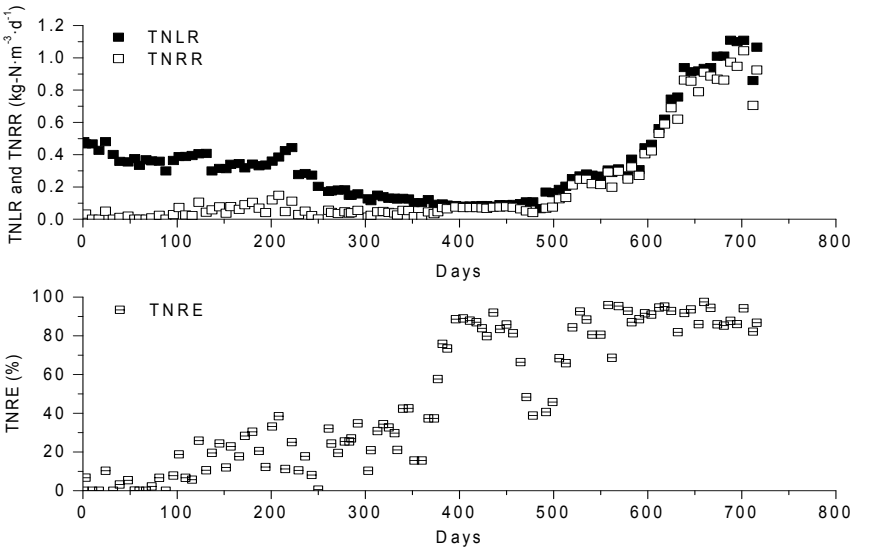

Figure 9. Time cources of TNLR, TNRR and TNRE in DeamMBBR

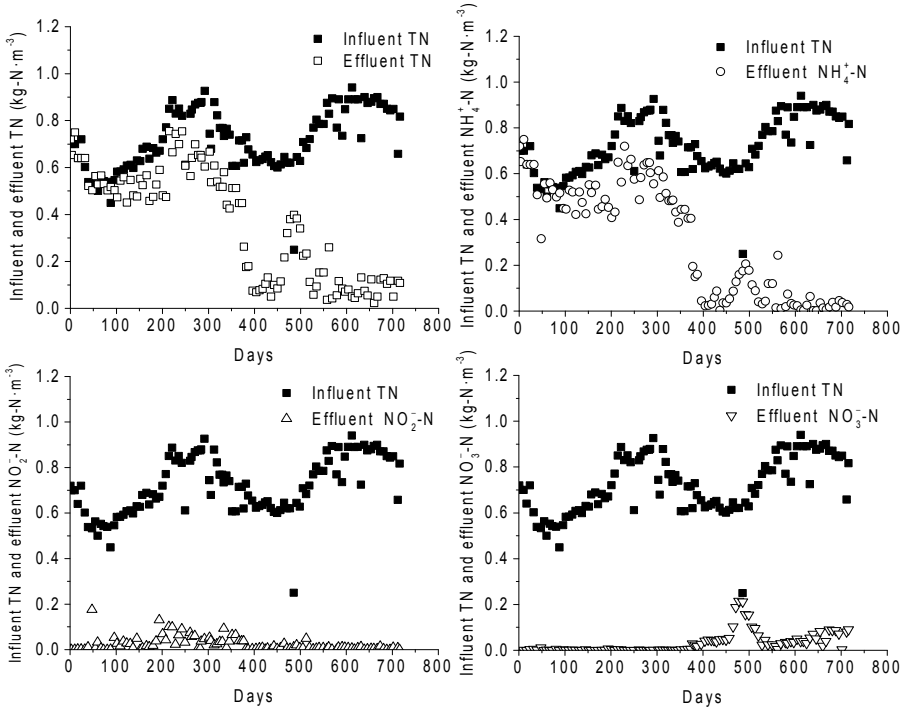

Figure 10. Time courses of TN, NH_4^+, NO_2^- and NO_3^- in the effluent of DeamMBBR

4.2.3. Operation of DeamSBR

The performance of DeamSBR was similar to DeamMBBR during period I and the main operation parameters showed similar values (Tab 3). As in DeamMBBR, propagation of deammonifying biomass was inhibited and NH_3 stripping was assumed to play the main role in TN removal. Similarly to the DeamMBBR, denitrification was estimated to contribute 10–30% of total nitrogen removal, with a COD removal of 13%, and it was limited by low NO_3^--N (as in the DeamMBBR, at <10 mg-N·L^{-1}).

During period II, pH, alkalinity and FA decreased similarly with DeamMBBR. Accumulation of NO_2^--N over a period of approximately 200 days was observed with concentrations of NO_2^--N reaching up to 120 mg-N·L^{-1} (Fig 12) and FNA up to 21·µg-HNO_2-N·L^{-1}. No accumulation of NO_3^--N occurred. Denitrification was estimated to contribute less than 10% of TN removal, with an average COD removal of 19%. Closer to neutral pH value curtailed the NH_3 stripping (the average ratio of NO_3^--N_{formed} / $TN_{removed}$ was 0.013). Despite a pH shock on day 304, when HCl was accidentally released into the reactor and pH dropped to 2, the TN removal recovered within two months (Fig 11). By day 411, a TNRE of 50% was achieved (TNRR=0.04 kg-N·m^{-3}·d^{-1}) indicating the end of start-up period.

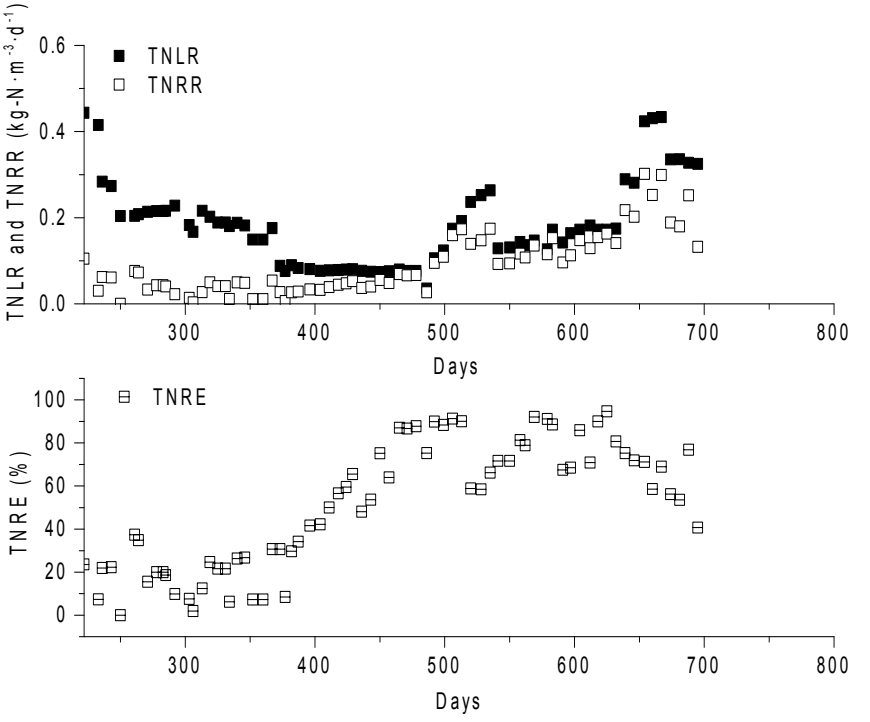

Figure 11. Time cources of TNLR, TNRR and TNRE in DeamSBR

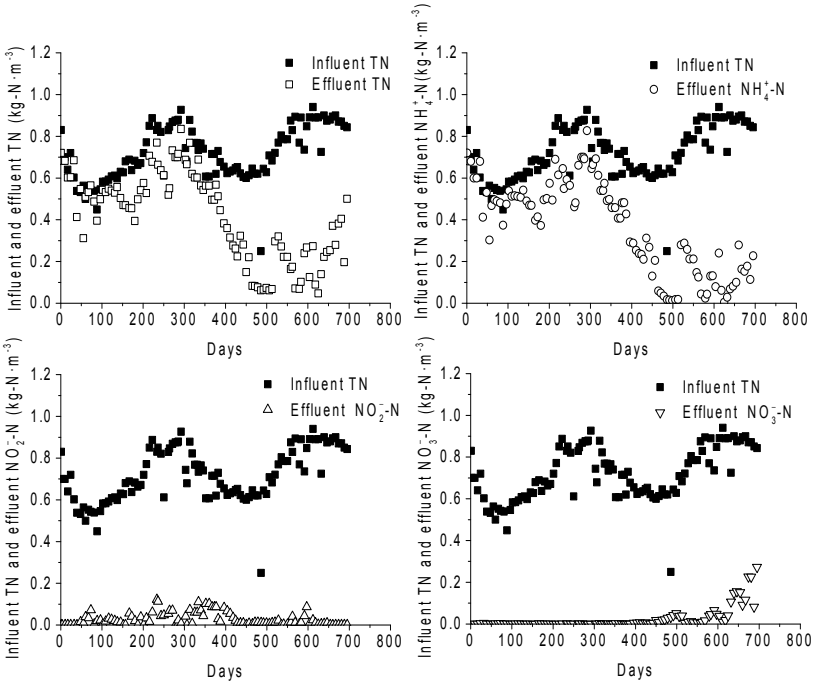

Figure 12. Time cources of TN, NH_4^+, NO_2^- and NO_3^- in the effluent of DeamSBR

Although the highest TNRE values exceeded 90% in period III, the reactor's performance was less stable compared to DeamMBBR and the maximum TNRR was about ⅓ of the value achieved in DeamMBBR. The instability was related both to wash-out of sludge around day 520 and prodigious growth of NOB by the end of the period, when denitrification using dissolved organics increased to over 10% of TN removal. The aeration control strategy was the same for both reactors, but it turned out to be less efficient in DeamSBR. Even lower bicarbonate alkalinity than in the DeamMBBR might have facilitated NOB activity and ensuing accumulation of nitrate.

4.2.4. Operation of NitriSBR

The performance of NitriSBR was unstable for the first 220 days of operation, when sludge retention time (SRT) equaled HRT (1÷2 days). The nitritation process was repeatedly disrupted by "shock loads" of solids (over 1000 $mg \cdot L^{-1}$) in the influent. Application of SRT control strategy since day 263 resulted in the stable and efficient performance of the NitriSBR after 300 days of operation.

The NO_2^--N to (NH_X-N + NO_2^--N) ratio shows a very efficient selection of AOB over NOB. The NO_2^--N to (NO_2^--N + NO_3^--N) ratio was in a nearly optimal range for the subsequent anammox process in accordance with Eq 2. The main parameters of the steady-state operation of the NitriSBR are listed in

Tab 4. The NH_X-N to alkalinity ratio of the reject water fed into the NitriSBR was 0.87±0.06, almost equal to 0.88, reported as the optimum value by Ganigué R et al [147].

Table 4. Operational parameters of NitriSBR

Parameter	Unit	Average (±SD)
NH_X-N	$mgN \cdot L^{-1}$	308 ±61
NO_2^--N	$mgN \cdot L^{-1}$	396 ±64
NO_3^--N	$mgN \cdot L^{-1}$	10 ±5
TNLR	$kgN \cdot m^{-3} \cdot d^{-1}$	0.67 ±0.13
NO_2^--N production rate	$kgN \cdot m^{-3} \cdot d^{-1}$	0.35 ±0.08
NO_2^--N to (NH_X-N + NO_2^--N) ratio	$mol \cdot mol^{-1}$	0.56 ±0.03
NO_2^--N to (NO_2^--N + NO_3^--N) ratio	$mol \cdot mol^{-1}$	0.97 ±0.01
Alkalinity	$mmol \cdot L^{-1}$	4.40 ±1.62

4.2.5. Operation of AnamMBBR

During period I, the performance of AnamMBBR was perturbed by both FA concentrations exceeding 30 g-N m^{-3} and unstable operation of NitriSBR that inhibited the propagation of anammox bacteria. Thus, TN removal was negligible.

By period II, the operation of NitriSBR was stabilised and FA control by pH adjustment resulted in estimated FA concentration below 10 $g\text{-}N \cdot m^{-3}$. The discrepancy between removal of NH_X-N and NO_2^--N, 8% vs > 80%, showed that denitritation using both soluble and suspended organic matter was the main pathway of TN removal. The removal of soluble COD was below 50%. Due to lack of aeration, stripping of NH_3 was insignificant compared to other reactors.

In period III, the TNRE exceeded 50% on day 429. By day 450, also NH_X-N removal exceeded 50%, indicating that the anammox process had become the main N-removal pathway. The emergent biofilm was, however, vulnerable to pH increase (up to 8.6) owing to heterotrophic denitrification after the pH control using HCl was discontinued. Decreased alkalinity ($4 \div 7$ $mmol \cdot L^{-1}$) resulted in a reduced buffering capacity contributing to the pH increase. An accumulation of NO_2^--N occurred and inhibition of the biofilm anammox activity ensued. However, even during process perturbations of the concentration of FNA did not exceed 7 $\mu g\text{-}HNO_2\text{-}N \cdot L^{-1}$, indicating a mechanism of inhibition to anammox bacteria other than HNO_2. The possible cause might be inhibition by NO_2^- ions or pH>8. Concentrations exceeding 7 $\mu g\text{-}HNO_2\text{-}N \cdot L^{-1}$ were reported as short-term inhibitory to anammox bacteria [86]. Mixed influent with pH control was temporarily resumed (figures 13 and 14) and in the second half of period III a stable removal of both TN and NH_X-N over 80% was achieved. Due to limited volume of nitritation reactor, achieved TNLR and

TNRR remained below 0.1 kg-N·m^{-3}·d^{-1}. Denitrification was estimated to contribute to less than 20% of TN removal in the final stage of period III, but still most of NO_3^- produced by anammox bacteria was consumed.

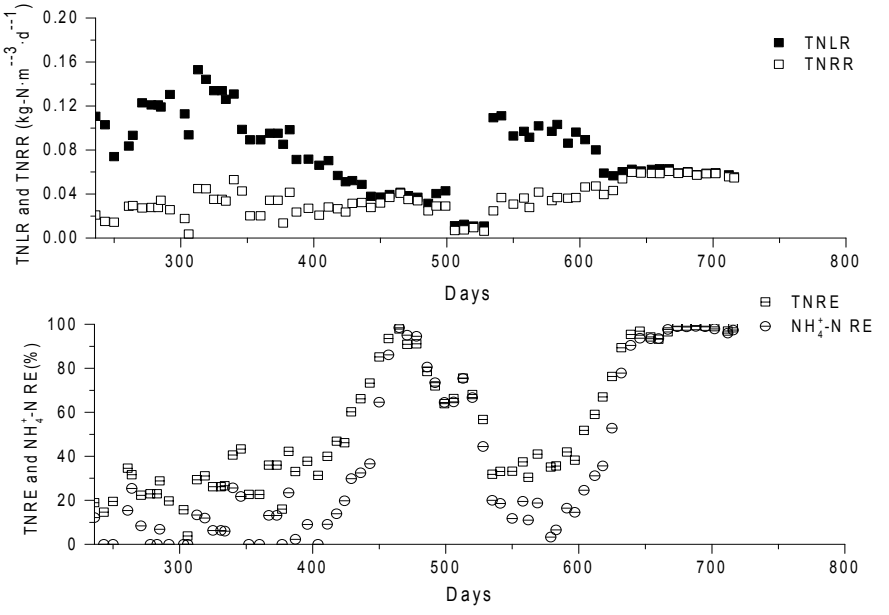

Figure 13. Time courses of TNLR, TNRR and TNRE in AnamMBBR

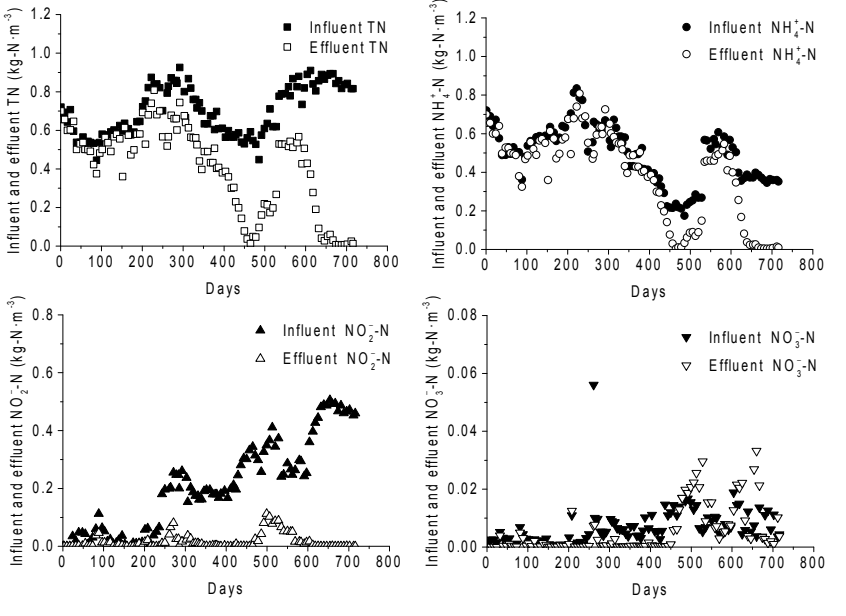

Figure 14. Time courses of TN, NH_4^+, NO_2^- and NO_3^- in the effluent of AnamMBBR

4.2.6. Quantitative analysis of 16S rRNA gene of anammox bacteria

The copy numbers of 16S rRNA gene of anammox bacteria per gram of total suspended solids (copies·g-TSS^{-1}) are given in Fig 15. In the DeamMBBR between days 318÷528, the number of 16S rRNA gene copies increased more than 500-fold, resulting in a 5-fold increase in TNRR. Between days 528÷681, the number of anammox gene copies decreased despite an increase in TNRR from 0.25÷0.86 kg-N·m^{-3}·d^{-1} (Fig 15). In the AnamMBBR and DeamMBBR the number of gene copies was comparable on day 318. By day 528, a 129-fold increase in abundance of anammox 16S rRNA gene copies was observed in the DeamMBBR. During this period, TNRR remained relatively stable while TNRE increased from 30 to 79%. By day 681, however, the number of gene copies had decreased again to nearly the same level as on day 318, although TNRR had risen to 0.060 kg-N·m^{-3}·d^{-1} and TNRE was over 90%. In the DeamSBR, the mixed liquor suspended solids were 2.30 g·L^{-1} on day 528 and 2.8 g·L^{-1} on day 681; the respective numbers of anammox 16S rRNA gene copies per gram of TSS were 3.93×10^{8} and 6.64×10^{6}. Before biomass sampling on day 528 there had been a period of steady increase in TNLR, TNRR and TNRE (Fig 9).

Thus, there was no clear correlation between anammox 16S rRNA gene copy numbers, TNRR and TNRE.

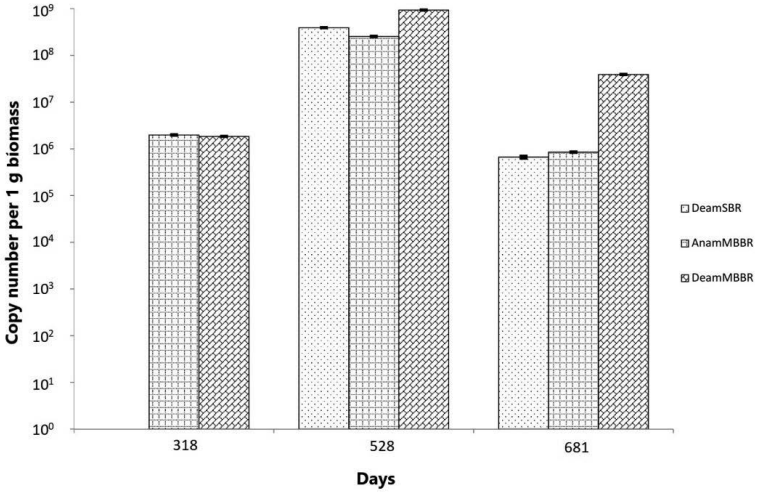

Figure 15. 16S rRNA gene copy numbers of anammox bacteria per gram of total suspended solids (copies·g-TSS^{-1}) during different periods of reactor operation. Error bars represent the standard deviation between three parallel qPCR tests

4.2.7. Implications for full-scale applications

Autotrophic nitrogen removal was successfully started-up in all three systems. In our earlier studies, various configurations, including SBR, one- and two-staged MBBR and upflow anaerobic sludge blanket reactor, have been started-up in bench-scale without anammox-specific *inoculum* [3, 16–23], indicating that many different configurations are applicable. Kanders L et al have shown in bench-scale that start-up of deammonification MBBRs can be done within a similar timeframe with or without seeding sludge, concluding that provision of the appropriate boundary conditions for anammox growth is most important factor [76]. Our studies allow us to extend this conclusion to other reactor configurations. The critical factors for start-up of a deammonification process in any scale, including full-scale applications, include:

1) FA control during the initial start-up stage maintaining the estimated FA below 10 mg-NH_3-N·L^{-1} is essential when start-up is performed with undiluted reject water. Inhibition by FA in reject water can be curtailed either by dilution with a low-nitrogen wastewater stream [8, 76] or by using pH adjustment as long as the microbial consortium is able to maintain the appropriate pH homeostatically (shown in the current thesis).
2) Fine-tuned aeration with a fast feedback and response should be applied in order to prevent both NO_2^--N inhibition of anammox process (at levels exceeding 40 mg-NO_2^--N·L^{-1}) and accumulation of NO_3^--N.
3) There should be an efficient control of suspended solid matter in the influent.

4.3. Modelling of carbonaceous equilibria

4.3.1. Modelling of open system $(CO_2)_G$–H_2O–$(CO_2)_W$–$(CaCO_3)_S$

The model is based on a structural scheme depicted in the Fig 16, showing the equilibrium distribution of carbonaceous species (ions and molecules) in the liquid phase. The novelty and importance of the given approach lays in a detailed interpretation of chemical processes taking place in an open ternary heterogeneous system $(CO_2)_G$–H_2O–$(CO_2)_W$–$(CaCO_3)_S$ as acid-base equilibria where H^+ ions play a central role in the evolution of the system to equilibrium and form a link that interconnects all equilibria in the system. The modelling of equilibrium in system $(CO_2)_G$–H_2O–$(CO_2)_W$–$(CaCO_3)_S$ is performed on assumption that the liquid phase (water) is in contact with gas (air) and solid phase ($CaCO_3$). The rates of mass transfer in gas-liquid and solid-liquid interfaces must be sufficient in both ways to assure equilibrium conditions in the whole ternary system.

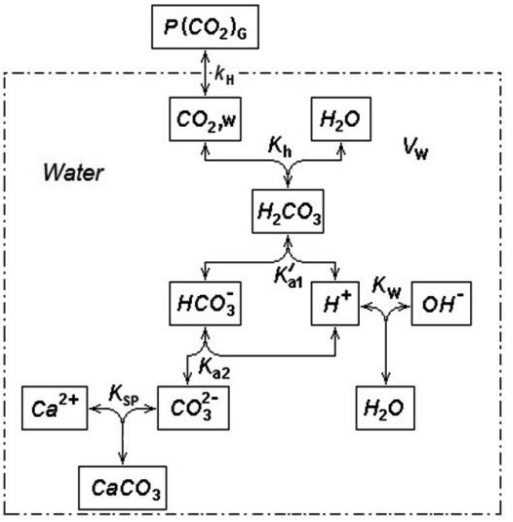

Figure 16. Structural scheme of the equilibrial distribution of ions and molecules in the ternary heterogeneous system $(CO_2)_G$–H_2O–$(CO_2)_W$–$(CaCO_3)_S$. In this scheme, k_H is Henry's constant—the distribution ratio of CO_2 between water and the gaseous phase; K_h is the coefficient of the equilibrium reaction of $(CO_2)_W + H_2O \rightleftharpoons H_2CO_3$; K'_{a1} is the acid dissociation constant of H_2CO_3; K_{a2} is the acid dissociation constant of HCO_3^-; K_{SP} is the solubility product of $CaCO_3$; K_W is the ion-product constant of water.

In addition to temperature, the equilibrium concentration of the species in the carbonic system is influenced by ionic strength. An increase in ionic strength reduces the activity of species. Consequently, for more concentrated solutions, the equilibrium equations are correct if expressed in terms of activity concentrations [105]. In current thesis, the ionic strength is neglected while in diluted solutions activity and concentration of species could be counted equal.

There are two main equilibrium processes in this system. The reaction between $(CO_2)_W$ and H_2O produces H_2CO_3 that dissociates, releasing H^+ and HCO_3^- ions. On the other hand, the dissolution of $CaCO_3$ produces CO_3^{2-} and Ca^{2+} ions. The CO_3^{2-} ions will take up H^+ ions and form HCO_3^- ions, leading to a decrease in the concentration of protons. These two concurrent processes produce a new equilibrium. The final pH of the equilibrium system depends on the concentration of dissolved CO_2. The reaction $(CO_2)_W + H_2O \rightleftharpoons H_2CO_3$ is slower than processes involving proton capture or release in liquid phase [148].

At equilibrium state, concentrations of all ions and molecules in liquid phase can be calculated on basis of following equations:

$$k_H = \frac{[CO_2]_W}{P(CO_2)_G} = 3.39\times10^{-2}\ \text{mol}\cdot\text{L}^{-1}\cdot\text{atm}^{-1}\ [149] \qquad (38)$$

$$K'_{a1} = \frac{[H^+]\times[HCO_3^-]}{[H_2CO_3]} = 1.72\times10^{-4}\ \text{mol}\cdot\text{L}^{-1}\ [150] \quad (39)$$

$$K_{a2} = \frac{[H^+]\times[CO_3^{2-}]}{[HCO_3^-]} = 4.70\times10^{-11}\ \text{mol}\cdot\text{L}^{-1}\ [150] \quad (40)$$

$$K_{SP} = [Ca^{2+}]\times[CO_3^{2-}] \cong 2.80\times10^{-9}\ (\text{mol}\cdot\text{L}^{-1})^2\ [151] \quad (41)$$

$$K_W = [H^+]\times[OH^-] = 1.01\times10^{-14}\ (\text{mol}\cdot\text{L}^{-1})^2\ [151] \quad (42)$$

The charge balance is expressed as follows:

$$2[Ca^{2+}] + [H^+] = 2[CO_3^{2-}] + [HCO_3^-] + [OH^-] \quad (43)$$

Concentrations of dissolved species is given as function of $[CO_2]_W$:

$$\left([Ca^{2+}],[CO_3^{2-}],[HCO_3^-],[H^+],[OH^-]\right) = f\,[CO_2]_W \quad (44)$$

The characterization of the equilibrium distribution of ions and molecules in the liquid phase is given on the basis of six explicit equations given above (38)–(43) containing six variables, concentrations of Ca^{2+}, CO_3^{2-}, HCO_3^-, H^+, OH^- and H_2CO_3. The equilibrium concentration of $(CO_2)_W$ at a given partial pressure of CO_2 in the gaseous phase $P(CO_2)_G$ is calculated using Eq 38 and the value of Henry's constant (k_H).

It is difficult to distinguish between unionized species H_2CO_3 and $(CO_2)_W$ by common analytical procedures such as acid-base titration. Therefore, the concentration H_2CO_3 and $(CO_2)_W$ is often summed up and the first pseudo-acid ionization constant K_{a1} is expressed as a product of two constants K_h (defined by Eq 50, chapter 4.3.3) and K'_{a1}, allowing to omit the concentration of H_2CO_3 from the calculations [152]. Also, in this thesis, the constant K_{a1} is used in order to decrease the number of unknowns. K_{a1} can be expressed as following:

$$K_{a1} = K_h \times K'_{a1} = \frac{[H^+]\times[HCO_3^-]}{[CO_2]_W} = (4.37 \pm 0.07)\times10^{-7}\ \text{mol}\cdot\text{L}^{-1} \quad (45)$$

The constant K_{a1} has a much smaller value ($K_{a1} = (4.30\div4.44)\times10^{-7}$ mol·L^{-1}) than the true acid dissociation constant K'_{a1} for H_2CO_3 (Eq 39). For pK'_{a1}, a range of values between 3.35÷3.80 have been reported, which makes the acidity of H_2CO_3 comparable to that of methanoic acid (HCOOH) [153]. Only less than 0.3% of total dissolved CO_2 (CO_2 in water + H_2CO_3), is present in the form of carbonic acid, while the rest is in the form of free dissolved carbon dioxide [105, 149, 152, 154–155].

For calculation of unknowns, the terms $[HCO_3^-]$, $[Ca^{2+}]$, $[OH^-]$ and $[CO_3^{2-}]$ were eliminated from the charge balance (Eq 43) by using equations (40)–(42) and (45). After these substitutions, the charge balance is converted into a form suitable for iterative solution. Eventually, the following expression is obtained (**paper IV**), which allows accurate calculations in a pH range up to 12:

$$[H^+] = \sqrt[3]{\frac{K_{a1} \times K_{a2} \times [CO_2]_W}{2 \times K_{SP}} \times \left\{ K_{a1} \times [CO_2]_W \times \left(2 \times \frac{K_{a2}}{[H^+]} + 1 \right) + K_W - [H^+]^2 \right\}} \qquad (46)$$

In practice, simplified solutions are sometimes used. Simplification, with the aim to eliminate some terms, is justified on the ground that such elimination does not produce any significant error [156]. A simplified method for the pH range 6÷9 has been presented in **paper IV**. This method is also compared with the method developed in this thesis.

The calculation of the pH and equilibrial $[Ca^{2+}]$, $[CO_3^{2-}]$ and $[HCO_3^-]$ is performed on the basis of the values for the equilibrium concentration of protons found by using an iterative method based on Eq 46. In the iteration series, different certain values of $[CO_2]_W$ are used in the range $2.74 \times 10^{-11} \div 8.02 \times 10^{-1}$ mmol·L^{-1}. Results of calculations are presented in Tab 5.

The $[HCO_3^-]$ and pH have a monotonous dependence on the $[CO_2]_W$. At the value of $[CO_2]_W$ 2.35×10^{-5} mmol·L^{-1} (correspondingly, $P(CO_2)_G$=0.692 ppm), the solubility of $CaCO_3$ passes through a minimum ($[Ca^{2+}]_{min} \cong 10^{-1}$ mmol·L^{-1}) and $[CO_3^{2-}]$ reaches a peak value ($[CO_3^{2-}]_{max} \cong 2.71 \times 10^{-2}$ mmol·L^{-1}). In the range of $[CO_2]_W$ ($2.35 \times 10^{-5} \div 2.74 \times 10^{-11}$) mmol·L^{-1}, the solubility of $CaCO_3$ consistently increases. This increase occurs due to the decrease in the concentration of CO_3^{2-} from 2.71×10^{-2} mmol·L^{-1} to 5.54×10^{-3} mmol·L^{-1}, which is compensated by an increase in concentration of Ca^{2+} ions, satisfying conditions of the equation of the solubility product of $CaCO_3$ (K_{SP}) (Tab 5). The decrease in the concentration of CO_3^{2-} ions, in turn, occurs along with the decrease in the concentrations of all carbonaceous ions and molecules in the water phase. The CO_3^{2-} and HCO_3^- ions bind protons, maintaining the equilibrium of $[CO_2]_W$ with the gas phase over a small equilibrium amount of H_2CO_3. These protons originate from the dissociation of water. Decrease in protons' concentration due to uptake by CO_3^{2-} and HCO_3^- ions is compensated by an increase in concentration of OH^- ions, maintaining a constant K_W value and leading to a rise in pH.

Table 5. Equilibrial $[CO_2]_W$, $[HCO_3^-]$, $[CO_3^{2-}]$, $\sum[CO_X]_W$, $[Ca^{2+}]$ and pH in the liquid phase and $P(CO_2)_G$ in the gas phase of the system $(CO_2)_G$–H_2O–$(CO_2)_W$–$(CaCO_3)_S$ at t=25 ºC. Boldface designates extremal values of Ca^{2+} and CO_3^{2-} corresponding to $[CO_2]_W \cong 2.35\times10^{-5}$ mmol·L^{-1}. $\sum[CO_X]_W$ shows summarised concentration of all dissolved carbonaceous species: $[CO_2]_W$, $[H_2CO_3]$, $[HCO_3^-]$ and $[CO_3^{2-}]$.

$[CO_2]_W$, mmol·L^{-1}	$P(CO_2)_G$, ppm	$[HCO_3^-]$, mmol·L^{-1}	$[CO_3^{2-}]$, mmol·L^{-1}	$\sum[CO_X]_W$ mmol·L^{-1}	$[Ca^{2+}]$ mmol·L^{-1}	pH
2.74×10^{-11}	8.08×10^{-7}	1.18×10^{-5}	5.54×10^{-3}	5.66×10^{-4}	5.05	12.00
8.66×10^{-10}	2.55×10^{-5}	1.18×10^{-4}	1.75×10^{-3}	1.87×10^{-3}	1.60	11.50
1.00×10^{-8}	2.95×10^{-4}	6.01×10^{-4}	3.94×10^{-3}	4.55×10^{-3}	0.71	11.15
1.00×10^{-7}	2.95×10^{-3}	2.77×10^{-3}	8.37×10^{-3}	1.11×10^{-2}	0.33	10.81
1.00×10^{-6}	2.95×10^{-2}	1.24×10^{-2}	1.67×10^{-2}	2.90×10^{-2}	0.17	10.46
1.00×10^{-5}	2.95×10^{-1}	4.88×10^{-2}	2.60×10^{-2}	7.48×10^{-2}	0.11	10.06
2.35×10^{-5}	**6.92×10^{-1}**	**7.63×10^{-2}**	**2.71×10^{-2}**	**1.03×10^{-1}**	**0.10**	**9.88**
1.00×10^{-4}	2.95×10^{0}	1.49×10^{-1}	2.42×10^{-2}	1.73×10^{-1}	0.12	9.54
1.00×10^{-3}	2.95×10^{1}	3.60×10^{-1}	1.41×10^{-2}	3.75×10^{-1}	0.20	8.92
3.00×10^{-3}	8.85×10^{1}	5.28×10^{-1}	1.01×10^{-2}	5.41×10^{-1}	0.28	8.61
1.00×10^{-2}	2.95×10^{2}	7.95×10^{-1}	6.91×10^{-3}	8.12×10^{-1}	0.41	8.27
1.32×10^{-2}	3.90×10^{2}	8.74×10^{-1}	6.31×10^{-3}	8.93×10^{-1}	0.44	8.19
3.00×10^{-2}	8.85×10^{2}	1.15	4.82×10^{-3}	1.19	0.58	7.95
1.00×10^{-1}	2.95×10^{3}	1.72	3.24×10^{-3}	1.82	0.86	7.60
8.02×10^{-1}	2.37×10	3.45	1.62×10^{-3}	4.25	1.73	7.00

At the value $[CO_2]_W = 1.32\times10^{-2}$ mmol·L^{-1} ($P(CO_2)_G = 390$ ppm) the total equilibrium concentration of calcium ions was approximately twice the sum of all carbonaceous species:

$$\sum[CO_X]_W \approx 2\times[Ca^{2+}] \tag{47}$$

Thus, the transfer of CO_2 from the gas phase accounts for nearly half the amount of carbonaceous ions and molecules in the liquid phase, with the other half of the carbonaceous species resulting from the transfer of CO_3^{2-} from the solid to the liquid phase. The increased solubility of $CaCO_3$ in the range of $[CO_2]_W \cong 2.35\times10^{-5} \div 8.02\times10^{-1}$ mmol·L^{-1} is driven by mass transfer of CO_2 from gas phase to liquid phase, dominating over CO_2 mass transfer in the opposite direction. At the value of $[CO_2]_W = 2.35\times10^{-5}$ mmol·L^{-1} ($P(CO_2)_G = 0.692$ ppm), the total equilibrium concentration of carbonaceous species in the liquid phase becomes nearly equal to the concentration of Ca^{2+} ions (Fig 17):

$$\sum[CO_X]_W \cong [Ca^{2+}] \tag{48}$$

$$\Delta[CO_2]_W = \sum[CO_X]_W - [Ca^{2+}] \cong 0 \tag{49}$$

In Eq 49, the term $\Delta[CO_2]_W$ indicates the amount of CO_2 transferred from the gas to the liquid phase per unit volume of the liquid. Consequently, there is no net transfer of CO_2 from the gas phase, which corresponds to the case of

equilibrium in a closed system without the gas phase. If $P(CO_2)_G < 0.692$ ppm and $[CO_2]_W < 2.35\times10^{-5}$ mmol·L^{-1}, escape of CO_2 from liquid phase to gas phase predominates over absorption of CO_2 from gas phase to liquid phase and the increased solubility of $CaCO_3$ is consequently driven by mass transfer of CO_2 from liquid phase to gas phase. Instead of interfacial transport, $(CO_2)_W$ may be consumed *in situ* in the liquid phase (water), e. g. by growing algae.

4.3.2. Model-predicted vs experimental data in the open system

The model allows to calculate pH values and concentrations of all ions and molecules over a wide range of pH at any equilibrium concentration of dissolved CO_2.The experimental results are shown in Tab 6 and Fig 17. In order to evaluate statistical similarity of data from the experiments and theoretical model, *p-values* of two-way *t-test* for both data sets were calculated (α=0.05).

Table 6. Experimentally measured and model-calculated values for pH and concentrations of Ca^{2+}, with p-values of two-way t-test

Composition of gas atmosphere	$[Ca^{2+}]$ measured, (mmol·L^{-1})	$[Ca^{2+}]$ calculated (mmol·L^{-1})	*p*-value, $[Ca^{2+}]$	pH value measured	pH value calculated	*p*-value, pH
A.	0.421±0.005	0.444	0.24	8.09±0.03	8.19	0.26
B.	0.113±0.012	<0.108	0.80	9.83±0.03	9.67	0.62
C.	0.100±0.016	0.104	0.84	10.02±0.03	9.88	0.24
D.	0.120±0.007	<0.126	0.52	10.06±0.03	10.25	0.23
E.	0.145±0.009	Not calculated		10.24±0.03	Not calculated	

The letters A, B, C, D, and E represent the following compositions of gas phase:
A – ambient air, $P(CO_2)_G$=390 ppm;
B – Ar of 99.999% purity, $P(CO_2)_G$<1.7 ppm;
C – Ar of 99.9999% purity, with added CO_2, $P(CO_2)_G$=0.836 ppm;
D – Ar of 99.9999% purity, $P(CO_2)$<0.1 ppm;
E – Ar of 99.999% purity, additionally purified by purging through 5.0 M NaOH.

The experimental data for $[Ca^{2+}]$, in accordance with the theoretical model, showed a minimum value of $[Ca^{2+}]$ at $P(CO_2)_G = 0.836$ ppm and $[CO_2]_W = 2.82\times10^{-5}$ mmol·L^{-1}, thus providing evidence in favour of the efficacy of the theoretical model developed in this study. The statistical similarity between experimental data and calculated data obtained by the theoretical model was shown by the two-way t-test (Tab 6).

A graphical expression of the dependence of pH and the solubility of $CaCO_3$ on the $[CO_2]_W$ is presented in Fig 17.

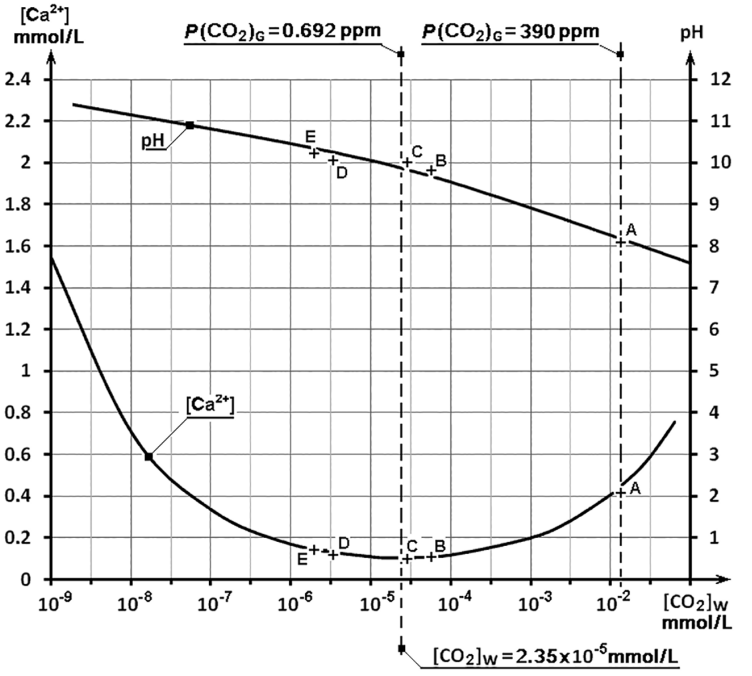

Figure 17. Calculated and experimentally determined values $[Ca^{2+}]$ and pH. Experimental data points A-E are specified in Tab 6. $P(CO_2)_G$=390 ppm represents ambient air and $P(CO_2)_G$=0.692 ppm represents the composition of gas phase corresponding to situation when net interfacial CO_2 transfer between gas and liquid phases is equal to zero.

According to the literature, the aqueous solutions of Ca^{2+} may also contain complexated cationic and neutral species such like ion pairs $CaOH^+$, $CaHCO_3^+$ and $CaCO_3^0$ [113, 157–158]. There is little evidence supporting the formation of higher order complexes in $CaCO_3$ solutions [157]. The concentration of the $Ca(OH)^+$ under experimental conditions of this study (pH<10) is inappreciably low, allowing the occurrence of $CaOH^+$ to be neglected. Under standard laboratory conditions (temperature 25 ºC and atmospheric pressure 100 kPa), most of calcium in solution is in the non-complexated Ca^{2+} form [113]. At the lower (close to atmospheric) CO_2 partial pressure, Ca^{2+} is by far the most abundant calcium-containing species at pH<9 [103]. Although $CaHCO_3^+$ forms a substantial fraction of total dissolved Ca^{2+} at the partial pressure of $[CO_2]_G = 10^6$ ppm, the inclusion or exclusion of $CaHCO_3^+$ into calculations affects the pH value only by ± 0.01 unit in the system $(CO_2)_G$–H_2O–$(CO_2)_W$–$(CaCO_3)_S$ without any other acid or base added [103]. The electrically neutral ion pair $CaCO_3^0$ does not influence pH of the stock solution, as no protons are taken up or released when ion pairing occurs. $CaCO_3^0$ concentration is independent on both pH and $[CO_2]_W$, provided solid $CaCO_3$ is in the equilibrium with the stock solution [103]. Due to an insignificant effect on the pH of liquid phase, $CaHCO_3^+$ and $CaCO_3^0$ were also neglected from calculations.

4.3.3. Modelling of closed system H_2O–$(CO_2)_W$–$(CaCO_3)_S$

Initial equilibrium system H_2O–$(CO_2)_W$

The modelling of equilibrium in a closed system H_2O–$(CO_2)_W$–$(CaCO_3)_S$ is performed on an assumption that solid $CaCO_3$ is led into contact with water containing dissolved CO_2. Thus, the original equilibrium system is defined as homogenous system H_2O–$(CO_2)_W$ without $CaCO_3$ where the distribution of carbonaceous ions and molecules in the liquid phase is determined by the equilibrium constants, as outlined on the structural scheme in Fig 18.

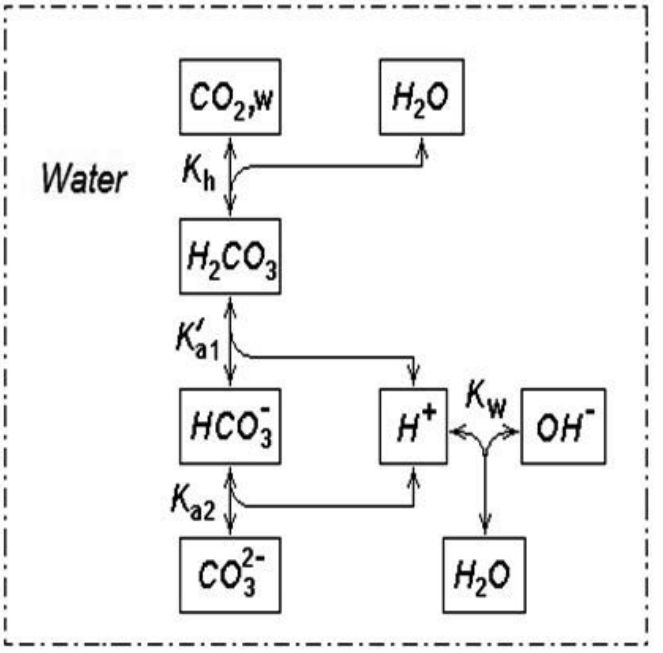

Figure 18. Structural scheme of the speciation of ions and molecules in the equilibrium system H_2O–$(CO_2)_W$. K_h is the hydration constant of CO_2, K'_{a1} the true acid dissociation constant of H_2CO_3, K_{a2} the acid dissociation constant of HCO_3^-, and K_W the ion-product constant of water

The values for $[CO_2]_{W0}$ in the liquid phase were calculated on the basis of Eq 38 and taken as invariable. The values of the equilibrium constants of K'_{a1}, K_{a2} and K_W of the system under investigation were given by the equations (39), (40) and (42). K_h was expressed as Eq (50):

$$K_h = \frac{[H_2CO_3]_0}{[CO_2]_{W0}} = 2.58\times10^{-3}\ \text{mol}\cdot\text{L}^{-1}\ [155] \qquad (50)$$

The charge balance equation for the initial equilibrium system is expressed as Eq (51):

$$[H^+]_0 = 2[CO_3^{2-}]_0 + [HCO_3^-]_0 + [OH^-]_0 \quad (51)$$

The set of equations describing the given ternary heterogeneous equilibrium system includes five unknowns, which are $[H_2CO_3]_0$, $[HCO_3^-]_0$, $[CO_3^{2-}]_0$, $[H^+]_0$ and $[OH^-]_0$ (subscripted index '0' indicates initial concentration).

In order to calculate these initial concentrations, it is necessary to solve five independent equations (39, 40, 42, 50 and 51) in relation to the predetermined $[CO_2]_{W0}$. Selected parameters account for all other parameters in the equilibrium system. If water has a pH of ≤7, then $[CO_3^{2-}]_0 << [HCO_3^-]_0$ and thus $[CO_3^{2-}]_0$ can be eliminated:

$$[H^+]_0 = [HCO_3^-]_0 + [OH^-]_0 \quad (52)$$

This assumption further simplifies the calculation procedure. In order to calculate the $[H^+]_0$, the unknown variables $[HCO_3^-]_0$ and $[OH^-]_0$ are excluded on the basis of equations (39, 40, 42 and 50), and the resulting quadratic equation is then converted to the following expression (**paper V)**:

$$[H^+]_0 \cong \sqrt{K'_{a1} \times K_h \times [CO_2]_{W0} + K_W} \quad (53)$$

Calculation of the $[H_2CO_3]_0$, $[HCO_3^-]_0$, $[CO_3^{2-}]_0$ and pH is performed on the basis of the values of $[H^+]_0$, calculated from Eq 53. Different certain values of $[CO_2]_{W0}$ ranging from $3.39 \times 10^{-7} \div 33.9$ mmol·L^{-1} are used in the iterative series. The summarized initial concentrations of all carbonaceous ions and molecules are calculated as follows:

$$\sum[CO_x]_{W0} \cong [CO_2]_{W0} + [H_2CO_3]_0 + [HCO_3^-]_0 + [CO_3^{2-}]_0 \quad (54)$$

Results of the calculations of $[H_2CO_3]_0$, $[HCO_3^-]_0$, $[CO_3^{2-}]_0$, $\sum[CO_X]_{W0}$, and pH on the basis of $[CO_2]_{W0}$ are presented in Tab 7.

Table 7. The initial concentrations of all carbonaceous species and pH in the closed system H_2O–$(CO_2)_W$ over the range of $[CO_2]_{W0}=3.39\times10^{-7}\div3.39\times10^{1}$ mmol·L^{-1} at t=25 ºC

$[CO_2]_{W0}$ mmol·L^{-1}	$[H_2CO_3]_0$ mmol·L^{-1}	$[HCO_3^-]_0$ mmol·L^{-1}	$[CO_3^{2-}]$ mmol·L^{-1}	$\sum[CO_x]_{W0}$ mmol·L^{-1}	$[H^+]_0$ mmol·L^{-1}	pH_0
3.39×10^{-7}	8.75×10^{-10}	1.54×10^{-6}	7.13×10^{-10}	1.88×10^{-6}	1.01×10^{-4}	6.99
1.02×10^{-5}	2.62×10^{-8}	3.84×10^{-5}	1.49×10^{-8}	4.86×10^{-5}	1.22×10^{-4}	6.92
2.37×10^{-5}	6.12×10^{-8}	7.52×10^{-5}	2.44×10^{-8}	9.90×10^{-5}	1.45×10^{-4}	6.84
3.39×10^{-5}	8.75×10^{-8}	9.72×10^{-5}	2.85×10^{-8}	1.31×10^{-4}	1.60×10^{-4}	6.80
3.39×10^{-4}	8.75×10^{-7}	3.82×10^{-4}	4.41×10^{-8}	7.22×10^{-4}	4.07×10^{-4}	6.39
3.05×10^{-3}	7.87×10^{-6}	1.18×10^{-3}	4.67×10^{-8}	4.24×10^{-3}	1.19×10^{-3}	5.93
1.32×10^{-2}	3.41×10^{-5}	2.46×10^{-3}	4.69×10^{-8}	1.57×10^{-2}	2.47×10^{-3}	5.61
3.39×10^{-2}	8.75×10^{-5}	3.94×10^{-3}	4.70×10^{-8}	3.79×10^{-2}	3.95×10^{-3}	5.40
3.39×10^{-1}	8.75×10^{-4}	1.25×10^{-2}	4.70×10^{-8}	3.52×10^{-1}	1.25×10^{-2}	4.90
2.50	6.46×10^{-3}	3.39×10^{-2}	4.70×10^{-8}	2.54	3.39×10^{-2}	4.47
3.39	8.75×10^{-3}	3.95×10^{-2}	4.70×10^{-8}	3.44	3.95×10^{-2}	4.40
1.02×10^{1}	2.62×10^{-2}	6.83×10^{-2}	4.70×10^{-8}	1.03×10^{1}	6.83×10^{-2}	4.17
3.39×10^{1}	8.75×10^{-2}	1.85×10^{-1}	4.70×10^{-8}	3.41×10^{1}	1.25×10^{-1}	3.90

Final equilibrium distribution of the ions and molecules CO_3^{2-}, HCO_3^-, H_2CO_3, and CO_2 after adding solid $CaCO_3$ to the initial closed equilibrium system of H_2O–$(CO_2)_{W0}$

To the initial homogenous equilibrium system H_2O–$[CO_2]_{W0}$, with a summarized concentrations of all carbonaceous ions and molecules $\sum[CO_x]_{W0}$, solid $CaCO_3$ is added, leading to a release Ca^{2+} ions and an additional amount of CO_3^{2-} ions due to the dissolution and dissociation of $CaCO_3$. This results in a change of concentrations of all ions and molecules and in a transformation of the initial homogenous equilibrium system H_2O–$(CO_2)_{W0}$ to a new binary heterogeneous equilibrium system H_2O–$[CO_2]_W$–$CaCO_3$. The ions and molecules in the system are quantitatively distributed in accordance with the equilibrium constants as shown in Fig 19.

The values of the equilibrium constants of $K_{a1}^{/}$, K_{a2}, K_{SP}, K_w, and K_h of the system under investigation are given by equations (39)–(42) and (50).

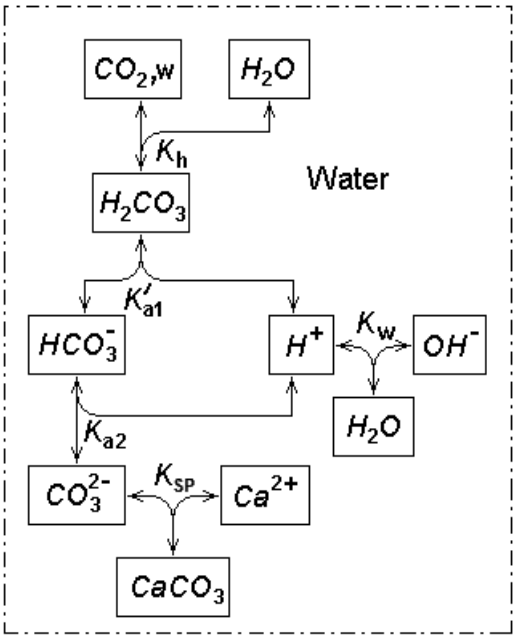

Figure 19. Structural scheme of the equilibrium distribution of ions and molecules in the final closed system of H_2O–$[CO_2]_W$–$(CaCO_3)_S$. K_h is the hydration constant of CO_2, K'_{a1} the true acid dissociation constant of H_2CO_3, K_{a2} the acid dissociation constant of HCO_3^-, K_W the ion-product constant of water and K_{SP} the solubility product of $CaCO_3$

The electrical neutrality condition for closed system H_2O–$(CO_2)_W$–$(CaCO_3)_S$ is the same as Eq 43 for the open system described in Chapter 4.3.1:

$$2[Ca^{2+}]+[H^+]=2[CO_3^{2-}]+[HCO_3^-]+[OH^-] \tag{55}$$

and the molar balance equation can be expressed as:

$$\sum[CO_X]_W = \Delta[CO_X]_{W0}+\Delta[CO_3^{2-}]= [CO_3^{2-}]+[H_2CO_3]+[HCO_3^-]+[CO_2]_W, \tag{56}$$

where $\Delta[CO_3^{2-}]=[Ca^{2+}]$ is equal to the additional amount of CO_3^{2-} ions, which is transferred to the system from dissolved $CaCO_3$.

Calculation of the concentrations of $[CO_2]_W$, $[CO_3^{2-}]$, $[H_2CO_3]$, $[HCO_3^-]$, $[H^+]$, $[OH^-]$, and $[Ca^{2+}]$ in the observed equilibrium system requires solution of a system of seven equations (39)–(42), (50), (55) and (56). As in case of the open system $(CO_2)_G$–H_2O–$(CO_2)_W$–$(CaCO_3)_S$, using composite constant K_{a1} defined by Eq 43 allows to decrease the number of unknowns, in this case to six.

The variables $[OH^-]$, $[Ca^{2+}]$, $[CO_3^{2-}]$ and $[CO_2]_W$, as in the case of open system, can be eliminated in equations (55) and (56) by replacing concentrations with their algebraic expressions, using equations (40–42) and (45). Equations (55) and (56) are eventually converted into following forms (**paper V**):

$$[HCO_3^-]_Z = \frac{-\left(\frac{K_W}{[H^+]} - [H^+]\right) + \sqrt{\left(\frac{K_W}{[H^+]} - [H^+]\right)^2 + 4\left(2 \times \frac{K_{a2}}{[H^+]} + 1\right) \times \left(2\,\frac{K_{SP} \times [H^+]}{K_{a2}}\right)}}{2\left(2 \times \frac{K_{a2}}{[H^+]} + 1\right)}, \qquad (57)$$

$$[HCO_3^-]_M = \frac{\sum[CO_X]_{W0} + \sqrt{\left(\sum[CO_X]_{W0}\right)^2 + 4\left(\frac{K_{a2}}{[H^+]} + 1 + \frac{[H^+]}{K_{a1}}\right) \times \frac{K_{SP} \times [H^+]}{K_{a2}}}}{2\left(\frac{K_{a2}}{[H^+]} + 1 + \frac{[H^+]}{K_{a1}}\right)}, \qquad (58)$$

$[HCO_3^-]_Z$ is the concentration of HCO_3^-, based on the charge balance (Eq 57) and $[HCO_3^-]_M$ – the concentration of HCO_3^-, based on the molar balance (Eq 58). As a result we have two equations, (57) and (58), for two unknown concentrations of $[HCO_3^-]$ and $[H^+]$. At equilibrium state, the next conditions must be fulfilled:

$$[HCO_3^-] = [HCO_3^-]_Z \text{ and } [HCO_3^-] = [HCO_3^-]_M. \qquad (59)$$

Now, there is only one unknown parameter, $[H^+]$, in the equations (57) and (58). The equilibrium values of $[HCO_3^-]$ and $[H^+]$ are calculated by an iterative method, using different values of the $[H^+]$ fulfilling the condition of difference between $[HCO_3^-]_Z$ and $[HCO_3^-]_M$, $\Delta[HCO_3^-]$, approaching zero:

$$\Delta[HCO_3^-] = [HCO_3^-]_M - [HCO_3^-]_Z \rightarrow 0. \qquad (60)$$

The calculation of the final equilibrium values of $[CO_2]_W$, $[Ca^{2+}]$, $[H_2CO_3]$, $\sum[CO_X]_W$, and pH is performed on the basis of the calculated equilibrium values of $[HCO_3^-]$ and $[H^+]$. The results of these calculations are presented in Tab 8.

Using both charge balance and molar balance equations for modelling of closed system H_2O–$(CO_2)_W$–$(CaCO_3)_S$ has not been referred in the surveyed literature [103, 111, 152]. These sources rely on the solution of a set of equations for charge balance and equilibrium constants.

The data in Tab 8 show that at the given range of $\sum[CO_X]_{W0}$ from 1.88×10^{-6} mmol·L^{-1} to 3.41×10^{1} mmol·L^{-1}, adding solid $CaCO_3$ causes the calculated value for pH to increase up to a maximum value of 9.88.

Table 8. Equilibrium values of $[CO_2]_W$, $[HCO_3^-]$, $[CO_3^{2-}]$, $\sum[CO_X]_{W0}$, $\sum[CO_X]_W$, $[Ca^{2+}]$, and pH in the closed system H_2O–$(CO_2)_W$–$(CaCO_3)_S$ at t=25°C

$[CO_2]_{W0}$ mmol·L^{-1}	$\sum[CO_X]_{W0}$ mmol·L^{-1}	$[Ca^{2+}]$ mmol·L^{-1}	$\sum[CO_X]_W$ mmol·L^{-1}	$[CO_2]_W$ mmol·L^{-1}	$[HCO_3^-]$ mmol·L^{-1}	$[CO_3^{2-}]$ mmol·L^{-1}	pH
3.39×10^{-7}	1.88×10^{-6}	1.03×10^{-1}	1.03×10^{-1}	2.20×10^{-5}	7.63×10^{-2}	2.71×10^{-2}	9.88
1.02×10^{-5}	4.86×10^{-5}	1.03×10^{-1}	1.03×10^{-1}	2.20×10^{-5}	7.63×10^{-2}	2.71×10^{-2}	9.88
2.37×10^{-5}	9.90×10^{-5}	1.03×10^{-1}	1.04×10^{-1}	2.20×10^{-5}	7.64×10^{-2}	2.71×10^{-2}	9.88
3.39×10^{-5}	1.31×10^{-4}	1.03×10^{-1}	1.04×10^{-1}	2.21×10^{-5}	7.64×10^{-2}	2.71×10^{-2}	9.88
3.39×10^{-4}	7.22×10^{-4}	1.03×10^{-1}	1.04×10^{-1}	2.24×10^{-5}	7.70×10^{-2}	2.71×10^{-2}	9.87
3.05×10^{-3}	4.24×10^{-3}	1.03×10^{-1}	1.08×10^{-1}	2.46×10^{-5}	8.06×10^{-2}	2.71×10^{-2}	9.85
1.32×10^{-2}	1.57×10^{-2}	1.04×10^{-1}	1.20×10^{-1}	3.32×10^{-5}	9.32×10^{-2}	2.68×10^{-2}	9.79
3.39×10^{-2}	3.79×10^{-2}	1.09×10^{-1}	1.47×10^{-1}	5.86×10^{-5}	1.21×10^{-1}	2.57×10^{-2}	9.65
3.39×10^{-1}	3.52×10^{-1}	3.56×10^{-1}	7.09×10^{-1}	6.28×10^{-3}	6.95×10^{-1}	7.86×10^{-3}	8.38
2.50	2.54	1.76	4.30	7.89×10^{-1}	3.51	1.60×10^{-3}	6.99
3.39	3.44	2.09	5.53	1.34	4.19	1.34×10^{-3}	6.83
1.02×10^{1}	1.03×10^{1}	3.57	1.38×10^{1}	6.67	7.15	7.83×10^{-4}	6.37
3.39×10^{1}	3.41×10^{1}	5.78	3.99×10^{1}	2.83×10^{1}	1.16×10^{1}	4.84×10^{-4}	5.95

In referred source [103], Butler JN calculated the equilibrium pH in a binary system H_2O–$(CaCO_3)_S$ without gas phase, based on the charge balance and including both ion pairs and activity coefficients. The calculations returned an equilibrium pH value of 9.90 and showed that inclusion of ion pairs $CaOH^+$, $CaHCO_3^+$ and $CaCO_3^0$ had an insignificant role on outcome. Concentrations of ion pairs were low, compared to the principal (most prevalent) species (HCO_3^-, CO_3^{2-}, Ca^{2+} and OH^-) in the binary closed system, and ion pairs could be neglected [103].

In order to identify the proton donors and acceptors, the proton transfers related to carbonate ions, water, and H_2CO_3 ($\Delta[H^+]_{CO_3^{2-}}$, $\Delta[H^+]_{H_2O}$, and $\Delta[H^+]_{H_2CO_3}$, respectively) are calculated. During the evolution of the system H_2O–$(CO_2)_W$–$CaCO_3$ to an equilibrium, the CO_3^{2-} ions are released when $CaCO_3$ dissolves and dissociates; then the CO_3^{2-} ions accept a certain amount of protons ($\Delta[H^+]_{CO_3^{2-}}$), which originate from two sources, either the reversible dissociation of water ($\Delta[H^+]_{H_2O}$) or H_2CO_3 ($\Delta[H^+]_{H_2CO_3}$), formed in the reaction between $(CO_2)_{W0}$ and H_2O. Thus, the H^+ ions carry a central role in the evolution of this equilibrium system and form a link between acid–base equilibrium processes. The proton transfers are presented in Tab 9.

The smaller is the $[CO_2]_{W0}$, the fewer protons is produced on the basis of the dissociation of H_2CO_3. Thus, dissociation of water at lower values of $[CO_2]_{W0}$ produces the main amount of protons, which bind to CO_3^{2-} ions, resulting in an increase in $[OH^-]$ and a rise in pH, while the value of K_W remains constant. The maximum value of pH=9.88 is related to the K_{SP} of $CaCO_3$ and the K_W as the dissociation of H_2CO_3 can be neglected at small values of $[CO_2]_{W0}$.

Table 9. Calculated proton transfers between different species, concentrations of $[CO_2]_{W0}$, $[Ca^{2+}]$ and $[HCO_3^-]$, and pH in the closed system H_2O–$(CO_2)_W$–$(CaCO_3)_S$ at t = 25 ºC

$[CO_2]_{W0}$ mmol·L^{-1}	$\Delta[H^+]_{H_2O}$ mmol·L^{-1}	$\Delta[H^+]_{H_2CO_3}$ mmol·L^{-1}	$\Delta[H^+]_{CO_3^{2-}}$ mmol·L^{-1}	pH	$[Ca^{2+}]$ mmol·L^{-1}	$[HCO_3^-]$ mmol·L^{-1}
$3.39\cdot10^{-7}$	$7.63\cdot10^{-2}$	$-2.03\cdot10^{-5}$	$-7.63\cdot10^{-2}$	9.88	$1.03\cdot10^{-1}$	$7.63\cdot10^{-2}$
$1.00\cdot10^{-6}$	$7.63\cdot10^{-2}$	$-1.68\cdot10^{-5}$	$-7.63\cdot10^{-2}$	9.88	$1.03\cdot10^{-1}$	$7.63\cdot10^{-2}$
$1.02\cdot10^{-5}$	$7.63\cdot10^{-2}$	$2.65\cdot10^{-5}$	$-7.63\cdot10^{-2}$	9.88	$1.03\cdot10^{-1}$	$7.63\cdot10^{-2}$
$2.37\cdot10^{-5}$	$7.62\cdot10^{-2}$	$7.67\cdot10^{-5}$	$-7.63\cdot10^{-2}$	9.88	$1.03\cdot10^{-1}$	$7.64\cdot10^{-2}$
$3.39\cdot10^{-5}$	$7.62\cdot10^{-2}$	$1.09\cdot10^{-4}$	$-7.63\cdot10^{-2}$	9.88	$1.03\cdot10^{-1}$	$7.64\cdot10^{-2}$
$3.39\cdot10^{-4}$	$7.56\cdot10^{-2}$	$7.00\cdot10^{-4}$	$-7.63\cdot10^{-2}$	9.87	$1.03\cdot10^{-1}$	$7.70\cdot10^{-2}$
$3.05\cdot10^{-3}$	$7.22\cdot10^{-2}$	$4.21\cdot10^{-3}$	$-7.64\cdot10^{-2}$	9.85	$1.03\cdot10^{-1}$	$8.06\cdot10^{-2}$
$1.32\cdot10^{-2}$	$6.19\cdot10^{-2}$	$1.57\cdot10^{-2}$	$-7.75\cdot10^{-2}$	9.79	$1.04\cdot10^{-1}$	$9.32\cdot10^{-2}$
$3.39\cdot10^{-2}$	$4.55\cdot10^{-2}$	$3.79\cdot10^{-2}$	$-8.34\cdot10^{-2}$	9.65	$1.09\cdot10^{-1}$	$1.21\cdot10^{-1}$
$3.39\cdot10^{-1}$	$2.43\cdot10^{-3}$	$3.46\cdot10^{-1}$	$-3.49\cdot10^{-1}$	8.38	$3.56\cdot10^{-1}$	$6.95\cdot10^{-1}$
2.01	$5.07\cdot10^{-5}$	1.53	–1.53	7.11	1.53	3.05
2.15	$3.27\cdot10^{-5}$	1.59	–1.59	7.07	1.60	3.19
2.45	$\mathbf{-1.55\cdot10^{-7}}$	**1.73**	**–1.73**	**7.00**	**1.73**	**3.46**
3.39	$-7.86\cdot10^{-5}$	2.09	–2.09	6.83	2.10	4.19
$1.02\cdot10^{1}$	$-4.30\cdot10^{-4}$	3.58	–3.58	6.37	3.58	7.16
$3.39\cdot10^{1}$	$-1.11\cdot10^{-3}$	5.78	–5.78	5.95	5.78	$1.16\cdot10^{1}$

As seen from Tab 9, at small values of $[CO_2]_{W0}$, the $[HCO_3^-] \cong [H^+]$ released from the dissociation of water. In this case, the dissociation of water and solubility of $CaCO_3$ determine the equilibrium of the system. The data in the Tab 9 show that at $[CO_2]_{W0} = 2.45$ mmol·L^{-1}, the corresponding pH is equal to 7.0,. indicating a neutral environment. At $[CO_2]_{W0} < 2.5$ mmol·L^{-1}, the liquid phase is basic, with a pH value exceeding 7. At $[CO_2]_{W0} > 2.5$ mmol·L^{-1}, the liquid phase is acidic, with a pH value dropping below 7 and the evolution of the equilibrium system is determined by the reaction between $(CO_2)_{W0}$ and H_2O, which produces HCO_3^- and H^+ ions over the intermediary formation and dissociation of H_2CO_3. A certain amount of protons participates in the reaction between CO_3^{2-} and H^+ that forms HCO_3^- ions increasing the equilibrium concentration of the latter; another part of H^+ ions remain in solution resulting a decrease in pH.

The positive values of $\Delta[H^+]_{H_2O}$ is the outcome of the dissociation reaction of water, which acts as a proton donor and ($\Delta[H^+]_{H_2CO_3}$) has the negative value, as CO_3^{2-} ion is an acceptor of protons. At higher values of $[CO_2]_{W0}$, when the dissociation of H_2CO_3 elevates the concentration of released protons, the reversible dissociation of water is suppressed to satisfy the condition K_w=constant. The protons are bound to OH^- ions and $\Delta[H^+]_{H_2O}$ acquires a negative value. If the value of $[CO_2]_{W0} \leq 1.00\times10^{-6}$ mmol·L^{-1}, $\Delta[H^+]_{H_2CO_3}$ has a negative value as a reversible dehydration of H_2CO_3 takes place.

4.3.4. Model-calculated vs experimental data in the closed system

Experimentally measured and model-calculated [Ca^{2+}] and pH values are presented in Tab 10.

Table 10. Experimentally measured and model-calculated [Ca^{2+}] and corresponding final pH values in the closed H_2O–$[CO_2]_W$–$(CaCO_3)_S$ system

$[CO_2]_{W0}$ (mmol L^{-1})	$\sum[CO_X]_W$ calculated (mmol L^{-1})	$[Ca^{2+}]$ measured (mmol L^{-1})	$[Ca^{2+}]$ calculated (mmol L^{-1})	pH value measured in water with $CaCO_3$	pH value calculated
1.32×10^{-2}	1.20×10^{-1}	0.11±0.01	0.10	9.74±0.05	9.79
3.39×10^{-2}	1.47×10^{-1}	0.12±0.01	0.11	9.61±0.04	9.65
3.39×10^{-1}	7.09×10^{-1}	0.37±0.01	0.36	8.32±0.06	8.38
3.39	5.53	2.07±0.02	2.09	6.68±0.09	6.83
1.02×10^{1}	1.38×10^{1}	3.62±0.04	3.57	6.29±0.08	6.37
3.39×10^{1}	3.99×10^{1}	5.80±0.04	5.78	5.91±0.04	5.95

The experimental data for the [Ca^{2+}] were in compliance with the developed theoretical model: values were in the range of 0.11÷5.80 mmol·L^{-1} (Tab 10). Thus, we found evidence in favour of the validity of the theoretical model developed during this study.

Fig 20 shows that the final pH value in the water phase does not depend on the amount of added $CaCO_3$. A higher initial amount of $CaCO_3$ resulted in a faster increase in pH value due to the larger total surface area of salt particles ($m^2 \cdot kg^{-1}$) and hence larger interfacial surface. Experimentally measured stabilized pH values in the range of initial summarized concentrations of $\sum[CO_2]_{W0}$ from 1.20×10^{-1} to 3.99×10^{1} mmol·L^{-1} are shown in Tab 10.

As seen in Fig 21 in page 60 and tables (9) and (10), the experimental results correspond to the theoretical model to the accuracy of approximately 0.1 pH units. Adding 1000 mg of $CaCO_3$, the stabilisation of pH value (achieving a 'plateau') took about two minutes.

For comparison, an experimental pH value of 9.95 (at temperature of 25 °C) was reported by Garrels RM and Christ CL via adding $CaCO_3$ to the equilibrium system of water–air [159].

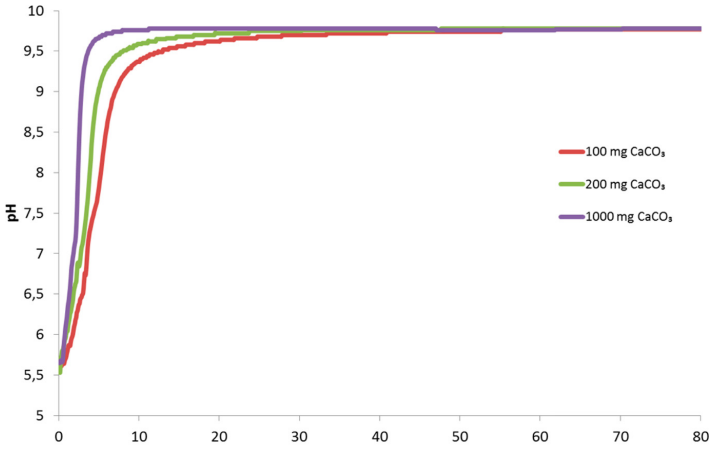

Figure 20. Measured pH values of the closed equilibrium system H_2O–$[CO_2]_W$–$(CaCO_3)_S$ at different added amounts of $CaCO_3$ ($mg \cdot L^{-1}$)

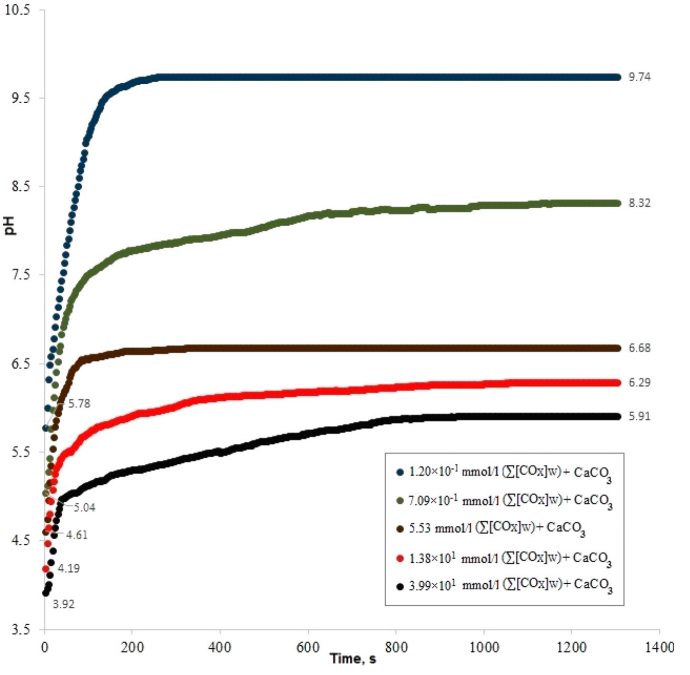

Figure 21. Experimentally measured pH values of the closed equilibrium system H_2 $[CO_2]_W$–$(CaCO_3)_S$ in the range of $\sum[COx]_{W0}$ from 1.20×10^{-1} to 3.99×10^{1} $mmol \cdot L^{-1}$ (t = 25 ºC)

4.4. Modelling of closed equilibrium system H_2O–$[CO_2]_W$–$(CaCO_3)_S$–NH_4Cl

4.4.1. Modelling of the system H_2O–$[CO_2]_W$–$(CaCO_3)_S$–NH_4Cl

In order to research the interconnection between carbonaceous and ammoniacal equilibria, a closed equilibrium system H_2O–$[CO_2]_W$–$(CaCO_3)_S$–NH_4Cl has been modelled and a series of experiments have been conducted in order to validate the model. The closed equilibrium system H_2O–$(CO_2)_W$–$(CaCO_3)_S$, where selected initial values of $[CO_2]_{W0}$ were taken as constants, served as a base for modelling. To this system, solid NH_4Cl was added, resulting in a transformation to the final equilibrium system H_2O–$(CO_2)_W$–$(CaCO_3)_S$–NH_4Cl where the ions and molecules were quantitatively distributed in accordance with the equilibrium constants as shown in Fig 22.

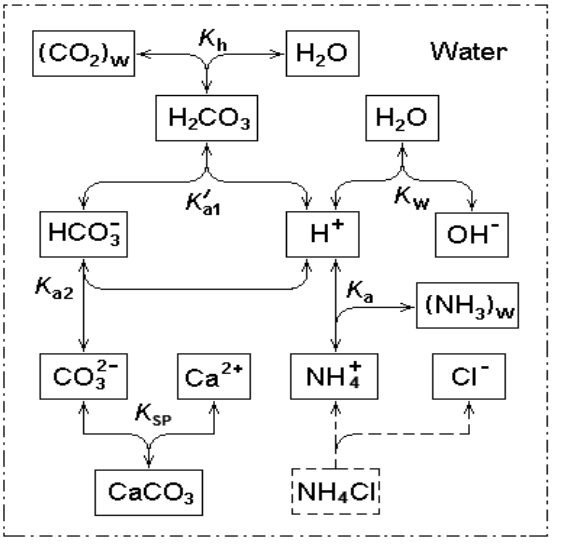

Figure 22. Structural scheme of the equilibrium distribution of ions and molecules in the final closed equilibrium system H_2O–$[CO_2]_W$–$(CaCO_3)_S$–NH_4Cl. K_h is the hydration constant of CO_2, K'_{a1} the true acid dissociation constant of H_2CO_3, K_{a2} the acid dissociation constant of HCO_3^-, K_{SP} is the solubility product constant of $CaCO_3$, K_W the ion–product constant of water, and K_a the acid dissociation constant of NH_4^+ ions

The values of the equilibrium constants for carbonaceous species and water in the equilibrium system are given by equations (39)-(42) and 50. The acid dissociation constant of the NH_4^+ ions is expressed as:

$$K_a = \frac{[NH_3]_W \times [H^+]}{[NH_4^+]} \cong 5.6 \times 10^{-10} \text{ mol} \cdot \text{L}^{-1} \text{ [160]} \qquad (61)$$

In the closed system H_2O–$(CO_2)_w$–$(CaCO_3)_S$–NH_4Cl, the charge balance is:

$$2[Ca^{2+}]+[H^+]+[NH_4^+]=2[CO_3^{2-}]+[HCO_3^-]+[OH^-]+[Cl^-], \quad (62)$$

The molar balance of carbonaceous ions and molecules is:

$$\sum[CO_X]_W=\sum[CO_X]_{W0}+[Ca^{2+}]=[CO_3^{2-}]+[H_2CO_3]+[HCO_3^-]+[CO_2]_W \quad (63)$$

where $\sum[CO_X]_W$ is the total amount of carbonaceous ions and molecules and $\sum[CO_X]_{W0}$ is the initial total amount of carbonaceous ions and molecules. It is the same as the molar balance equation in the closed system H_2O–$(CO_2)_W$–$(CaCO_3)_S$ (Eq 56). Thus, the mass conservation criterion for carbonaceous ions and molecules is not changed by the adding of NH_4Cl.

The molar balance equation of ammoniacal ions and molecules is:

$$[NH_4Cl]_S=[NH_4^+]+[NH_3]_W=[Cl^-]\ = constant, \quad (64)$$

where $[NH_4Cl]_S$ is the amount of NH_4Cl added to the equilibrium system of H_2O–$(CO_2)_W$–$(CaCO_3)_S$.

Calculation of $[CO_2]_W$, $[CO_3^{2-}]$, $[H_2CO_3]$, $[HCO_3^-]$, $[H^+]$, $[OH^-]$, $[Ca^{2+}]$, $[NH_4^+]$, and $[NH_3]$ in the final equilibrium system requires solution of nine equations (39-42), (50) and (61-64). To decrease the number of unknowns, the composite constant K_{a1} given by Eq 45 as in chapters 3.3.1 and 3.3.3 is used. On the basis of equations (61) and (64) the next equation is developed:

$$[NH_4^+]=[Cl^-]\times\frac{[H^+]}{[H^+]+K_a}. \quad (65)$$

The concentration variables in charge and molar balance equations are eliminated by replacing them with their algebraic expressions using equations (40-42), (45), (50) and (65). As a result of these replacements, two equations with two unknown concentrations ($[HCO_3^-]$ and $[H^+]$) are obtained. The charge and molar balance equations are converted to the following forms (**paper VI**):

$$[HCO_3^-]_Z=\frac{-\left(\frac{K_W}{[H^+]}-[H^+]+\frac{[Cl^-]\times K_a}{[H^+]+K_a}\right)+\sqrt{\left(\frac{K_W}{[H^+]}-[H^+]+\frac{[Cl^-]\times K_a}{[H^+]+K_a}\right)^2+8\left(\frac{2K_{a2}}{[H^+]}+1\right)\times\frac{K_{SP}\times[H^+]}{K_{a2}}}}{2\left(2\times\frac{K_{a2}}{[H^+]}+1\right)}, \quad (66)$$

$$[HCO_3^-]_M = \frac{\sum[CO_X]_{W0} + \sqrt{\left(\sum[CO_X]_{W0}\right)^2 + 4\left(\frac{K_{a2}}{[H^+]} + 1 + \frac{[H^+]}{K_{a1}}\right) \times \frac{K_{SP} \times [H^+]}{K_{a2}}}}{2\left(\frac{K_{a2}}{[H^+]} + 1 + \frac{[H^+]}{K_{a1}}\right)} \quad . \qquad (67)$$

The equations (66) and (67) contain only one unknown: the $[H^+]$. The equilibrium values of $[HCO_3^-]$ and $[H^+]$ are calculated by an iterative method, using different values of $[H^+]$ (analogously with chapters 4.3.1 and 4.3.3, **papers IV** and **V**).

The calculation of equilibrium values of $[Ca^{2+}]$, $[NH_3]$, $\sum[CO_X]_W$, and pH is performed on the basis of calculated equilibrium values of $[HCO_3^-]$ and $[H^+]$. The uptake of protons by CO_3^{2-} ions ($\Delta[H^+]_{CO_3^{2-}}$), the quantity of protons released from the dissociation of water ($\Delta[H^+]_{H_2O}$), H_2CO_3 ($\Delta[H^+]_{H_2CO_3}$), and from the dissociation of NH_4^+ ions ($\Delta[H^+]_{NH_4^+}$) at a concentration of NH_4Cl = 71 mmol·L^{-1} (with concentrations of $[CO_2]_{W0}$, $[NH_3]$, $[Ca^{2+}]$, $[HCO_3^-]$, and pH) are presented in Tab 11. The concentration of NH_4Cl = 71 mmol·L^{-1} roughly corresponds to the concentration of ammoniacal species in the reject water from anaerobic digestion of municipal sewage sludge [23, 45].

In the range of $[CO_2]_{W0}$ from 33.9 mmol·L^{-1} to 3.39×10^{-7} mmol·L^{-1}, adding NH_4Cl to the initial closed system H_2O–$[CO_2]_{W0}$–$(CaCO_3)_S$ results in a drop in pH in the new equilibrium system H_2O–$[CO_2]_{W0}$–$(CaCO_3)_S$–NH_4Cl as presented in Tables (11) and (12). The lower is the initial concentration of CO_2 in water, $[CO_2]_{W0}$, the fewer protons are released from dissociation of H_2CO_3, and the main amount of protons that will react with CO_3^{2-} are taken from the dissociation of NH_4^+. As seen from Tab 12, in the range of $[CO_2]_{W0}$ from 3.39×10^{-7} mmol·L^{-1} to 3.39×10^{-2} mmol·L^{-1}, the concentration of bicarbonate ion, $[HCO_3^-]$, is less than the $[H^+]$ released from the dissociation of NH_4^+. The difference between the $\Delta[H^+]_{NH_4^+}$ and $\Delta[H^+]_{CO_3^{2-}}$ is equal to the negative proton transfer value of $\Delta[H^+]_{H_2CO_3}$, which is related to the reversible dehydration of H_2CO_3 that is taking place in the given range of $[CO_2]_{W0}$. In this case, the dissociation of NH_4^+, dehydration of H_2CO_3, and dissolution of $CaCO_3$ determine the equilibrium processes.

Table 11. Results of the calculations of the equilibrium parameters after adding 71 mmol·L^{-1} NH_4Cl to the closed initial system of H_2O–$(CO_2)_{W0}$–$(CaCO_3)_S$ containing $[CO_2]_{W0}$ 3.39×10^{-7} to 33.9 mmol·L^{-1} at t = 25°C

$[CO_2]_{W0}$ mmol·L^{-1}	$\Delta[H^+]_{H_2O}$ mmol·L^{-1}	$\Delta[H^+]_{H_2CO_3}$ mmol·L^{-1}	$\Delta[H^+]_{CO_3^{2-}}$ mmol·L^{-1}	$\Delta[H^+]_{NH_4^+}$ mmol·L^{-1}	pH	$[NH_3]$ mmol·L^{-1}	$[Ca^{2+}]$ mmol·L^{-1}	$[HCO_3^-]$ mmol·L^{-1}
3.39×10^{-7}	3.63×10^{-4}	-6.85×10^{-2}	–1.28	1.35	7.59	1.35	1.28	1.21
1.00×10^{-6}	3.63×10^{-4}	-6.85×10^{-2}	–1.28	1.35	7.59	1.35	1.28	1.21
1.02×10^{-5}	3.63×10^{-4}	-6.84×10^{-2}	–1.28	1.35	7.59	1.35	1.28	1.21
2.37×10^{-5}	3.63×10^{-4}	-6.84×10^{-2}	–1.28	1.35	7.59	1.35	1.28	1.21
3.39×10^{-5}	3.63×10^{-4}	-6.83×10^{-2}	–1.28	1.35	7.59	1.35	1.28	1.21
3.39×10^{-4}	3.63×10^{-4}	-6.78×10^{-2}	–1.28	1.35	7.59	1.35	1.28	1.21
3.05×10^{-3}	3.62×10^{-4}	-6.47×10^{-2}	–1.28	1.34	7.58	1.34	1.28	1.21
1.32×10^{-2}	3.59×10^{-4}	-5.43×10^{-2}	–1.28	1.331	7.58	1.33	1.28	1.22
3.39×10^{-2}	3.52×10^{-4}	-3.44×10^{-2}	–1.28	1.310	7.57	1.31	1.28	1.24
3.39×10^{-1}	2.70×10^{-4}	2.41×10^{-2}	–1.30	1.052	7.48	1.052	1.29	1.53
2.01	1.29×10^{-5}	1.40	–1.77	3.78×10^{-1}	7.03	3.78×10^{-1}	1.77	3.18
2.15	$\mathbf{3.29\times10^{-8}}$	**1.47**	**–1.82**	$\mathbf{3.52\times10^{-1}}$	**7.00**	$\mathbf{3.52\times10^{-1}}$	**1.82**	**3.29**
2.45	-2.54×10^{-7}	1.61	–1.92	3.11×10^{-1}	6.94	3.11×10^{-1}	1.92	3.53
3.39	-9.27×10^{-5}	1.99	–2.22	2.26×10^{-1}	6.80	2.26×10^{-1}	2.22	4.21
10.2	-4.12×10^{-4}	3.51	–3.63	1.21×10^{-1}	6.36	1.21×10^{-1}	3.63	7.14
33.9	-1.12×10^{-3}	5.76	–5.79	3.17×10^{-2}	5.95	3.17×10^{-2}	5.79	11.56

The $[H^+]$ released from dissociation of NH_4^+ ions ($\Delta[H^+]_{NH_4^+}$) is equal to the concentration of NH_3. At higher $[CO_2]_{W0}$, in the range of 2.45 mmol·L^{-1} to 33.9 mmol·L^{-1}, the dissociation of H_2CO_3 predominates and produces more protons than are released by the dissociation of NH_4^+, with a corresponding decrease in pH below 7. After adding solid NH_4Cl into sytem, the interval, where $\Delta[H^+]_{H_2CO_3}$ values are negative, is widened towards higher values of $[CO_2]_{W0}$ and lies in the range of 3.39×10^{-7} to 3.39×10^{-2} mmol·L^{-1}. If the initial concentration of dissolved CO_2 is 2.15 mmol·L^{-1} and added NH_4Cl (solid) concentration is 71 mmol L^{-1}, the corresponding pH value is 7.00. In the range of $[CO_2]_{W0}$ values from 2.45 to 33.9 mmol L^{-1}, values of $\Delta[H^+]_{H_2O}$ are negative, while dissociation of water is suppressed.

Tab 12 shows the calculated values of $\sum[CO_X]_W$, $[Ca^{2+}]$, $[NH_3]_W$, $[NH_4^+]$ and pH, when various amounts of NH_4Cl are added to the system H_2O–$[CO_2]_{W0}$–$(CaCO_3)_S$ with different initial concentrations of CO_2. It can be seen that both, higher $[CO_2]_{W0}$ and higher dose of NH_4Cl, cause an increase in solubility of Ca^{2+} ions and decrease of pH, as well as a decrease in $[NH_3]_W$ to $[NH_4^+]$ ratio, indicating the interdependency of carbonaceous and ammoniacal equilibria.

However, in real reject water the NH_4^+ ions are counterbalanced with HCO_3^- ions rather than Cl^-, thus, the proton balance is different from that of the model, and the $[NH_3]_W$ to $[NH_4^+]$ ratio is correspondingly affected.

Table 12. The calculated values of $\sum[CO_X]_W$, $[Ca^{2+}]$, $[NH_3]_W$, $[NH_4^+]$ and pH, when $CaCO_3$ and various amounts of NH_4Cl are added to the system H_2O–$[CO_2]_{W0}$ with different initial concentrations of CO_2 at t=25 ºC

$[CO_2]_{W0}$ mmol·L^{-1}	Variable	Initial values	Added $[NH_4Cl]_S$, mmol·L^{-1}				
			0.0	**27.0**	**55.0**	**71.0**	**105.0**
0.00	$\sum[CO_X]_W$, mmol·L^{-1}	0.00	0.10	0.92	1.17	1.28	1.46
	$[Ca^{2+}]$, mmol·L^{-1}	–	0.10	0.92	1.17	1.28	1.46
	$[NH_3]_W$, mmol·L^{-1}	–	0.00	0.95	1.22	1.35	1.56
	$[NH_4^+]$, mmol·L^{-1}	–	0.00	26.06	53.78	69.66	103.44
	pH	**7.00**	**9.88**	**7.86**	**7.66**	**7.59**	**7.48**
1.32×10^{-2}	$\sum[CO_X]_W$, mmol·L^{-1}	1.57×10^{-2}	0.12	0.94	1.19	1.29	1.48
	$[Ca^{2+}]$, mmol·L^{-1}	–	0.10	0.92	1.17	1.28	1.46
	$[NH_3]_W$, mmol·L^{-1}	–	0.00	0.93	1.21	1.33	1.54
	$[NH_4^+]$, mmol·L^{-1}	–	0.00	26.07	53.79	69.67	103.46
	pH	**5.61**	**9.78**	**7.85**	**7.65**	**7.58**	**7.47**
3.39×10^{-1}	$\sum[CO_X]_W$, mmol·L^{-1}	3.52×10^{-1}	0.71	1.31	1.55	1.65	1.82
	$[Ca^{2+}]$, mmol·L^{-1}	–	0.36	0.96	1.19	1.29	1.47
	$[NH_3]_W$, mmol·L^{-1}	–	0.00	0.66	0.93	1.05	1.26
	$[NH_4^+]$, mmol·L^{-1}	–	0.00	26.34	54.07	69.95	103.74
	pH	**4.90**	**8.38**	**7.67**	**7.54**	**7.48**	**7.39**
3.39	$\sum[CO_X]_W$, mmol·L^{-1}	3.44	5.53	5.58	5.63	5.66	5.71
	$[Ca^{2+}]$, mmol·L^{-1}	–	2.09	2.14	2.19	2.22	2.28
	$[NH_3]_W$, mmol·L^{-1}	–	0.00	0.09	0.18	0.23	0.33
	$[NH_4^+]$, mmol·L^{-1}	–	0.00	26.91	54.82	70.77	104.68
	pH	**4.40**	**6.83**	**6.82**	**6.81**	**6.80**	**6.79**
33.9	$\sum[CO_X]_W$, mmol·L^{-1}	34.1	39.89	39.90	39.91	39.91	39.91
	$[Ca^{2+}]$, mmol·L^{-1}	–	5.78	5.79	5.79	5.79	5.80
	$[NH_3]_W$, mmol·L^{-1}	–	0.00	0.01	0.03	0.03	0.05
	$[NH_4^+]$, mmol·L^{-1}	–	0.00	26.99	54.98	70.97	104.95
	pH	**3.90**	**5.95**	**5.95**	**5.95**	**5.95**	**5.95**

4.4.2. Model-predicted vs experimental data in the system H_2O–$[CO_2]_W$–$(CaCO_3)_S$–NH_4Cl

The experiments were performed in a closed reaction cell, where $CaCO_3$ was added to the initial equilibrium system H_2O–$[CO_2]_{W0}$, and a supplementary amount of CO_3^{2-} and Ca^{2+} ions were released by the dissolution of $CaCO_3$. As shown in Fig 23, in the range of initial concentrations of CO_2 in water from 3.39×10^{-5} to 33.9 mmol L^{-1}, adding $CaCO_3$ to the equilibrium system caused the rise of pH value to about 2÷4 units, depending on the $[CO_2]_{W0}$. Maximum value of pH was 9.89±0.03 when $[CO_2]_{W0}$ was 3.39×10^{-5} mmol L^{-1}, which coincides with the theoretically calculated pH value. Adding solid $CaCO_3$ to the initial equilibrium system in the range of $[CO_2]_{W0}$ from 3.39 to 33.9 mmol L^{-1} resulted in the final pH value remaining below 7.

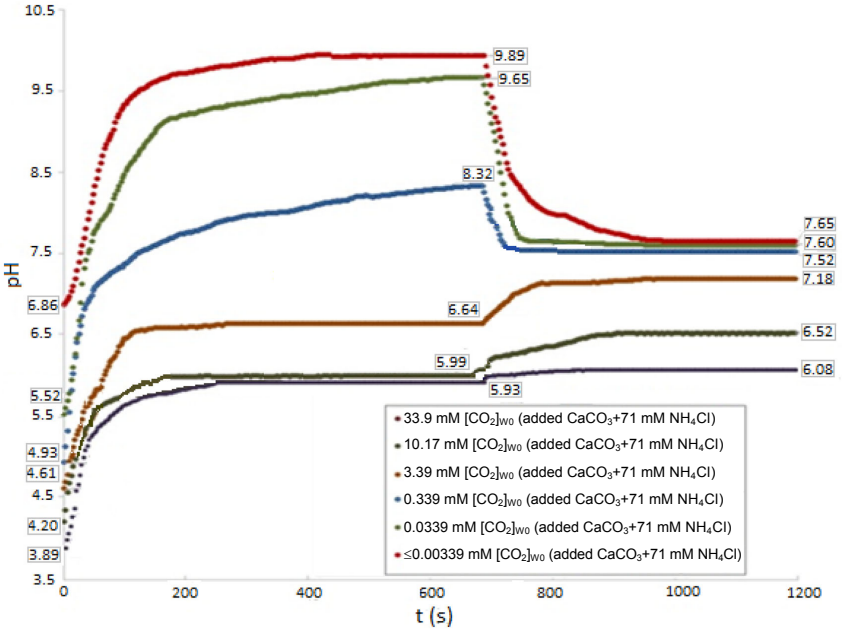

Figure 23. Experimentally measured pH values of the closed equilibrium system H_2O–$[CO_2]_W$–$CaCO_3$–NH_4Cl at the concentration range of $[CO_2]_{W0}$ 3.39×10^{-5} to 33.9 mmol L^{-1} at t = 25 ºC

NH_4Cl (71 mmol·L^{-1}) was added, when at least ten minutes had passed from the addition of solid $CaCO_3$ and no significant change in pH of the equilibrium system was observed any more. The addition of NH_4Cl can be seen as an abrupt change of pH curve between 600 and 800 seconds from the beginning of the experiment. As seen on Fig 23, at initial concentrations of $(CO_2)_W$ from 3.39×10^{-5} to 3.39×10^{-1} mmol L^{-1}, the pH values decreased after NH_4Cl was added to the initial system of H_2O–$(CO_2)_W$–$CaCO_3$. The maximum change in pH value was 2.24±0.02 units at $[CO_2]_{W0}$ 3.39×10^{-5} mmol L^{-1}, with the final pH value reaching 7.65±0.02. However, at higher initial concentrations of $(CO_2)_W$ in the range from 3.39 to 33.9 mmol L^{-1}, the final pH values increased up to 7.18±0.03 after NH_4Cl was added to the initial system of H_2O–$(CO_2)_W$–$(CaCO_3)_S$. The maximum change in pH was 0.54±0.03, when initial concentration of CO_2 in water was 3.39 mmol L^{-1}. This indicates that pH values of final system were significantly affected by higher $[CO_2]_{W0}$ in the solutions.

As shown in Tab 13, experimentally measured final stabilized pH values of the closed equilibrium system H_2O–$[CO_2]_W$–$(CaCO_3)_S$–NH_4Cl were generally close to the theoretical ones. Small differences (ΔpH_{max}=0.12 pH units) in these obtained values might be caused by the inaccurate gas preparation and flow control system.

Table 13. Experimental and model-predicted concentrations of $[Ca^{2+}]$ and corresponding final pH values in the closed H_2O–$[CO_2]_{W0}$–$(CaCO_3)_S$–NH_4Cl equilibrium system after adding 71 mmol L^{-1} NH_4Cl

$[CO_2]_{W0}$, mmol·L^{-1}	$[Ca^{2+}]$ measured, mmol·L^{-1}	$[Ca^{2+}]$ theoretically predicted, mmol·L^{-1}	pH value measured after addition of NH_4Cl	pH value theoretically predicted
3.39×10^{-5}	0.11±0.01	0.10	7.65±0.06	7.59
1.32×10^{-2}	0.12±0.01	0.11	7.60±0.03	7.58
3.39×10^{-1}	0.37±0.01	0.36	7.52±0.04	7.48
3.39	2.07±0.02	2.09	7.18±0.06	6.80
10.2	3.62±0.04	3.57	6.52±0.05	6.36
33.9	5.82±0.04	5.78	6.08±0.04	5.95

The values of the concentration of Ca^{2+} ions determined experimentally were in accordance with the developed theoretical model being in the range from 0.11÷5.82 mmol·L^{-1} (Tab 13). As seen in Fig 23 and Tables (11)–(13), the experimental results corresponded to the theoretical model, which supported the validity of our novel proton transfer model linking different acid-base equilibria. The same approach can be applied to complex self-regulating systems involving more acid-base equilibria (e.g. phosphoric acid equilibrium). Thus, the validity of developed theoretical model was confirmed as a result of the present empirical study.

5. CONCLUSIONS

SRAO studies:

- The SRAO process was started up both in a MBBR system and in an UASBR system, using different inocula;
- However, compared to the conventional Anammox UASBR, the SRAO was significantly less efficient and less stable, whereas there was no significant difference between the SRAO MBBR system and SRAO UASBR system. Only about one fourth of influent total nitrogen was removed by SRAO process, while in conventional anammox, ca two thirds of influent total nitrogen was removed;
- The SRAO process took place as one reaction of the multiple complex interactions between nitrogen compounds, sulphur compounds and organic matter (containing quinoid groups). This resulted in a significantly higher removal ratio of NH_4^+ than the SRAO stoichiometry predicts. The presence of denitrifying sulphur-oxidizing microorganism *Sulfurimonas denitrificans* DSM 1251 in the seeding sludge of SRAO UASBR and in the reactor's sludge sample provided evidence in favor of this denitrification process.

Pilot studies:

- Pilot-scale (3 m^3) deammonification process was started-up in three configurations without anammox-specific inoculation using high-strength undiluted reject water as the sole source of functional bacteria. The process conditions were dictated by the realtime technological conditions of the sludge dewatering process in Tallinn municipal wastewater treatment plant;
- It was demonstrated that the autotrophic nitrogen removal could be started up independently of applied technological concept. However, the most stable and efficient nitrogen removal occurred in single-reactor biofilm system. Total nitrogen removal rates up to 1.04 kg-N m^{-3} d^{-1} and 0.3 kg-N m^{-3} d^{-1} were achieved in the single-reactor biofilm- and sludge-based deammonification processes, respectively. In the two-stage system, the maximum total nitrogen removal rate was much lower mainly owing to the limited volume of nitritation reactor. The average total nitrogen removal efficiencies (in %) in the final stage of operation were 82±15, 73±14, and 72±24 in the single-stage deammonification biofilm reactor, single-stage SBR and anammox reactor, respectively;
- The critical factors for successful start-up and stable operation were keeping pH below 7.5, dissolved oxygen at 0.3 ÷ 0.8 mg-O_2 L^{-1} and concentration of suspended solids in the influent below 1000 NTU;
- Free ammonia was the main inhibitory factor for deammonifying and anammox consortia of microorganisms prior to application of pH adjustment. The pH adjustment below 7.5 in order to maintain the estimated free ammonia concentration below 10 mg-NH_3-N L^{-1} resulted in a successful start-up for all reactors achieving a total nitrogen removal efficiency of over 50% within 4 ÷ 6 months.

Studies of chemical equilibria:

- Matematical models for an open system $(CO_2)_G$–H_2O–$(CO_2)_W$–H_2CO_3–HCO_3^-–CO_3^{2-}–$(CaCO_3)_S$ and for two closed systems, H_2O–$(CO_2)_W$–H_2CO_3–HCO_3^-–CO_3^{2-}–$(CaCO_3)_S$ and H_2O–$(CO_2)_W$–$(CaCO_3)_S$–NH_4Cl, were developed and experimentally verified. These models allowed the calculation on pH and concentrations of all species (ions and molecules) in the liquid phase;
- In the open system $(CO_2)_G$–H_2O–$(CO_2)_W$–H_2CO_3–HCO_3^-–CO_3^{2-}–$(CaCO_3)_S$ with $P(CO_2)_G$ = 390 ppm at t = 25 °C, the equilibrium value of pH was 8.2. The minimum solubility of $(CaCO_3)_S$ was ≅ 0.1 mmol L^{-1} at t = 25°C and $P(CO_2)_G$= 0.692 ppm. Under these conditions, the net interfacial transfer of CO_2 equalled zero, corresponding to the case of closed system;
- In the closed system H_2O–$(CO_2)_W$–H_2CO_3–HCO_3^-–CO_3^{2-}–$(CaCO_3)_S$, the pH of liquid phase is alkaline when $\sum[CO_X]_{W0}$ ranged from 1.88×10^{-6} to 0.352 mmol L^{-1} with the maximum value of 9.88 ± 0.03. In the range of $\sum[CO_X]_{W0}$ from 2.54 to 34.10 mmol L^{-1}, the pH of liquid phase is acidic. When the closed system H_2O–$(CO_2)_W$–H_2CO_3–HCO_3^-–CO_3^{2-}–$(CaCO_3)_S$, is formed, CO_3^{2-} ions in the liquid phase will accept protons ($\Delta[H^+]_{CO_3^{2-}}$) originating either from the dissociation of water ($\Delta[H^+]_{H_2O}$) or H_2CO_3 ($\Delta[H^+]_{H_2CO_3}$). The smaller was the initial concentration of CO_2 in water, the fewer protons were released from H_2CO_3. Thus, the dissociation of water at lower concentrations of $[CO_2]_{W0}$ gives the main amount of protons that will be bound to CO_3^{2-} ions and the pH of liquid phase will rise;
- In the system H_2O–$(CO_2)_W$–$(CaCO_3)_S$–NH_4Cl, at lower $[CO_2]_{W0}$ the main source of protons in the liquid phase are NH_4^+ ions and at higher initial concentrations of $(CO_2)_W$ the main source of protons is H_2CO_3;
- Content of toxic NH_3 in water was affected by the interaction between carbonaceous and ammoniacal equilibrium processes and can be estimated on the basis of developed model with a greater accuracy than on the basis of earlier published methods. The developed models allow one to assess the impact of anthropogenic processes on the environment and could be applied in water and wastewater treatment. The models are useful in the development of innovative methods for measuring concentrations of CO_2 and NH_3 in water.

6. REFERENCES

1. Gilbert EM, Agrawal S, Karst SM, Horn H, Nielsen PH, Lackner S. (**2014**) Low temperature partial nitritation/anammox in a moving bed biofilm reactor treating low strength wastewater. *Environ Sci Technol* 48(15): 8784–8792; 10.1021/es501649m.
2. Lotti T, Kleerebezem R, Hu Z, Kartal B, de Kreuk MK, van Erp Taalman Kip C, Kruit J, Hendrickx TL, van Loosdrecht MCM. (**2015**) Pilot-scale evaluation of Anammox-based mainstream nitrogen removal from municipal wastewater. *Environ Technol* 36: 1167–1177; 10.1080/09593330.2014.982722.
3. Zekker I, Rikmann E, Tenno T, Vabamäe P, Tomingas M, Menert A, Loorits L, Tenno T. (**2012**) Anammox bacteria enrichment and phylogenetic analysis in moving bed biofilm reactors. *Environ Eng Sci* 29(10): 946–950; 10.1080/09593330.2011.588962.
4. Kartal B, Kuenen JG and van Loosdrecht MCM. (**2010**) Sewage treatment with Anammox. *Science* 328(5979): 702-703; 10.1126/science.1185941.
5. Terada A, Zhou S and Hosomi M. (**2011**) Presence and detection of anaerobic ammonium oxidizing (Anammox) bacteria and appraisal of Anammox process for high-strength nitrogenous wastewater treatment. *Clean Technol Environ Policy* 13(6): 759–781; 10.1007/s10098-011-0355-3.
6. Ma B, Zhang S, Zhang L, Yi P, Wang J, Wang S and Peng Y. (**2011**) The feasibility of using a two-stage autotrophic nitrogen removal process to treat sewage. *Bioresour Technol* 102(17): 8331-8334; 10.1016/j.biortech.2011.06.017.
7. Driessen W, Abma W, Van Zessen E, Reitsma G and Haarhuis R. Sustainable Treatment of Reject Water and Industrial Effluent by Producing Valuable By-Products. (**2009)** In: *Proceedings of the 14th European Biosolids and Organic Resources Conference*, 9th–11th November, Leeds, UK.
8. Mehrdad M, Park H, Ramalingam K, Fillos J, Beckmann K, Deur A, Chandran K. (**2014**) Anammox moving bed biofilm reactor pilot at the 26th Ward wastewater treatment plants in Brooklyn, New York: start-up, biofilm population diversity and performance optimization. *Water Sci Technol* 70: 1448–55; 10.2166/wst.2014.362.
9. Abma WR, Schultz CE, Woutres JW, Mulder JW, van Loosdrecht MCM, van der Star W, Strous M, Tokutomi T. (**2006)** Full Scale Granular Sludge ANAMMOX® process. In: *Proceedings of the 4th CIWEM Annual Conference*, 4th 12th–14th September, Newcastle, UK.
10. Liu S, Yang F, Gong Z, Meng F, Chen H, Xue Y, Furukawa K. (**2008**) Application of anaerobic ammonium-oxidizing consortium to achieve completely autotrophic ammonium and sulfate removal. *Bioresour Technol* 99: 6817–6825; 10.1016/j.biortech.2008.01.054.
11. Lei Z, Ping Z, YuHui H and RenCun J. (**2009**) Performance of sulfate-dependent anaerobic ammonium oxidation. *Sci China B* 52(1): 86–92; 10.1007/s11426-008-0161-x.
12. Yang Z, Zhou S and Sun Y. (**2009**) Start-up of simultaneous removal of ammonium and sulfate from an anaerobic ammonium oxidation (anammox) process in an anaerobic up-flow bioreactor. *J Hazard Mater* 169: 113–118; 10.1016/j.jhazmat.2009.03.067.
13. Prachakittikul P, Wantawin C, Noophan PL, Boonapatcharoen N. (**2016**) ANAMMOX-like performances for nitrogen removal from ammonium-sulfate-

rich wastewater in an anaerobic sequencing batch reactor. *J Environ Sci Health A Tox Hazard Subst Environ Eng* 50(3): 220-228; 10.1080/10934529.2015.1094336.
14. Zhao Q-I, Li W and You S-J. (**2006**) Simultaneous removal of ammonium-nitrogen and sulfate from wastewaters with an anaerobic attached-growth bioreactor. *Water Sci Technol* 54(8): 27–35; 10.2166/wst.2006.762.
15. Jing C, JianXiang J & Ping Z. (**2010**) Isolation and identification of bacteria responsible for simultaneous anaerobic ammonium and sulfate removal. *Sci China Chem* 53(3): 645–650; 10.1007/s11426-010-0053-8.
16. Zekker I, Rikmann E, Tenno T, Menert A, Lemmiksoo V, Saluste A, Tomingas M, Tenno T. (**2011**) Modification of nitrifying biofilm into nitritating one by combination of increased free ammonia concentrations, lowered HRT and dissolved oxygen concentration. *J Environ Sci* 23(7): 1113–1121; 10.1016/S1001-0742(10)60523-2.
17. Zekker I, Rikmann E, Tenno T, Menert A, Loorits L, Vabamäe P, Tomingas M, Tenno T. (**2012**) Anammox enrichment from reject water on blank biofilm carriers and carriers containing nitrifying biomass: operation of two moving bed biofilm reactors (MBBR). *Biodegradation* 23(4): 547–560; 10.1007/s10532-011-9532-7.
18. Zekker I, Rikmann E, Tenno T, Vabamäe P, Kroon K, Loorits L, Saluste A, Tenno T. (**2012**) Effect of HCO_3^- concentration on anammox nitrogen removal rate in a moving bed biofilm reactor. *Environ Technol* 33(20): 2263–2271; 10.1080/09593330.2012.665487.
19. Zekker I, Rikmann E, Tenno T, Kroon K, Vabamäe P, Salo E, Loorits L, DC Rubin SSC, Vlaeminck S; Tenno T. (**2013**) Deammonification process start-up after enrichment of anammox microorganisms from reject water in a moving bed biofilm reactor (MBBR). *Environ Technol* 34(23): 3095–3101; 10.1080/09593330.2013.803134.
20. Zekker I, Rikmann E, Tenno T, Kroon K, Seiman A, Loorits L, Fritze H, Tuomivirta T, Vabamäe P, Raudkivi M, Mandel A, Tenno T. (**2015**) Start-up of low-temperature anammox in UASB from mesophilic yeast factory anaerobic tank inoculum. *Environ Technol* 36(2): 214–225; 10.1080/09593330.2014.941946.
21. Zekker I, Rikmann E, Tenno T, Seiman A, Loorits L, Kroon K, Tomingas M, Vabamäe P, Tenno T. (**2014**) Nitritating-anammox biomass tolerant to high dissolved oxygen concentration and C/N ratio in treatment of yeast factory wastewater. *Environ Technol* 35(12): 1565–1576; 10.1080/09593330.2013.874492.
22. Zekker I, Rikmann E, Tenno T, Loorits L, Kroon K, Fritze H, Tuomivirta T, Vabamäe P, Raudkivi M, Mandel A, DC Rubin SSC and Tenno T. (**2015**) Nitric oxide for anammox recovery in a nitrite-inhibited deammonification system. *Environ Technol* 36(19): 2477–2487; 10.1080/09593330.2015.1034791.
23. Zekker, I, Rikmann, E, Kroon, K, Mandel, A, Mihkelson, J, Tenno, T, Tenno, T. (**2017**) Ameliorating nitrite inhibition in a low-temperature nitritation–anammox MBBR using bacterial intermediate nitric oxide. *Int J Environ Sci Technol* 14(11): 2343–2356; 10.1007/s13762-017-1321-3.
24. Richard FA. (**1965**) Anoxic basins and Fjords. In: *Chemical Oceanography*, edited by Ripley JP and Skirrow G. pp. 611-643; Manhattan: Academic Press.
25. Broda E. (1977) Two kinds of lithotrophs missing in nature. *Z Allg Mikrobiol*, 17: 491–493; 10.1002/jobm.19770170611.
26. Strous M, Pelletier E, Mangenot S, Rattei T, Lehner A, Taylor MW, Horn M, Daims H, Bartol-Mavel D, Wincker P, Barbe V, Fonknechten N, Vallenet D,

Segurens B, Schenowitz-Truong C, Médigue C, Collingro A, Snel B, Dutilh BE, Op den Camp HJM, van der Drift C, Cirpus I, van de Pas-Schoonen KT, Harhangi HR, van Niftrik L, Schmid M, Keltjens J, van de Vossenberg J, Kartal B, Meier H, Frishman D, Huynen MA, Mewes H-W, Weissenbach J, Jetten MSM, Wagner M & Le Paslier D. (**2006**) Deciphering the evolution and metabolism of an anammox bacterium from a community genome. *Nature* 440: 790-794; 10.1038/nature04647.

27. Mulder A, Graaf AA, Robertson LA, Kuenen JG. (**1995**) Anaerobic ammonium oxidation discovered in a denitrifying fluidized bed reactor. *FEMS Microbiol Ecol* 16: 177–183; 10.1016/0168-6496(94)00081-7.
28. Lotti T, Kleerebezem R, Lubello C, van Loosdrecht MCM. (**2014**) Physiological and kinetic characterization of a suspended cell anammox culture. *Water Res* 60: 1–14; 10.1016/j.watres.2014.04.017.
29. Zekker I, Rikmann E, Tenno T, Saluste A, Tomingas M, Menert A, Loorits L, Lemmiksoo V & Tenno T. (**2012**) Achieving nitritation and anammox enrichment in a single moving-bed biofilm reactor treating reject water. *Environ Technol* 33(6): 703–710; 10.1080/09593330.2011.588962.
30. Ahn Y-H. (**2006**) Sustainable nitrogen elimination biotechnologies: A review. *Process Biochem* 41: 1709–1721; 10.1016/j.procbio.2006.03.033.
31. van de Graaf AA, de Bruijn P, Robertson LA, Jetten MSM, Kuenen GJ. (**1996**) Autotrophic growth of anaerobic ammonium-oxidizing micro-organisms in a fluidized bed reactor. *Microbiology* 142: 2187–2196; 10.1099/13500872-142-8-2187.
32. Strous M, Heijnen JJ, Kuenen JG, Jetten MSM. (**1998**) The sequencing batch reactor as a powerful tool for the study of slowly growing anaerobic ammonium-oxidizing microorganisms. *Appl Microbiol Biotechnol* 50(5): 589–596; 10.1007/s002530051340.
33. Jeanningros Y, Vlaeminck SE, Kaldate A, Verstraete W and Graveleau L. (**2010**) Fast start-up of a pilot-scale deammonification sequencing batch reactor from an activated sludge inoculum. *Water Sci Technol* 61(6): 1393–1400; 10.2166/wst.2010.019.
34. Yu YC, Gao DW and Tao Y. (**2013**) Anammox start-up in sequencing batch biofilm reactors using different inoculating sludge. *Appl Microbiol Biotechnol* 97: 6057–6064; 10.1007/s00253-012-4427-z.
35. Ni SQ, Gao BY, Wang CC, Lin JG, Sung S. (**2011**) Fast start-up, performance and microbial community in a pilot-scale anammox reactor seeded with exotic mature granules. *Bioresour Technol* 102: 2448–2454; 10.1016/j.biortech.2010.11.006.
36. Wang T; Zhang H; Yang F; Liu S; Fu Z; Chen H. (**2009**) Startup of the Anammox Process from the Conventional Activated Sludge in a Membrane Bioreactor. *Biotechnol Bioeng* 100: 2501–2506; 10.1016/j.biortech.2008.12.011.
37. Bi Z, Qiao S, Zhou J, Tang X and Cheng Y. (**2014**) Inhibition and recovery of Anammox biomass subjected to short-term exposure of Cd, Ag, Hg and Pb. *Chem Eng J* 244: 89–96; 10.1016/j.cej.2014.01.062.
38. Ali M and Okabe S. (**2015**) Anammox-based technologies for nitrogen removal: Advances in process start-up and remaining issues. *Chemosphere* 141: 144–153; 10.1016/j.chemosphere.2015.06.094.
39. Van Dongen U, Jetten MSM and Van Loosdrecht MCM. (**2001**). The SHARON-Anammox process for treatment of ammonium rich wastewater. *Water Sci Technol* 44(1): 153–160.

40. Sliekers AO, Derwort N, Campos Gomez JL, Strous M, Kuenen JG, Jetten MSM. (**2002**) Completely autotrophic nitrogen removal over nitrite in one single reactor. *Water Res* 36: 2475–2482; 10.1016/S0043-1354(01)00476-6.
41. De Clippeleir H, Yan X, Verstraete W, Vlaeminck SE. (**2011**) OLAND is feasible to treat sewage-like nitrogen concentrations at low hydraulic residence times. *Appl Microbiol Biotechnol* 90: 1537–45; 10.1007/s00253-011-3222-6.
42. Kalyuzhnyi S, Gladchenko M, Mulder A, Versprille B. (**2006**) DEAMOX-New biological nitrogen removal process based on anaerobic ammonia oxidation coupled to sulphide-driven conversion of nitrate into nitrite. *Water Res* 40: 3637–3645; 10.1016/j.watres.2006.06.010.
43. Hartwig P, Schmidtlein F, Beier M, Schneider Y and Rosenwinkel K-H. (2011) Nitritation/Denitritation with PANDA/PANDA+: Practical experience from WWTP with high industrial loading. *Proceedings of AGRO 2011, 8th IWA International Symposium on Waste Management Problems in Agroindustries*, Cesme, Izmir, Turkey, 22–24 June, pp. 431–438.
44. Hartwig P. (**2017**) Combined Treatment of Sewage Sludge and Solid Waste Organic Fraction – the Duplex-Technology. *IJEE* 8(1): 44–47; 10.5829/idosi.ijee.2017.08.01.08.
45. Berends DHJ, Salem G, van der Roest SHF and van Loosdrecht MCM. (**2005**) Boosting nitrification with the BABE technology. *Water Sci Technol* 52: 63–70.
46. Rosenwinkel KH and Cornelius A. (**2005**) Deammonification in the moving-bed process for the treatment of wastewater with high ammonia content. *Chem Eng Technol* 28: 49–52; 10.1002/ceat.200407070.
47. Regmi P, Bunce R, Miller MW, Park H, Chandran K, Wett B, Murthy S, Bott CB. (**2015**) Ammonia-based intermittent aeration control optimized for efficient nitrogen removal. *Biotechnol Bioeng* 12: 2060–67; 10.1002/bit.25611.
48. Christensson M, Ekström S, Andersson Chan A, Le Vaillant E and Lemaire R. (**2013**) Experience from start-ups of the first ANITA Mox Plants *Water Sci Technol* 67(12): 2677–2684; 10.2166/wst.2013.156.
49. Scherson YD, Wells GF, Woo SG, Lee J, Park J, Cantwell BJ, Criddle CS. (**2013**) Nitrogen removal with energy recovery through N_2O decomposition. *Energy Environ Sci* 6: 241–248; 10.1039/C2EE22487A.
50. Kartal B, van Niftrik L, Keltjens JT, Op den Camp HJ, Jetten MS. (**2012**). Anammox–Growth Physiology, Cell Biology, and Metabolism. *Adv Microb Physiol* 60: 211–262; 10.1016/B978-0-12-398264-3.00003-6.
51. Starke R, Müller M, Gaspar M, Marz M, Küsel K, Totsche KU, von Bergen M and Jehmlich N. (**2017**) Candidate Brocadiales dominates C, N and S cycling in anoxic groundwater of a pristine limestone-fracture aquifer. *J Proteomics* 152: 153–160; 10.1016/j.jprot.2016.11.003.
52. Fdz-Polanco F, Fdz-Polanco M, Fernández N, Urueña MA, Garciá PA, Villaverde S. (**2001**) Combining the biological nitrogen and sulfur cycles in anaerobic conditions. *Water Sci Technol* 44(8): 77-84; 10.2166/wst.2001.0469.
53. Strous M, Kuenen JG, Fuerst JA, Wagner M. and Jetten MSM. (**2002**) The anammox case – A new experimental manifesto for microbiological ecophysiology. *Antonie van Leeuwenhoek* 81(1–4): 693–702; 10.1023/A:1020590413079.
54. Schrum HN, Spivack AJ, Kastner M, and D'Hondt S. (**2009**) Sulfate-reducing ammonium oxidation: A thermodynamically feasible metabolic pathway in subseafloor sediment. *Geology* 37(10): 939–942; 10.1130/G30238A.1.

55. Yuan Y, Huang Y, Li X, Zhang C-L, Zhang Li, Pan Y, Liu F-X. (**2015**) Characteristics of Sulfate Reduction–Ammonia Oxidation under Anaerobic Conditions. *J Residuals Sci Tech* 12(S1): S155–S121; 10.12783/issn.1544-8053/12/S1/17.
56. Amend JP, Rogers KL, Shock EL, Gurrieri S and Inguaggiato S. (**2003**) Energetics of chemolithoautotrophy in the hydrothermal system of Vulcano Island, southern Italy. *Geobiology* 1: 37–58. 10.1046/j.1472-4669.2003.00006.x.
57. Sabumon PC. (**2007**) Anaerobic ammonia removal in presence of organic matter: A novel route. *J Hazard Mater* 149: 49–59; 10.1016/j.jhazmat.2007.03.052.
58. Sabumon PC. (**2008**) Development of a novel process for anoxic ammonia removal with sulfidogenesis. *Process Biochem* 43: 984–991; 10.1016/j.procbio.2008.05.004.
59. Sabumon PC. (**2009**) Effect of potential electron acceptors on anoxic ammonia oxidation in the presence of organic carbon. *J Hazard Mater* 172: 280–288; 10.1016/j.jhazmat.2009.07.006.
60. Zhang Z and Liu S (**2014**). Insight into the overconsumption of ammonium by anammox consortia under anaerobic conditions. *J Appl Microbiol* 117: 1830–1838; 10.1111/jam.12649.
61. Rios-Del Toro EE and Cervantes FJ. (**2016**) Coupling between anammox and autotrophic denitrification for simultaneous removal of ammonium and sulfide by enriched marine sediments. *Biodegradation* 27(2–3): 107–118; 10.1007/s10532-016-9759.
62. Aranda-Tamaura C, Estrada-Alvarado MI, Texier A-C, Cuervo F, Gómez J, Cervantes FC. (**2007**) Effects of different quinoid redox mediators on the removal of sulphide and nitrate via denitrification. *Chemosphere*, 69: 1722–1727. 10.1016/j.chemosphere.2007.06.004.
63. Wenk CB, Blees J, Zopfi J, Veronesi M, Bourbonnais A, Schubert CJ, Niemann H, and Lehmann MF (**2013**) Anaerobic ammonium oxidation (anammox) bacteria and sulfide-dependent denitrifiers coexist in the water column of a meromictic south-alpine lake. *Limnol Oceanogr* 58(1): 1–12; 10.4319/lo.2013.58.1.0001.
64. Russ L, Speth DR, Jetten MSM, Op den Camp HJM and Kartal B. (**2014**) Interactions between anaerobic ammonium and sulfur-oxidizing bacteria in a laboratory scale model system. *Environ Microbiol* 16(11): 3487–3498; 10.1111/1462-2920.12487.
65. Yin Z, Xie L, Zhou Q. (**2015**) Effects of sulfide on the integration of de-nitrification with anaerobic digestion. *J Biosci and Bioeng* 120(4): 426–431; 10.1016/j.jbiosc.2015.02.004.
66. Cervantes FJ, Monroy O, and Gómez J. (**1999**) Influence of ammonium on the performance of a denitrifying culture under heterotrophic conditions. *Appl Biochem Biotechnol* 81(1): 13–21; 10.1385/ABAB:81:1:13.
67. Cervantes FJ, De la Rosa DA, and Gómez J. (**2001**) Nitrogen removal from wastewaters at low C/N ratios with ammonium and acetate as electron donors. *Bioresour Technol* 79(2): 165–170; 10.1016/S0960-8524(01)00046-3.
68. González-Blanco G, Beristain-Cardoso R, Cuervo-López F, Cervantes FJ, Gómez J. (**2012**) Simultaneous oxidation of ammonium and p-cresol linked to nitrite reduction by denitrifying sludge. *Bioresour Technol* 103: 48–55; 10.1016/j.biortech.2011.09.086.

69. González-Blanco G, Cervantes FJ, Beristain-Cardoso R, Gómez J. (**2015**) Concurrence of anaerobic ammonium oxidation and organotrophic denitrification in presence of p-cresol. *Appl Biochem Biotechnol* 176: 2120–2130; 10.1007/s12010-015-1702-3.
70. Korb T. (**2016**) Microbial consortia with biodegrading potential from Estonian graptolite argillite. Master Thesis, University of Tartu, 77 pp.
71. van der Star WRL, Abma WR, Blommers D, Mulder JW, Tokutomi T, Strous M, Picioreanu C, van Loosdrecht MCM. (**2007**) Startup of reactors for anoxic ammonium oxidation: Experiences from the first full-scale anammox reactor in Rotterdam. *Water Res* 41: 4149–4163; 10.1016/j.watres.2007.03.044.
72. Tsushima I, Ogasawara Y, Kindaichi T, Satoh H, Okabe S. (**2007**) Development of high-rate anaerobic ammonium- oxidizing (anammox) biofilm reactors. *Water Res* 41: 1623–1634; 10.1016/j.watres.2007.01.050.
73. Tang C-J, Zheng P, Hu B-L, Chen J-W, Wang C-H. (**2010**) Influence of substrates on nitrogen removal performance and microbiology of anaerobic ammonium oxidation by operating two UASB reactors fed with different substrate levels. *J Hazard Mater* 181(1–3): 19–26; 10.1016/j.jhazmat.2010.04.015.
74. Suneethi S and Joseph K. (**2011**) Batch culture enrichment of ANAMMOX populations from anaerobic and aerobic seed cultures. *Bioresour Technol* 102: 585–591; 10.1016/j.biortech.2010.07.121.
75. Dapena-Mora A, Campos JL, Mosquera-Corral A, Méndez R. (**2006**) Anammox process for nitrogen removal from anaerobically digested fish canning effluents. *Water Sci Technol* 53: 265–274; 10.2166/wst.2006.429.
76. Kanders L, Areskoug T, Schneider Y, Ling D, Punzi M, Beier M. (**2014**) Impact of seeding on the start-up of one-stage deammonification MBBRs, *Environ Technol* 35(22): 2767–2773; 10.1080/09593330.2014.920421.
77. Schneider Y, Beier M and Rosenwinkel K. (**2009**) Impact of seeding on the start-up of the deammonification process with different sludge systems. *Proceedings of 2nd IWA Specialized Conference on Nutrient Management in Wastewater*. Krakow, Poland, 6th–9th September.
78. Chen H, Hu H-Y, Chen Q-Q, Shi M-L, Jin R-C. (**2016**) Successful start-up of the anammox process: Influence of the seeding strategy on performance and granule properties. *Bioresour Technol* 211: 594–602; 10.1016/j.biortech.2016.03.139.
79. Dapena-Mora A, Fernández I, Campos JL, Mosquera-Corral A, Méndez R and Jetten MSM. (**2007**) Evaluation of activity and inhibition effects on Anammox process by batch tests based on the nitrogen gas production. *Enzyme Microb Technol* 40: 859–865; 10.1016/j.enzmictec.2006.06.018.
80. Jung JY, Kang SH, Chung YC, Ahn DH. (**2007**) Factors affecting the activity of anammox bacteria during start up in the continuous culture reactor. *Water Sci Technol* 55: 459–468; 10.2166/wst.2007.023.
81. Jaroszynski LW, Cicek N, Sparling R, Oleszkiewicz J. (**2012**) Impact of free ammonia on anammox rates (anoxic ammonium oxidation in a moving bed biofilm reactor. *Chemosphere* 88: 188–195; 10.1016/j.chemosphere.2012.02.085.
82. Wang T, Zhang H and Fenglin Y. (**2016**) Performance of Anammox process and low-oxygen adaptability of Anammox biofilms in a FBR with small ring non-woven carriers. *Ecol Eng* 86: 126–134; 10.1016/j.ecoleng.2015.11.025.

83. Raudkivi M, Zekker I, Rikmann E, Vabamäe P, Kroon K, Tenno T. (**2017**) Nitrite inhibition and limitation–the effect of nitrite spiking on anammox biofilm, suspended and granular biomass. *Water Sci Technol* 75(2): 313–321; 10.2166/wst.2016.456.
84. Anthonisen AC, Loehr RC, Prakasam TBS, Srinath EG. (**1976**) Inhibition of nitrification by ammonia and nitrous acid. *J Water Pollut Control Fed* 48: 835–852; 10.2307/25038971.
85. Tang C-J, Zheng P, Hu B-L, Chen J-W, Wang C-H. (**2010**) Influence of substrates on nitrogen removal performance and microbiology of anaerobic ammonium oxidation by operating two UASB reactors fed with different substrate levels. *J Hazard Mater* 181(1–3): 19–26; 10.1016/j.jhazmat.2010.04.015.
86. Fernández I, Dosta J, Fajardo C, Campos JL, Mosquera-Corral A, Méndez R. (**2010**) Short- and long-term effects of ammonium and nitrite on the anammox process. *J Environ Manage* 95(S): 5170–5174. 10.1016/j.jenvman.2010.10.044.
87. Aktan CK, Yapsakli K and Mertoglu B. (**2012**) Inhibitory effects of free ammonia on Anammox bacteria. *Biodegradation* 23(5): 751–762; 10.1007/s10532-012-9550-0.
88. Lu X, Yin Z, Sobotka D, Wisniewski K, Czerwionka K, Xie L, Zhou Q and Makinia J. (**2017**) Modeling the pH effects on nitrogen removal in the anammox-enriched granular sludge. *Water Sci Technol* 75(2): 378–386; 10.2166/wst.2016.530
89. Waki M, Tokutomi T, Yokoyama H, Tanaka Y. (**2007**) Nitrogen removal from animal waste treatment water by Anammox enrichment. *Bioresour Technol* 98(14): 2775–80; 10.1016/j.biortech.2006.09.031
90. Mosquera-Corral A, González F, Campos JL and Méndez R. (**2005**) Partial nitrification in a SHARON reactor in the presence of salts and organic carbon compounds *Process Biochem* 40(9): 3109–3118; 10.1016/j.procbio.2005.03.042.
91. Park S and Bae W. (**2009**) Modeling kinetics of ammonium oxidation and nitrite oxidation under simultaneous inhibition by free ammonia and free nitrous acid. *Process Biochem* 44(6): 631–640; 10.1016/j.procbio.2009.02.002.
92. Zhou Y, Oehmen A, Lim M, Vadivelu V and Jern Ng, W. (**2011**) The role of nitrite and free nitrous acid (FNA) in wastewater treatment plants. *Water Res* 45(15): 4672–4682; 10.1016/j.watres.2011.06.025.
93. Ma H, Niu Q, Zhang Y, He S and Li Y-Y. (**2017**) Substrate inhibition and concentration control in an UASB-Anammox process. *Bioresour Technol* 238: 263–272; 10.1016/j.biortech.2017.04.017.
94. Hafner SD and Bisogni JJ Jr. (**2009**) Modeling of ammonia speciation in anaerobic digesters. *Water Res* 43: 4105–4114; 10.1016/j.watres.2009.05.044.
95. Carvajal-Arroyo JM, Puyol D, Li G, Lucero-Acuña A, Sierra-Álvarez R, Field JA. (**2014**) Pre-exposure to nitrite in the absence of ammonium strongly inhibits anammox. *Water Res* 48: 52–60; 10.1016/j.watres.2013.09.015.
96. Lackner S, Thoma K, Gilbert EM, Gander W, Schreff D and Horn H. (**2015**) Start-up of a full-scale deammonification SBR-treating effluent from digested sludge dewatering. *Water Sci Technol* 71(4): 553–559; 10.2166/wst.2014.421.
97. Scaglione D, Ficara E, Corbellini V, Tornotti G, Teli A, Canziani R. Malpei F. (**2015**) Autotrophic nitrogen removal by a two-step SBR process applied to mixed agrodigestate. *Bioresour Technol* 176: 98–105; 10.1016/j.biortech.2014.
98. Wett B. (**2007**) Development and implementation of a robust deammonification process. *Water Sci Technol* 56(7): 81–88; 10.2166/wst.2007.611

99. Ivlev AA. (**2015**) Global redox cycle of biospheric carbon: Interaction of photosynthesis and earth crust processes. *BioSystems* 137: 1–11; 10.1016/j.biosystems.2015.10.001.
100. Wang Y, Wang L, Tsang YF, Fu X, Hu J, Li H, Le Y. (**2016**) The variability in carbon fixation characteristics of several typical chemoautotrophic bacteria at low and high concentrations of CO_2 and its mechanism. *Int Biodeterior Biodegradation* 113: 105–112; 10.1016/j.ibiod.2016.03.002.
101. Heisler N. (**1986**) Buffering and transmembrane ion transfer processes. In: Heisler N. (ed.) *Acid–base regulation in animals*. Elsevier Science, Amsterdam, pp. 3–47.
102. Snoeyink VL, Jenkins D. (**1980**) Water Chemistry. John Wiley & Sons Inc. New York.
103. Butler, JN. (**1991**) Carbon Dioxide Equilibria and Their Applications. Lewis Publishers Inc. CRC Press, Michigan.
104. Jones B. (**2017**) Review of calcium carbonate polymorph precipitation in spring systems. *Sediment Geol* 353: 64–75; 10.1016/j.sedgeo.2017.03.006.
105. Panthi SR. (**2003**) Carbonate chemistry and calcium carbonate saturation state of rural water supply projects in Nepal. In: *Proceedings of the 7th IWTC*, Cairo, Egypt, June 3–5, pp. 545–560.
106. Feely RA, Sabine CL, Lee K, Berelson W, Kleypas J, Fabry VJ and Millero FJ. (**2004**) Impact of Anthropogenic CO_2 on the $CaCO_3$ System in the Oceans. *Science* 305(5682): 362–366; 10.1126/science.1097329.
107. U.S. Department of Commerce/National Oceanic & Atmospheric Administration/ NOAA Research. Earth System Research Laboratory, Global Monitoring Division. Trends in Atmospheric Carbon Dioxide, https://www.esrl.noaa.gov/gmd/ccgg/trends/global.html Last accessed 06-22-2018.
108. Hoegh-Guldberg O, Mumby PJ, Hooten AJ, R. Steneck S, Greenfield P, Gomez E, Harvell CD, Sale PF, Edwards AJ, Caldeira K, Knowlton N, Eakin CM, Iglesias-Prieto R, Muthiga N, Bradbury RH, Dubi A and Hatziolos ME. (**2007**) Coral Reefs Under Rapid Climate Change and Ocean Acidification. *Science* 318(5857): 1737–1742; 10.1126/science.1152509.
109. Arakaki T and Mucci A. (**1995**) A Continuous and Mechanistic Representation of Calcite Reaction-Controlled Kinetics in Dilute Solutions at 25°C and 1 Atm Total Pressure. *Aquat Geochem* 1: 105–130; 10.1007/BF01025233.
110. Mitchell MJ, Jensen OE Cliffe KA and Maroto-Valer MM. (**2010**) A model of carbon dioxide dissolution and mineral carbonation kinetics. *Proc. R. Soc. A* 466: 1265–1290; 10.1098/rspa.2009.0349.
111. Mook WG (**2001**) Chemistry of Carbonic Acid in Water. IHP-IX pp 87-98. In: *Environmental Isotopes in the Hydrological Cycle. Principles and Applications. Technical Documents in Hydrology*. Water Resources Programme, International Atomic Energy Agency and United Nations Educational, Scientific and Cultural Organization, Paris. Edited by Mook WG. No. 39, vol. 1. Retrived from: http://www-naweb.iaea.org/napc/ih/documents/global_cycle/Environmental%20Isotopes%20in%20the%20Hydrological%20Cycle%20Vol%201.pdf. Last accessed 06-22-2018.
112. Chibowski E, Hotysz L, Szcześ A. (**2003**) Time dependent changes in zeta potential of freshly precipitated calcium carbonate. *Colloids and Surfaces A: Physicoche. Eng Aspects* 222: 41–54; 10.1016/S0927-7757(03)00232-2.

113. Eriksson R, Merta J, Rosenholm JB. (**2007**) The calcite/water interface I. Surface charge in indifferent electrolyte media and the influence of low-molecular-weight polyelectrolyte. *J Colloid Interface Sci* 313: 184–193; 10.1016/j.jcis.2007.04.034.
114. IUPAC Gold Book. (**1997**) Retrieved from: https://goldbook.iupac.org/index.html. Last accessed 06-22-2018.
115. Heberling F, Trainor TP, Lützenkirchen J, Eng P, Denecke MA Bosbach D. (**2011**) Structure and reactivity of the calcite–water interface. *J Colloid Interface* 354: 843–857; 10.1016/j.jcis.2010.10.047.
116. Website of Tallinna Vesi Ltd, drinking water quality: https://tallinnavesi.ee/en/ettevote/activities/water-treatment/drinking-water-quality/ (last accessed 05-01-2019).
117. Gut L, Płaza E, Długołęcka M and Hultman B. (**2005**) Partial Nitritation Process Assessment. *Vatten* 61(3): 175–182.
118. Kim H-T, Bae S-Y and Yoo K-O. (**1991**) Correlation of pitzer ion interaction parameters. *Korean J Chem Eng* 8(2): 105–113; 10.1007/BF02697384.
119. APHA. (**1992**) Standard Methods for the Examination of Water and Wastewater, 16th ed. Washington, DC: American Public Health Association.
120. George M, Nagaraja KS, Balasubramanian N. (**2008**) Spectrophotometric determination of hydrazine. *Talanta* 75(1): 27-31; 10.1016/j.talanta.2007.09.002.
121. Frear DS and Burrell RC. (**1955**) Spectrophotometric method for determining hydroxylamine reductase activity in higher plants. *Anal Chem* 27(10): 1664–1665; 10.1021/ac60106a054.
122. Ibrahim MBM, Moursy AS, Bedair AH, Radwan EK. (**2008**) Comparison of DAX-8 and DEAE for isolation of humic substances from surface water. *J Environ Sci Tech* 1: 90-96; 10.3923/jest.2008.90.96.
123. Lane DJ. (**1991**) 16/23S rRNA Sequencing. Nucleic Acid Techniques in Bacterial Systematics. Chichester: John Wiley and Sons, pp 177–204.
124. Neef A, Amann RI, Schlesner H, and Schleifer KHG. (**1998**) Monitoring a widespread bacterial group: in situ detection of planctomycetes with 16S rRNA-targeted probes. *Microbiol* 144: 3257-3266; 10.1099/00221287-144-12-3257.
125. Sànchez-Melsió A, Cáliz J, Balaguer MD, Colprim J, Vila X. (**2009**) Development of batch-culture enrichment coupled to molecular detection for screening of natural and manmade environments in search of anammox bacteria for N-removal bioreactors systems. *Chemosphere* 75: 169–179; 10.1016/j.chemosphere.2008.12.017.
126. Dionisi HM, Layton AC, Harms G, Gregory IR, Robinson KG and Sayler GS. (**2002**) Quantification of Nitrosomonas oligotropha-like ammonia-oxidizing bacteria and Nitrospira spp. from full-scale wastewater treatment plants by competitive PCR. *Appl Environ Microbiol* 68: 245–253; 10.1128/AEM.68.1.245-253.2002.
127. Muyzer G, de Waal EC and Uitterlinden (**1993**) AG Profiling of complex microbial populations by denaturing gradient gel electrophoresis analysis of polymerase chain reaction amplified genes coding for 16S rRNA. *Appl Environ Microbiol* 59(3): 695–700.
128. Muyzer G, Hottenträger S, Teske A, Waver C (**1996**) Denaturing gradient gel electrophoresis of PCR amplified 16S rDNA – a new molecular approach to analyze the genetic diversity of mixed microbial communities. In: Akermanns AD, van Elsas JD, de Brujin FJ (eds) *Molecular microbial ecology manual*. Kluwer academic publishers, Dordrecht.

129. Koskinen PE, Kaksonen AH and Puhakka JA. (**2006**) The relationship between instability of H_2 production and compositions of bacterial communities within a dark fermentation fluidized-bed bioreactor. *Biotechnol Bioeng* 97: 742–758; 10.1002/bit.21299.
130. Ni B-J, Hu B-L, Fang F, Xie W-M, Kartal B, Liu X-W, Sheng G-P, Jetten M, Zheng P and Yu H-Q. (**2010**) Microbial and physicochemical characteristics of compact anaerobic ammonium-oxidizing granules in an upflow anaerobic sludge blanket reactor. *Appl Environ Microbiol* 76: 2652–2656; 10.1128/AEM.02271-09.
131. Hu Z and Ma R. (**2016**) Distribution and characteristic of nitrite-dependent anaerobic methane oxidation bacteria by comparative analysis of wastewater treatment plants and agriculture fields in northern China. *PeerJ* 4: e2766; 10.7717/peerj.2766.
132. Li W, Zhao Q-L, and Liu H. (**2009**) Sulfide removal by simultaneous autotrophic and heterotrophic desulfurization–denitrification process. . *J Hazard Mater* 162(2–3):848-853; 10.1016/j.jhazmat.2008.05.108.
133. Han Y and Perner M. (**2016**) Sulfide Consumption in Sulfurimonas denitrificans and Heterologous Expression of Its Three Sulfide-Quinone Reductase Homologs. *J Bacteriol* 198(8): 1260-1267; 10.1128/JB.01021-15.
134. Bassin JP, Pronk M, Kraan R, Kleerebezem R, van Loosdrecht MCM (**2011**) Ammonium adsorption in aerobic granular sludge, activated sludge and anammox granules. *Water Res* 45(16):5257–5265; 10.1016/j.watres.2011.07.034.
135. Yu X, Wan C, Lei Z, Liu X, Zhang Y, Lee D-J, Tay J-H. (**2014**) Adsorption of ammonium by aerobic granules under high ammonium levels. *J Taiwan Inst Chem Eng* 45: 202–206; 10.1016/j.jtice.2013.04.017.
136. Coates JD, Cole KA, Chakraborty R, O'Connor SM, Achenbach LA. (**2002**) Diversity and ubiquity of bacteria capable of utilizing humic substances as electron donors for anaerobic respiration. *Appl Environ Microb* 68: 2445–2452.
137. Cervantes FJ, van der Velde S, Lettinga G, Field JA. (**2000**). Quinones as terminal electron acceptors for anaerobic microbial oxidation of phenolic compounds. *Biodegradation* 11: 313–321; 10.1023/A:1011118826386.
138. Cervantes FJ, van der Velde S, Lettinga G, Field JA. (**2000**) Competition between methanogenesis and quinone respiration for ecologically important substrates in anaerobic consortia. *FEMS Microbiol Ecol* 34(2): 161–171.
139. Cervantes FJ, Dijksma W, Duong-Dac T, Ivanova A, Lettinga G, Field JA. (**2001**) Anaerobic mineralization of toluene by enriched sediments with quinones and humus as terminal electron acceptors. *Appl Environ Microb* 67: 4471–4478.
140. van der Zee FP, Bisschops IAE, Blanchard VG, Bouwman RHM, Lettinga G, Field JA. (**2003**) The contribution of biotic and abiotic processes during azo dye reduction in anaerobic sludge. *Water Res* 37: 3098–3109; 10.1016/S0043-1354(03)00166-0.
141. Lovley DR, Coates JD, Blunt-Harris EL, Philips EJD, Woodward JC. (**1996**) Humic substances as electron acceptors for microbial respiration. *Nature* 382: 445–448.
142. Bruce RA, Achenbach LA, Coates JD. (**1999**) Reduction of (per)chlorate by a novel organism isolated from a paper mill waste. *Environ Microbiol* 1: 319–331.
143. Lovley DR, Fraga JL, Coates JD, Blunt-Harris EL. (**1999**) Humics as an electron donor for anaerobic respiration. *Environ Microbiol* 1: 89–98.

144. Zub S, Kurissoo T, Menert A, Blonskaja V. (**2008**) Combined biological treatment of high-sulfate wastewater from yeast production. *Water Environ J* 22(4): 274–286; 10.1111/j.1747-6593.2007.00097.x.
145. Reungsang A, Pattra S and Sittijunda S. (**2012**) Optimization of Key Factors Affecting Methane Production from Acidic Effluent Coming from the Sugarcane Juice Hydrogen Fermentation Process. *Energies* 5: 4746-4757; 10.3390/en5114746.
146. Sànchez-Melsió A, Cáliz J, Balaguer MD, Colprim J, Vila X. (**2009**) Development of batch-culture enrichment coupled to molecular detection for screening of natural and man-made environments in search of anammox bacteria for N-removal bioreactors systems. *Chemosphere* 75(2): 169–79; 10.1016/j.chemosphere.2008.12.017.
147. Ganigué R, López H, Ruscalleda M, Dolors Balaguer M, Colprim J. (**2008**) Operational strategy for a partial nitritation–sequencing batch reactor treating urban landfill leachate to achieve a stable influent for an anammox reactor. *J Chem Technol Biotechnol* 83: 365–371; 10.1002/jctb.1822.
148. Dreybrodt W. (**2008**) Evolution of the isotopic composition of carbon and oxygen in a calcite precipitating H_2O–CO_2–$CaCO_3$ solution and the related isotopic composition of calcite in stalagmites. *Geochim Cosmochim Acta* 72: 4712–4724; 10.1016/j.gca.2008.07.022.
149. Stumm W, Morgan JJ. (**1996**) Aquatic Chemistry, 3rd ed.; John Wiley & Sons Inc. New York.
150. Segal BG. (**1989**) Chemistry, Experiment and Theory; John Wiley & Sons, Inc. New York.
151. Dean, JA. (**1992**) Lange's Handbook of Chemistry; McGraw-Hill, Inc. New York.
152. Snoeyink VL; Jenkins D. (**1980**) Water Chemistry; John Wiley & Sons Inc. New York.
153. Reddy SK and Balasubramanian S. (**2014**) Carbonic acid: molecule, crystal and aqueous solution. *Chem Commun* 50: 503-514; 10.1039/c3cc45174g.
154. Moran D. (**2010**) Carbon dioxide degassing in fresh and saline water. I: Degassing performance of a cascade column. *Aquat Eng* 43(1): 29–36; 10.1016/j.aquaeng.2010.05.001
155. Chang R. (**1990**) Physical Chemistry with Applications to Biological Systems, 2nd ed.; Williams College, Macmillan Publishing Co., Inc. New York.
156. Skoog DA, West DM, and Holler FJ. (**1992**) Fundamentals of Analytical Chemistry. 6th ed. Saunders College Publishing.
157. Plummer LN and Busenberg E. (**1982**) The solubilities of calcite, aragonite and vaterite in CO_2-H_2O solutions between 0 and 90 °C, and an evaluation of the aqueous model for the system $CaCO_3$-CO_2-H_2O. *Geochim Cosmochim Acta* 46(6): 1011–1040; 10.1016/0016-7037(82)90056-4.
158. Genovese D, Montalti M, Otálora F, Gómez-Morales J, Sancho-Tomás M, Falini G, and García-Ruiz JM. (**2016**) Role of $CaCO_3^0$ Neutral Pair in Calcium Carbonate Crystallization. *Cryst Growth Des* 16(8):4173–4177; 10.1021/acs.cgd.6b00276.
159. Garrels RM, Christ CL. (**1967**) Solutions, Minerals and Equilibria; Harper and Row Publishing Co, New York.
160. Dickerson RE, Gray HB, and Haight GP. (**1979**) Chemical Principles. Third ed. The Benjamin/Cummings Publishing Company Inc., Menlo Park, CA.

7. SUMMARY IN ESTONIAN

Autotroofne lämmastikuärastus ja sellega seotud tasakaalulised protsessid

Käesoleva väitekirja aluseks olevad kuus publikatsiooni käsitlevad kolme alateemat:

a) sulfaatredutseeriva ammooniumi oksüdatsiooni uuringud;
b) deammonifikatsioniprotsessi käivitamine ja võrdlemine kolmes erineva konfiguratsiooniga pilootseadmes, mis realiseeriti vädu eeltöötluseta ning anammoks-spetsiifilise inokuleerimiseta tegeliku tehnoloogilise protsessi tingimustes;
c) reoveekäitluse seisukohalt oluliste tasakaaluliste protsesside – karbo-naatsete ja ammoniakaalsete tasakaalude teoreetiline matemaatiline modelleerimine ja arvutuslike tulemuste eksperimentaalne kontroll.

Sulfaatredutseeriv ammooniumi oksüdatsiooniprotsess (SRAO) käivitati nii liikuvate kandjatega biokilereaktoris (MBBR, aktiivruumalaga 3.3 L, t = 20 ºC) kui ka ülesvoolses heljuva mudakihiga anaeroobses reaktoris (UASBR, aktiivruumalaga 1.5 L, t = 36 ºC), kasutades erinevaid inokulume: vastavalt ettekasvatatud anammoks biokilet ja pärmitööstuse reoveepuhasti muda (**artikkel I**). Võrreldes UASBR-süsteemis teostatud tavapärase anammoks protsessiga, kus elektronaktseptorina kasutatakse NO_2^-, oli SRAO protsess oluliselt madalama efektiivsusega ning ebastabiilsem: UASBR ja SRAO protsessides ärastati vastavalt ca ⅔ ja ca ¼ lämmastikust (**artikkel II**). Samas ei olnud sulfaatredutseerivas ammooniumi oksüdatsiooniprotsessis MBBR-süsteemi ja UASBR-süsteemi vahel efektiivsuses olulist erinevust (**artikkel I**).

SRAO protsess toimus ühe reaktsioonina keerukast reaktsioonideahelast, mis hõlmas lämmastiku- ja väävliühendeid ning kinoonrühmi sisaldavaid orgaanilisi ühendeid. Tulemuseks oli oluliselt suurem ärastatud ammooniumlämmastiku suhe ärastatud sulfaatiooni koguse kohta kui võrrandi (6) stöhhiomeeriline vahekord seda näitab. Denitrifitseeriva väävlit oksüdeeriva mikroorganismi *Sulfurimonas denitrificans* DSM 1251 identifitseerimine sulfaatredutseeriva UASBR seemnemudas ja reaktori mudaproovis tõendas nimetatud denitrifikatsiooniprotsessi kulgemist.

Tuginedes varasemates laboratoorsetes uuringutes saadud kogemustele, teostati reoveepuhasti jääkmuda käitleva metaanitanki vädu autotroofse lämmastikuärastuse käivitamise uuring pilootskaalas reoveepuhastusjaama tegelikes tehnoloogilistes tingimustes (**artikkel III**). Täisautomatiseeritud pilootkatse-jaamas käivitati ühesugustel tingimustel kolm erinevat opereerimisüksust: vahelduva aeratsiooniga deammonifitseeriv liikuvate kandjatega biokilereaktor (V=3 m^3), deammonifitseeriv biomudapõhine annuspuhasti (V=3 m^3) ja kaheastmeline süsteem, mis koosnes eraldatud nitritatsioonireaktorist (V=0,3 m^3) ning liikuvate

kandjatega anammoks biokilereaktorist (V=3 m^3). Biokilereaktoritesse laaditi biomassita uued kandjad, autotroofsete bakterite allikaks oli käideldav vädu. Eksperimentide algfaasis, kui ei kasutatud automaatset pH kontrolli, esines kõigis süsteemides bioprotsessi tugev inhibitsioon, mis oli tingitud eelkõige vaba ammoniaagi kõrgest kontsentratsioonist vedelfaasis. Pärast automaatse pH kontrolli rakendamist saavutati kõigil kolmel opereerimisüksusel 4–6 kuu jooksul autotroofne lämmastikuärastus efektiivsusega üle 50%. Automaatne pH kontroll madalamatel pH väärtustel kui 7,5 võimaldas hoida vaba ammoniaagi kontsentratsiooni <10 mg-NH_3-N·L^{-1}, kõrvaldades sellega vaba ammoniaagi inhibeeriva mõju.

Näidati, et autotroofset lämmastikuärastust on võimalik käivitada sõltumatult rakendatavast tehnoloogilisest kontseptsioonist, kuid kõige stabiilsem ja efektiivsem lämmastikuärastus toimus vahelduva aeratsiooniga liikuvate kandjatega biokilereaktoris. Üldlämmastiku maksimaalseteks ärastuskiirusteks saadi 1.04 kg-N·m^{-3}·d^{-1}, 0.3 kg-N·m^{-3}·d^{-1} ja 0.11 kg-N·m^{-3}·d^{-1}, vastavalt vahelduva aeratsiooniga biokilereaktoris, annuspuhastis ja kaheastmelises süsteemis. Nitritatsioonireaktori piiratud mahu tõttu jäi üldlämmastiku maksimaalne ärastuskiirus kaheastmelises süsteemis tunduvalt madalamaks kui üheastmelistes süsteemides. Keskmine üldlämmastiku ärastusefektiivsus pilootkatsejaama opereerimise viimasel perioodil oli oli vahelduva aeratsiooniga biokilereaktoris, annuspuhastis ja anammoks biokilereaktoris oli vastavalt 82±15%, 73±14% ja 72±24%. Lämmastikuärastuse edukaks käivitamiseks ja stabiilse opereerimise tagamiseks tuli kontrollida järgmiste kriitiliste parameetrite väärtusi: pH < 7,5, lahustunud hapniku kontsentratsioon 0,3–0,8 mg-O_2·L^{-1} ning sissevoolu heljumisisaldus < 1000 NTU.

Vädu on keerulise koostisega süsteem, mille üksikute komponentide kontsentratsioonid on määratud mitme pH-st sõltuva, üksteisega prootonite kaudu seotud tasakaaluliste protsessidega. Neist tasakaaludest peamised on karbonaatne tasakaal $(CO_2)_W$–HCO_3^-–CO_3^{2-} ja ammoniakaalne tasakaal $(NH_3)_W$–NH_4^+. Vädu efektiivse käitluse seisukohalt on oluline teada vädu koostises olevate komponentide kontsentratsioone. Käesolevas töös võeti lähema vaatluse alla karbonaatsed tasakaalud süsteemide $(CO_2)_W$–H_2O–$(CaCO_3)_S$ näitel. Karbonaatsete ja ammoniakaalsete tasakaalude omavahelise vastasmõju uurimiseks vaadeldi olukorda, kus karbonaatsele süsteemile on lisatud NH_4Cl. Käesolevas töös tuletati teoreetiliselt matemaatilised mudelid alljärgnevatele heterogeensetele tasakaalulistele süsteemidele:

1) mudel, mis on esitatud **artiklis IV**, kirjeldab matemaatiliselt avatud süsteemis $(CO_2)_G$–H_2O–$(CO_2)_W$–H_2CO_3–HCO_3^-–CO_3^{2-}–$(CaCO_3)_S$ toi-muvaid keemilisi tasakaalu protsesse ning võimaldab arvutada süsteemi pH ja CO_3^{2-}, HCO_3^-, H_2CO_3, Ca^{2+}, H^+ ja OH^- kontsentratsioone antud süsteemi vedelfaasis erinevate etteantud süsihappegaasi kontsentrat-sioonide korral gaasifaasis.
2) mudel, mis on esitatud **artiklis V**, kirjeldab matemaatiliselt suletud süsteemis H_2O–$(CO_2)_W$–H_2CO_3–HCO_3^-–CO_3^{2-}–$(CaCO_3)_S$ toimuvaid tasakaalulisi

protsesse ja võimaldab arvutada pH ning kõikide kompo-nentide (CO_3^{2-}, HCO_3^-, H_2CO_3, $(CO_2)_W$, Ca^{2+}, H^+ ja OH^-) kontsentrat-sioone erinevate $[CO_2]_{W0}$ väärtuste korral.

3) mudel, mis on esitatud **artiklis VI**, kirjeldab matemaatiliselt suletud süsteemis H_2O–$(CO_2)_W$–$(CaCO_3)_S$–NH_4Cl toimuvaid tasakaalulisi protsesse ja võimaldab arvutada pH ning kõikide komponentide (CO_3^{2-}, HCO_3^-, H_2CO_3, $(CO_2)_W$, Ca^{2+}, H^+, OH^-, NH_4^+ ja $(NH_3)_W$) kontsentrat-sioone erinevate $[CO_2]_{W0}$ väärtuste ning erinevate lisatud NH_4Cl koguste korral.

Kõigile kolmele mudelile teostati ka eksperimentaalne valideerimine. Modelleerimisest tulenevad alljärgnevad järeldused:

- avatud süsteemis $(CO_2)_G$–H_2O–$(CO_2)_W$–H_2CO_3–HCO_3^-–CO_3^{2-}–$(CaCO_3)_S$ süsihappegaasi osarõhul $P(CO_2)_G = 390$ ppm ja $t = 25$ °C, on tasakaaluline pH = 8,2;
- avatud süsteemis $(CO_2)_G$–H_2O–$(CO_2)_W$–H_2CO_3–HCO_3^-–CO_3^{2-}–$(CaCO_3)_S$ on temperatuuril 25 °C ja CO_2 osarõhul $P(CO_2)_G = 0{,}692$ ppm tahke $CaCO_3$ lahustuvuse miinimum 0,1 mmol·L^{-1}. Neil tingimustel on süsinikdioksiidi faasidevaheline netoülekanne võrdne nulliga, mis vastab olukorrale suletud süsteemis;
- Suletud süsteemis H_2O–$(CO_2)_W$–H_2CO_3–HCO_3^-–CO_3^{2-}–$(CaCO_3)_S$ on vedelfaas aluseline, kui $\sum[CO_X]_{W0}$ on vahemikus $1{,}88\times10^{-6}$ kuni 0,352 mmol·L^{-1}, maksimumiga pH=9,88 ±0,03. Vahemikus $\sum[CO_X]_{W0}$ 2,54 mmol·L^{-1} kuni 34,10 mmol·L^{-1} on vedelfaas happeline;
- Kui moodustub suletud süsteem H_2O–$(CO_2)_W$–H_2CO_3–HCO_3^-–CO_3^{2-}–$(CaCO_3)_S$, liidavad CO_3^{2-} ioonid prootoneid, mis pärinevad kas vee või H_2CO_3 dissotsiatsioonist. Mida väiksem on süsteemi $[CO_2]_{W0}$, seda vähem vabaneb prootoneid H_2CO_3 dissotsieerumisest. Seega annab vee dissotsiatsioon madalamate $[CO_2]_{W0}$ korral peamise hulga prootoneid, mis seotakse CO_3^{2-} ioonide poolt ja vedelfaasi pH suureneb;
- Süsteemis H_2O–$(CO_2)_W$–$(CaCO_3)_S$–NH_4Cl on madalama $[CO_2]_{W0}$ korral peamiseks prootonite allikaks NH_4^+ ioonid ja kõrgematel vees lahustunud süsihappegaasi algkontsentratsioonidel on peamine prootonite allikas H_2CO_3;
- Toksilise vaba ammoniaagi kontsentratsiooni vesikeskkonnas $(NH_3)_W$ mõjutab karbonaatse ja ammoniakaalse tasakaaluprotsesside vastastikmõju ning seda saab väljatöötatud mudeli põhjal hinnata suurema täpsusega kui varem kirjanduses pakutud meetoditega;
- Väljatöötatud mudelid võimaldavad hinnata inimtekkeliste protsesside mõju keskkonnale ja neid saab rakendada mitmetes keskkonna-tehnoloogia valdkondades, eelkõige joogivee- ja reoveepuhastuses. Mudelid on kasulikud ka vees lahustunud süsihappegaasi ja ammoniaagi uuenduslike mõõtmismeetodite väljatöötamisel.

ACKNOWLEDGEMENTS

The present thesis is based on studies performed at the Chair of Colloidal and Environmental Chemistry of University of Tartu. I would like to express my sincere gratitude to all my colleagues in this research team, with whom I had an honour to collaborate with during the years of my study.

I would like to express my greatest gratitude to my doctoral supervisor Prof. Toomas Tenno for his support and assistance throughout the years of my study. I would also like to thank my co-supervisor Ph.D. Anne Menert for her contribution.

My very special thanks go to:

my good colleague Ph.D. Ivar Zekker for his collaboration;

to Ph.D. Taavo Tenno for his contribution to the inception and operation of pilot plant;

to Alar Saluste for his work related to the launch of pilot plant;

to Peka Tiidus for his help with the routine maintainance works of pilot plant;

to Anne Paaver for her help with the chemical analyses;

to Kalev Uiga for his participation in the experimental work connected to the validation of theoretical models;

to Alexey Mashirin for his advice about the matemathics;

to Karin Hellat for the proofreading the manuscript.

My warmest go to my family and friend for their unlimited support during the years of my studies.

The financial support from the following institutions is gratefully acknowledged: Estonian Science Foundation and Estonian Environmental Investment Center (grants and programs № SF0180135s08, ETF 9370, SLOTI08262, SLOKT11027T, SLOKT11119, IUT20-16, IWAMA) as well as the Doctoral School ‘Functional materials and Technologies’ receiving funding from the European Social Fund under project ‘1.2.0401.09-0079 in Estonia’.

PUBLICATIONS

CURRICULUM VITAE

Name: Ergo Rikmann
Date of birth: June 08.1973
Place of birth: Tallinn, Estonia
Citizenship: Estonian
Phone: +372 737 5181; +372 56 912 374
E-mail: ergo.rikmann@ut.ee, rikmannster@gmail.com
ORCID: 0000-0001-7469-2685

Education:

2009–present	University of Tartu, Faculty of Science and Technology, doctoral student in environmental technology, doctoral supervisor Prof. Toomas Tenno, co-supervisor Anne Menert
1997–2000	TalTech, Faculty of Chemistry, *M.Sc* in biotechnology and food technology
1992–1997	TalTech, Faculty of Chemistry, *B.Sc* in chemical and environmental technology

Professonal employment:

2011–present	University of Tartu, Faculty of Science and Technology, Institute of Chemistry, Chemist
1999–2005	PIC Eesti Ltd., engineer

Mentoring experience:
Supervisor of Anni Mandel *Master Thesis* 'Ammoniacal-carbonaceous equilibrium in liquid effluent of a methane digester and in landfill leachate' (2015)

Main scientific publications:

1 Zekker I, Kivirüüt A, **Rikmann E,** Mandel A, Jaagura M, Tenno T, Artemchuk O, Rubin SdC Tenno T. (**2019**) Enhanced Efficiency of Nitritating-Anammox Sequencing Batch Reactor Achieved at Low Decrease Rates of Oxidation-Reduction Potential. *Environ Eng Sci* 36 (3): 350–360; 10.1089/ees.2018.0225 [forthcoming].
2 **Rikmann E**, Zekker I, Tenno T, Saluste A, Tenno T. (**2018**) *Inoculum*-free start-up of biofilm- and sludge-based deammonification systems in pilot scale. *Int J Environ Sci Technol* 15(1): 133 –148; 10.1007/s13762-017-1374-3.
3 Liiv J, Teppand T, **Rikmann E**, Tenno T. (**2018**) Novel ecosustainable peat and oil shale ash-based 3D-printable composite material. *Sustainable Mater Technol* 17, UNSP e00067; 10.1016/j.susmat.2018.e00067.

4 Tenno T, **Rikmann E**, Uiga K, Zekker I, Mashirin A, and Tenno T. **(2018)**. A novel proton transfer model of closed equilibrium systems of H_2O–CO_2–$CaCO_3$–NH_X. *P Est Acad Sci Chem* 67(3): 260–270; 10.3176/proc.2018.3.04.
5 Tenno T, **Rikmann E**, Zekker I, Tenno T. (**2018**). Modelling the solubility of sparingly soluble compounds depending on their particles size. *P Est Acad Sci Chem* 67(3): 300–302; 10.3176/proc.2018.3.10.
6 Tenno T, Uiga K, Mashirin A, Zekker I and **Rikmann E**. (**2017**) Modeling Closed Equilibrium Systems of H_2O–Dissolved CO_2–Solid $CaCO_3$ *J Phys Chem A* 121: 3094–3100; 10.1021/acs.jpca.7b00237.
7 Raudkivi M, Zekker I, **Rikmann E**, Vabamäe P, Kroon K, Tenno T. (**2017**). Nitrite inhibition and limitation - the effect of nitrite spiking on anammox biofilm, suspended and granular biomass. *Water Sci Technol* 75(2): 313–321; 10.2166/wst.2016.456.
8 Tenno T, **Rikmann E**, Zekker I, Tenno T, Daija L, Mashirin A. (**2016**). Modelling equilibrium distribution of carbonaceous ions and molecules in a heterogeneous system of $CaCO_3$–water–gas. *P Est Acad Sci Chem* 65(1): 68–77; 10.3176/proc.2016.1.07.
9 Zekker I, **Rikmann E**, Mandel A, Kroon K, Seiman A, Mihkelson J, Tenno T, Tenno T. (**2016**). Step-wise temperature decreasing cultivates a biofilm with high nitrogen removal rates at 9 °C in short-term anammox biofilm tests. *Environ Technol* 37 (15): 1933–1946 ; 10.1080/09593330.2015.1135995.
10 Daija L, Selberg A, **Rikmann E**, Zekker I, Tenno T, Tenno T, (**2016**). The influence of lower temperature, influent fluctuations and long retention time on the performance of an upflow mode laboratory-scale septic tank. *Desalination Water Treat* 57(40): 18679–18687; 10.1080/19443994.2015.1094421.
11 **Rikmann E**, Zekker I, Tomingas M, Tenno T, Loorits L, Vabamäe P, Mandel A, Raudkivi M, Daija L, Kroon K, Tenno T, (**2015**). Sulfate-reducing Anammox for Sulfate and Nitrogen Containing Wastewaters. *Desalination Water Treat* 57(7): 3132–3141; 10.1080/19443994.2014.984339.
12 Zekker I, **Rikmann E**, Tenno T, Loorits L, Kroon K, Vabamäe P, Mandel A, Raudkivi M, Daija L, Rubin SSCdC, Tenno T. (**2015**) Nitric oxide for anammox recovery in nitrite-inhibited deammonification system. *Environ Technol* 36(19): 2477–2487; 10.1080/09593330.2015.1034791.
13 **Rikmann E**, Zekker I, Tomingas M, Vabamäe P, Kroon K, Saluste A, Tenno T, Menert A, Loorits L, Rubin SSCdC, Tenno T. (**2014**). Comparison of sulfate-reducing and conventional Anammox upflow anaerobic sludge blanket reactors. *J Biosci Bioeng* 118(4): 426–433; 10.1016/j.jbiosc.2014.03.012.

14 Zekker I, **Rikmann E**, Tenno T, Seiman A, Loorits L, Kroon K, Tomingas M, Vabamäe P, Tenno T. (**2014**). Nitritating-anammox biomass tolerant to high dissolved oxygen concentration and C/N ratio in treatment of yeast factory wastewater. *Environ Technol* 35(12): 1565–1576; 10.1080/09593330.2013.874492.
15 Zekker I, **Rikmann E**, Loorits L, Tenno T, Fritze H, Tuomivirta T, Kroon K, Vabamäe P, Seiman A, Raudkivi M, Mandel A, Tenno T. (**2014**). Start-up of low temperature anammox in UASB from mesophilic yeast factory anaerobic tank inoculum. *Environ Technol*, 36(2): 214–225; 10.1080/09593330.2014.941946.
16 Zekker I, **Rikmann E**, Tenno T, Kroon K, Vabamäe P, Salo E, Loorits L, Rubin SSCdC, Tenno T. (**2013**). Deammonification process start-up after enrichment of anammox microorganisms from reject water in a moving bed biofilm reactor (MBBR). *Environ Technol* 34(23): 3095–3101; 10.1080/09593330.2013.803134.
17 Zekker I, **Rikmann E**, Tenno T, Vabamäe P, Tomingas M, Menert A, Loorits L, Tenno T. (**2012**). Anammox Bacteria Enrichment and Phylogenic Analysis in Moving Bed Biofilm Reactors. *Environ Eng Sci* 29(10): 946–950; 10.1089/ees.2011.0146.
18 Zekker I, **Rikmann E**, Tenno T, Lemmiksoo V, Menert A, Loorits L, Vabamäe P, Tomingas M, Tenno T. (**2012**). Anammox enrichment from reject water on blank biofilm carriers and carriers containing nitrifying biomass: operation of two moving bed biofilm reactors (MBBR). *Biodegradation*, 23(4): 547–560; 10.1007/s10532-011-9532-7.
19 **Rikmann E**, Zekker I, Tomingas M, Tenno T, Menert A, Loorits L, Tenno T. (**2012**) Sulfate-reducing anaerobic ammonium oxidation as a potential treatment method for high nitrogen-content wastewater. *Biodegradation* 23(4): 509–524; 10.1007/s10532-011-9529-2.
20 Zekker I, **Rikmann E**, Tenno T, Saluste A, Tomingas M, Menert A, Loorits L, Lemmiksoo V, Tenno T. (**2012**). Achieving nitritation and anammox enrichment in single moving- bed biofilm reactor treating reject water. *Environ Technol* 33(6): 703–710; 10.1080/09593330.2011.588962.
21 Zekker I, **Rikmann E**, Kroon, K, Saluste A, Vabamäe P, Tenno T, Menert A, Loorits L, Tenno T. (**2012**). Sulfate- reducing and nitrite-dependent anammox for ammonium removal. *Commun Agric Appl Biol Sci* 77(1): 227–230.
22 Zekker I, Kroon, K, **Rikmann E**, Tenno T, Tomingas M, Vabamäe P, Vlaeminck SE, Tenno T. (**2012**). Accelerating effect of hydroxylamine and hydrazine on nitrogen removal rate in moving bed biofilm reactor. *Biodegradation*, 23(5): 739–749; 10.1007/s10532-012-9549-6.
23 Zekker I, **Rikmann E**, Tenno T, Vabamäe P, Kroon K, Loorits L Saluste, A, Tenno T. (**2012**). Effect of HCO_3^- concentration on anammox nitrogen removal rate in a moving bed biofilm reactor. *Environ Technol* 33(20): 2263–2271; 10.1080/09593330.2012.665487.

24 Zekker I, **Rikmann E**, Tenno T, Menert A, Lemmiksoo V, Saluste A, Tenno T, Tomingas M. (**2011**). Modification of nitrifying biofilm into nitritating one by combination of increased free ammonia concentrations, lowered HRT and dissolved oxygen concentration. Journal of Environmental Sciences, 23(7): 1113–1121; 10.1016/S1001-0742(10)60523-2.
25 Pikkov L, Kallas J, Rüütmann T, Rikmann E. (**2001**). Characteristics of activated carbon produced from biosludge and its use in wastewater post-treatment. *Environ Technol* 22(2): 229–236; 10.1080/09593332208618302.

ELULOOKIRJELDUS

Nimi: Ergo Rikmann
Sünniaeg: 08.06.1973
Sünnikoht: Tallinn, Eesti
Kodakondsus: Eesti
Telefon: +372 737 5181; +372 56 912 374
E-post: ergo.rikmann@ut.ee, rikmannster@gmail.com
ORCID: 0000-0001-7469-2685

Haridus:

2009–käesoleva	Tartu Ülikool, Loodus- ja täppisteaduste valdkond, ajani doktoriõppes õppija keskkonnatehnoloogia alal, akadeemiline juhendaja prof. Toomas Tenno, kaasjuhendaja Anne Menert
1997–2000	TalTech, Keemiateaduskond, *M.Sc* biotehnoloogia ja toiduainete tehnoloogia alal
1992–1997	TalTech, Keemiateaduskond, *B.Sc* keemia- ja keskkonnatehnoloogia alal

Erialase töö kogemus:

2011–present	Tartu Ülikool, Loodus- ja täppisteaduste valdkond, Keemia instituut, keemik
1999–2005	PIC Eesti AS, insener

Juhendamised:
2015. aastal juhendanud Tartu Ülikooli keskkonnatehnoloogia õppekava üliõpilase Anni Mandeli magistritööd "Ammoniakaalne-karbonaatne tasakaal metaankääriti settevees ja prügila nõrgvees".

Tähtsamad teaduspublikatsioonid (1.1 kategooria):

1 Zekker I, Kivirüüt A, **Rikmann E,** Mandel A, Jaagura M, Tenno T, Artemchuk O, Rubin SdC Tenno T. (**2019**) Enhanced Efficiency of Nitritating-Anammox Sequencing Batch Reactor Achieved at Low Decrease Rates of Oxidation-Reduction Potential. *Environ Eng Sci* 36 (3): 350–360; 10.1089/ees.2018.0225 [forthcoming].

2 **Rikmann E**, Zekker I, Tenno T, Saluste A, Tenno T. (**2018**) *Inoculum*-free start-up of biofilm- and sludge-based deammonification systems in pilot scale. *Int J Environ Sci Technol* 15(1): 133 –148; 10.1007/s13762-017-1374-3.

3 Liiv J, Teppand T, **Rikmann E**, Tenno T. (**2018**) Novel ecosustainable peat and oil shale ash-based 3D-printable composite material. *Sustainable Mater Technol* 17, UNSP e00067; 10.1016/j.susmat.2018.e00067.

4 Tenno T, **Rikmann E**, Uiga K, Zekker I, Mashirin A, and Tenno T. **(2018)**. A novel proton transfer model of closed equilibrium systems of H_2O–CO_2–$CaCO_3$–NH_X. *P Est Acad Sci Chem* 67(3): 260–270; 10.3176/proc.2018.3.04.
5 Tenno T, **Rikmann E**, Zekker I, Tenno T. (**2018**). Modelling the solubility of sparingly soluble compounds depending on their particles size. *P Est Acad Sci Chem* 67(3): 300–302; 10.3176/proc.2018.3.10.
6 Tenno T, Uiga K, Mashirin A, Zekker I and **Rikmann E**. (**2017**) Modeling Closed Equilibrium Systems of H_2O–Dissolved CO_2–Solid $CaCO_3$ *J Phys Chem A* 121: 3094–3100; 10.1021/acs.jpca.7b00237.
7 Raudkivi M, Zekker I, **Rikmann E**, Vabamäe P, Kroon K, Tenno T. (**2017**). Nitrite inhibition and limitation – the effect of nitrite spiking on anammox biofilm, suspended and granular biomass. *Water Sci Technol* 75(2): 313–321; 10.2166/wst.2016.456.
8 Tenno T, **Rikmann E**, Zekker I, Tenno T, Daija L, Mashirin A. (**2016**). Modelling equilibrium distribution of carbonaceous ions and molecules in a heterogeneous system of $CaCO_3$–water–gas. *P Est Acad Sci Chem* 65(1): 68–77; 10.3176/proc.2016.1.07.
9 Zekker I, **Rikmann E**, Mandel A, Kroon K, Seiman A, Mihkelson J, Tenno T, Tenno T. (**2016**). Step-wise temperature decreasing cultivates a biofilm with high nitrogen removal rates at 9 °C in short-term anammox biofilm tests. *Environ Technol* 37 (15): 1933–1946. 10.1080/09593330.2015.1135995.
10 Daija L, Selberg A, **Rikmann E**, Zekker I, Tenno T, Tenno T, (**2016**). The influence of lower temperature, influent fluctuations and long retention time on the performance of an upflow mode laboratory-scale septic tank. *Desalination Water Treat* 57(40): 18679–18687; 10.1080/19443994.2015.1094421.
11 **Rikmann E**, Zekker I, Tomingas M, Tenno T, Loorits L, Vabamäe P, Mandel A, Raudkivi M, Daija L, Kroon K, Tenno T, (**2015**). Sulfate-reducing Anammox for Sulfate and Nitrogen Containing Wastewaters. *Desalination Water Treat* 57(7): 3132–3141; 10.1080/19443994.2014.984339.
12 Zekker I, **Rikmann E**, Tenno T, Loorits L, Kroon K, Vabamäe P, Mandel A, Raudkivi M, Daija L, Rubin SSCdC, Tenno T. (**2015**) Nitric oxide for anammox recovery in nitrite-inhibited deammonification system. *Environ Technol* 36(19): 2477–2487; 10.1080/09593330.2015.1034791.
13 **Rikmann E**, Zekker I, Tomingas M, Vabamäe P, Kroon K, Saluste A, Tenno T, Menert A, Loorits L, Rubin SSCdC, Tenno T. (**2014**). Comparison of sulfate-reducing and conventional Anammox upflow anaerobic sludge blanket reactors. *J Biosci Bioeng* 118(4): 426–433; 10.1016/j.jbiosc.2014.03.012.

14 Zekker I, **Rikmann E**, Tenno T, Seiman A, Loorits L, Kroon K, Tomingas M, Vabamäe P, Tenno T. (**2014**). Nitritating-anammox biomass tolerant to high dissolved oxygen concentration and C/N ratio in treatment of yeast factory wastewater. *Environ Technol* 35(12): 1565–1576; 10.1080/09593330.2013.874492.
15 Zekker I, **Rikmann E**, Loorits L, Tenno T, Fritze H, Tuomivirta T, Kroon K, Vabamäe P, Seiman A, Raudkivi M, Mandel A, Tenno T. (**2014**). Start-up of low temperature anammox in UASB from mesophilic yeast factory anaerobic tank inoculum. *Environ Technol*, 36(2): 214–225; 10.1080/09593330.2014.941946.
16 Zekker I, **Rikmann E**, Tenno T, Kroon K, Vabamäe P, Salo E, Loorits L, Rubin SSCdC, Tenno T. (**2013**). Deammonification process start-up after enrichment of anammox microorganisms from reject water in a moving bed biofilm reactor (MBBR). *Environ Technol* 34(23): 3095–3101; 10.1080/09593330.2013.803134.
17 Zekker I, **Rikmann E**, Tenno T, Vabamäe P, Tomingas M, Menert A, Loorits L, Tenno T. (**2012**). Anammox Bacteria Enrichment and Phylogenic Analysis in Moving Bed Biofilm Reactors. *Environ Eng Sci* 29(10): 946–950; 10.1089/ees.2011.0146.
18 Zekker I, **Rikmann E**, Tenno T, Lemmiksoo V, Menert A, Loorits L, Vabamäe P, Tomingas M, Tenno T. (**2012**). Anammox enrichment from reject water on blank biofilm carriers and carriers containing nitrifying biomass: operation of two moving bed biofilm reactors (MBBR). *Biodegradation*, 23(4): 547–560; 10.1007/s10532-011-9532-7.
19 **Rikmann E**, Zekker I, Tomingas M, Tenno T, Menert A, Loorits L, Tenno T. (**2012**) Sulfate-reducing anaerobic ammonium oxidation as a potential treatment method for high nitrogen-content wastewater. *Biodegradation* 23(4): 509–524; 10.1007/s10532-011-9529-2.
20 Zekker I, **Rikmann E**, Tenno T, Saluste A, Tomingas M, Menert A, Loorits L, Lemmiksoo V, Tenno T. (**2012**). Achieving nitritation and anammox enrichment in single moving- bed biofilm reactor treating reject water. *Environ Technol* 33(6): 703–710; 10.1080/09593330.2011.588962.
21 Zekker I, **Rikmann E**, Kroon, K, Saluste A, Vabamäe P, Tenno T, Menert A, Loorits L, Tenno T. (**2012**). Sulfate- reducing and nitrite-dependent anammox for ammonium removal. *Commun Agric Appl Biol Sci* 77(1): 227–230.
22 Zekker I, Kroon, K, **Rikmann E**, Tenno T, Tomingas M, Vabamäe P, Vlaeminck SE, Tenno T. (**2012**). Accelerating effect of hydroxylamine and hydrazine on nitrogen removal rate in moving bed biofilm reactor. *Biodegradation*, 23(5): 739–749; 10.1007/s10532-012-9549-6.
23 Zekker I, **Rikmann E**, Tenno T, Vabamäe P, Kroon K, Loorits L Saluste, A, Tenno T. (**2012**). Effect of HCO_3^- concentration on anammox nitrogen removal rate in a moving bed biofilm reactor. *Environ Technol* 33(20): 2263–2271; 10.1080/09593330.2012.665487.

24 Zekker I, **Rikmann E**, Tenno T, Menert A, Lemmiksoo V, Saluste A, Tenno T, Tomingas M. (**2011**). Modification of nitrifying biofilm into nitritating one by combination of increased free ammonia concentrations, lowered HRT and dissolved oxygen concentration. Journal of Environmental Sciences, 23(7): 1113–1121; 10.1016/S1001-0742(10)60523-2.
25 Pikkov L, Kallas J, Rüütmann T, Rikmann E. (**2001**). Characteristics of activated carbon produced from biosludge and its use in wastewater post-treatment. *Environ Technol* 22(2): 229–236; 10.1080/09593332208618302

DISSERTATIONES TECHNOLOGIAE CIRCUMIECTORUM UNIVERSITATIS TARTUENSIS

1. **Sille Teiter.** Emission rates of N_2O, N_2, CH_4 and CO_2 in riparian grey alder forests and subsurface flow constructed wetlands. Tartu, 2005, 134 p.
2. **Kaspar Nurk.** Relationships between microbial characteristics and environmental conditions in a horizontal subsurface flow constructed wetland for wastewater treatment. Tartu, 2005, 123 p.
3. **Märt Öövel.** Performance of wastewater treatment wetlands in Estonia. Tartu, 2006, 148 p.

   Sergei Yurchenko. Determination of some carcinogenic contaminants in food. Tartu, 2006, 143 p. Published in *Dissertation Chimicae Universitatis Tartuensis,* 51.
4. **Alar Noorvee.** The applicability of hybrid subsurface flow constructed wetland systems with re-circulation for wastewater treatment in cold climates. Tartu, 2007, 117 p.

   Ülle Jõgar. Conservation and restoration of semi-natural floodplain meadows and their rare plant species. Tartu, 2008, 99 p. Published in *Dissertation Biologicae Universitatis Tartuensis*, 139.
5. **Christina Vohla.** Phosphorus removal by various filter materials in subsurface flow constructed wetlands. Tartu, 2008, 103 p.
6. **Martin Maddison.** Dynamics of phytomass production and nutrient standing stock of cattail and its use for environment-friendly construction. Tartu, 2008, 87 p.
7. **Marika Truu.** Impact of land use on microbial communities in Estonian soils. Tartu, 2008, 126 p.
8. **Elar Põldvere.** Removal of organic material, nitrogen and phosphorus from wastewater in hybrid subsurface flow constructed wetlands. Tartu, 2009, 107 p.
9. **Margit Kõiv.** Treatment of landfill leachate and municipal wastewater in subsurface flow filters using mineralized peat and hydrated oil shale ash. Tartu, 2010, 147 p.
10. **Jaanis Juhanson.** Impact of phytoremediation and bioaugmentation on the microbial community in oil shale chemical industry solid waste. Tartu, 2010, 95 p.

    Aare Selberg. Evaluation of environmental quality in Northern Estonia by the analysis of leachate. Tartu, 2010, 117 p. Published in *Dissertation Chimicae Universitatis Tartuensis,* 99.
11. **Riho Mõtlep.** Composition and diagenesis of oil shale industrial solid wastes. Tartu, 2010, 127 p.
12. **Igor Zaytsev.** Bioaugmentation in LWA-filled horizontal subsurface flow filters for wastewater treatment: Impact of flow regime, temperature and donor system Tartu, 2010, 97 p.

13. **Siiri Velling.** Microbial BOD biosensor for wastewater analysis. Tartu, 2011, 79 p.
14. **Riina Lepik.** Biodegradability of phenolic compoundsas single and mixed substrates by activated sludge. Tartu, 2011, 153 p.
15. **Liis Marmor.** Ecology and bioindicative value of epiphytic lichens in relation to air pollution and forest continuity. Tartu, 2011, 98 p.
16. **Martin Liira.** Active filtration of phosphorus in Ca-rich hydrated oil shale ash: precipitation mechanisms and recovery. Tartu, 2012, 84 p.
17. **Kristjan Karabelnik.** Advanced design and management of hybrid constructed wetlands: environmental and water purification effects. Tartu, 2012, 128 p.
18. **Hiie Nõlvak.** Influence of qPCR workflow on target gene enumeration from environmental samples in the case of bioremediation potential estimation. Tartu, 2012, 136 p.
19. **Merlin Raud.** Study of semi-specific BOD biosensors for biosensor-array. Tartu, 2013, 103 p.
20. **Ivar Zekker.** Enrichment of anaerobic ammonium oxidizing bacteria for nitrogen removal from digester effluent and anammox process acceleration by intermediate compounds. Tartu, 2013, 142 p.
21. **Annika Uibopuu**. Communities of arbuscular mycorrhizal fungi in spruce forest ecosystem and their effect on performance of forest understorey plant species. Tartu, 2013, 104 p.
22. **Jekaterina Jefimova.** Leaching of polycyclic aromatic hydrocarbons (PAHs) and heavy metals from the oil shale processing wastes and from waste-based products. Tartu, 2015, 184 p.
23. **Teele Ligi**. Bacterial community structure and its genetic potential for nitrogen removal in the soils and sediments of a created riverine wetland complex. Tartu, 2015, 127 p.
24. **Kuno Kasak**. Greenhouse gas emissions and water treatment efficiency in subsurface flow filters using various substrates. Tartu, 2016, 128 p.
25. **Martin Ligi**. Application of close range remote sensing for monitoring aquatic environment. Tartu, 2017, 146 p.
26. **Mikk Espenberg.** Impact of management on peatland microbiome and greenhouse gas emissions. Tartu, 2017, 152 p.
27. **Jens-Konrad Preem.** Forest soil bacterial community analysis using high-throughput amplicon sequencing. Tartu, 2017, 108 p.
28. **Taavi Vaasma.** Enrichment, atmospheric dispersion and deposition of naturally occurring radionuclides from oil shale-fired power plants. Tartu, 2017, 175 p.
29. **Kristjan Oopkaup.** Microbial community and its relationship with pollutant removal in treatment wetlands. Tartu, 2018, 154 p.